Biomechanics Of Human Temporomandibular Joint.

Order Number 8909390

Biomechanics of human temporomandibular joint

Kang, Q-Seop, Ph.D.

Lehigh University, 1989

U·M·I

300 N. Zeeb Rd.
Ann Arbor, MI 48106

BIOMECHANICS OF HUMAN TEMPOROMANDIBULAR JOINT

by

Q-Seop Kang

A Dissertation

Presented to the Graduate Committee

of Lehigh University

in Candidacy for the Degree of

Doctor of Philosophy

in

Applied Mechanics

Lehigh University

1988

Approved and recommended for acceptance as a dissertation in partial fulfillment of the requirements for the degree of Doctor of Philosophy.

October 26, 1988

Dean P. Updike

Dr. Dean P. Updike,
Professor in Charge

Accepted Dec. 5, 1988

Special Committee directing
the doctoral work of
Q-seop Kang

Eric P. Salathe'

Dr. Eric P. Salathe,
Chairman

Jacob Y. Kazakia

Dr. Jacob Y. Kazakia

Arkady Voloshin

Dr. Arkady Voloshin

Dr. David Cundall

Dean P. Updike

Dr. Dean P. Updike,
Professor in Charge

ACKNOWLEDGEMENTS

I express my sincerest thanks to Professor Dean P. Updike, the dissertation adviser, and Professor Eric P. Salathe, the chairman of the advising committee, for their supervision, encouragement and critical review of this work. I also express my sincere appreciation to the members of my doctoral committee, Professors Jacob Y. Kazakia, Arkady Voloshin and David Cundall for their time and interest in this work.

I thank my fellow graduate students for their interest and discussions throughout this work. I thank my wife, Mee-Young for her assistance with the preparation of this manuscript.

I wish to express my special thanks to my father in law, Mr. Chong-In Hahn, for his financial support and encouragement during my graduate study.

TABLE OF CONTENTS

LIST OF TABLES

LIST OF FIGURES

NOMENCLATURE

A	a nonlinear elastic constant of ligaments
a_j	physiological cross sectional area of a ligament
A_t	physiological cross sectional area of the temporalis
A_{t0}	area of the origin of the temporalis
$A_{i,j}$	elements of coefficient matrix [A]
B	a nonlinear elastic constant of ligaments
B_i	elements of column matrix {B}
C, C_1, C_2	constants of the reduced relaxation function
E	tangent modulus of ligaments
E_1	exponential integral
$\vec{f}_i$	individual muscle fiber force
$\vec{F}_j$	ligamentous force
$\vec{F}_M$	muscle force
$\tilde{G}$	stress relaxation of ligaments
G	reduced relaxation function of ligaments
G^*	dynamic modulus
G'	storage modulus
G''	loss modulus
$\tilde{J}$	creep compliance of ligaments
J	reduced creep function of ligaments
$\vec{L}$	bite force or external force
L, L_j	length of a ligament

L_0, L_{j0}	free length of a ligament
L', L_j'	length of a ligament after incremental movement
L_{c1}, L_{c2}	lengths of the capsular ligaments
L_l	length of the lateral ligament
L_{sp}	length of the sphenomandibular ligament
L_{st}	length of the stylomandibular ligament
M	moment
n	number of the temporalis muscle fibers (chapter 4)
P^k	location of a point on the mandible after k° normal opening
P_0	center of the condyle
P_1	the origin of a muscle or a ligament
P_2	the insertion of a muscle or a ligament
R	joint reaction force
S_k	the center of rotation of the mandible from k° to $(k+1)^\circ$
T_1, T_2	components of the external pterygoidal force
t	time
U_j	strain energy of a ligament
u, v	translations along the x and y directions respectively
W_m	work done by a muscle
W_R	work done by the joint reaction force

Greek letters

α	constant strain rate
Γ	maximum allowable muscle stress
γ	Euler's number
δ_x, δ_y	amounts of incremental translation of P_2 along the x and y directions

	respectively
$\Delta(\ )$	incremental quantity
ϵ_j	ligamentous strain
ϵ_{j1}, ϵ_{j2}	ligamentous strain before and after incremental movement respectively
ϵ_r	ligamentous strain at the threshold between linear and nonlinear zones
θ_i	angle between i-th muscle fiber and the total muscle force in the temporalis
η_e	efficiency of the external pterygoidal force
ϕ	direction of the joint reaction force
ϕ_{opt}	optimum direction of the joint reaction force
Π	total potential energy
σ_j	ligamentous stress
σ_{j1}, σ_{j2}	ligamentous stress before and after incremental movement respectively
σ_r	ligamentous stress at the threshold between linear and nonlinear zones
σ^e	time independent elastic stress of a ligament
τ	time
τ_1, τ_2	time constants associated with the reduced relaxation function
ω	frequency in cyclic stress
ζ_1, ζ_2, ζ_e	reference angles of the external pterygoid (see Fig.4.3)

Superscripts

*	quantity associated with the starting of relaxation

Subscripts

e	quantity associated with the external pterygoid
i	quantity associated with the internal pterygoid

j	quantity associated with a ligament
M	quantity associated with a muscle
m	quantity associated with the masseter
o	quantity associated with the opener
t	quantity associated with the temporalis

ABSTRACT

The biomechanics of the human temporomandibular joint is examined. A simplified craniomandibular model is put forth to analyze normal opening and bite motion of the jaw. The locus of the instantaneous center of rotation is interpolated from several discrete data points given in the literature, and the corresponding motion of the mandible during normal opening is regenerated. The motion of the mandible is regarded as due to its muscle forces and constrained by the ligaments of the temporomandibular joint.

The available limit of the mandibular translation, other than normal opening, is determined on the basis of maximum allowable lengths of ligaments, which are taken appropriately with marginal safety. To predict the related muscle forces and corresponding joint reaction force during the motion of the mandible, a nonlinear elastic behavior of ligaments is expressed in an exponential form, and all the ligaments of the temporomandibular joint are assumed to have the same elastic and viscoelastic properties. A linear optimization procedure with an appropriate optimizing condition is developed to predict the muscle forces during the motion of the mandible. The procedure is composed of a parametric representation of the direction of the joint reaction force and utilization of a commercial subroutine package. To confirm the method, comparison is performed for the bite motion, for which the experimental results are available in the literature. Satisfactory agreement is shown between theoretically predicted results and experimental data from the literature on muscle forces for different levels of bite force.

Analysis of the normal opening of the mandible is performed in the same procedure. The external force exerted to give the mandibular translation is also determined in a similar fashion.

The viscoelastic behavior of ligaments is examined using the reduced relaxation function. The reduced relaxation function proposed by Y. C. Fung is approximated into a simple, sectionally continuous form and fitted into experimental data given in the literature. The transient and long term behaviors of stress relaxation are determined for different levels of strain rate. Also, the reduced creep function of ligaments is deduced from the reduced relaxation function and applied to determine the creep behavior for time dependent stress history. The time dependent structural behavior of the mandible can easily be determined through the viscoelastic behavior of individual ligaments.

Through this analysis, we can obtain insight into the behavior of the temporomandibular joint that provides significant guidance to the design of a suitable traction device that will open the joint during arthroscopic surgery performed to treat the failure of the articular capsule.

CHAPTER 1

INTRODUCTION

1.1 The Temporomandibular Joint

The structural arrangements at which bones come together are called joints. The joint system is the functional connection between bones of the skeleton. Without some kind of stable union of the many separate bones the skeletal system would lose much of its effectiveness in providing rigidity and support for the body. However, an equally important function of the joint is to make movement possible at many points of skeletal union. Some joints that provide fixed union are called fibrous joints or synarthroses. In fibrous joints the bones are united by fibrous connective tissues of various length. In these joints the motion of the skeletal system is prohibited or severely limited. But other joints are characterized by a flexible union with varying degrees of movement allowed. They are called movable joints. In these joints, the allowance of movement depends on the nature of the joint surfaces and the arrangement of reinforcing structures. The movable joints are divided into two different classes called cartilaginous and synovial joints. In the synovial joints, the bone surfaces are completely separated; the bones forming the joints are expanded for convenience of mutual connection, covered by articular cartilage and surrounded by the articular capsules of fibrous tissues. The articular capsules are filled with an internal lubricating fluid called synovial fluid.

The temporomandibular joint [TMJ] is a synovial joint connecting the temporal bone of the cranium and the condyle of the mandible. It provides the mandible with combined motion of rotation and translation. Also it gives constraint to the motion of

the mandible. Voluntary motions of the mandible, like those of other skeletal systems of the body, is brought about by the contraction of muscles, whose ends are secured on the bones by tendons. Bones are also connected by ligaments at the joints; thus the constraints of the ligaments limit the effect of causes of the mandibular motion which are forces generated by muscles or some external force. The connective tissue varies in thickness, in density, in accumulation of fat, and in relative amount of collagenous fibers, elastic fibers, and tissue fluid, according to local requirements [1].

A complete understanding of the mechanics of the TMJ is important in the diagnosis and treatment of joint disorders resulting from injury or disease, in the quantitative assessment of treatment, and in the design of fixing devices to aid surgical operations. TMJ diseases may be diagnosed by a variety of means, including the patients medical history, a physical evaluation, or supplemental diagnostic aids. One of the supplemental aids which facilitates the diagnosis and surgery of internal joint derangements is TMJ arthroscopy. Arthroscopy is a technique for direct visual inspection of joint structure through a thin hollow tube-shaped arthroscope that enters the joint cavity. The diameter of arthroscopes used in TMJ is now less than 2 *mm* [2,3]. As a practical application, the present analysis will provide information useful in securing the maximum available space in the joint for the protrusion of arthroscopic tools during TMJ surgery, and in determining the basic design data of a jaw fixing device to aid the surgery.

1.2 Modelling of the Mandibular Motion

To analyze the human mandibular motion, the geometry of the cranium and the mandible were drawn from the atlas of human anatomy [4] utilizing computer graphics.

This is shown in Fig.1.1, which represents the projection of the cranium and the mandible on the plane of symmetry. Here the x-y coordinates are taken as the horizontal and the vertical lines on the plane of symmetry, with the origin at the projection of the center of the condyle at the jaw closed position. The z axis is directed along the intercondyle axis.

The hard tissues, such as bones and teeth, are generally modelled to be perfectly rigid when considered in conjunction with soft connective tissues. Ligaments are modelled to be tension springs. The muscle forces are modelled to be external forces applied to the mass-spring system composed of the mandible and the ligaments attached on the cranium. The cranium is modelled as a rigid boundary.

1.3 Ligaments of the Temporomandibular Joint

The ligaments of the temporomandibular joint are the capsular, the sphenomandibular, the stylomandibular and the lateral ligaments, shown in Fig.1.1. Ligaments are composed mainly of bundles of collagen fibers placed parallel with, or closely interlaced with, one another. They are inserted into bones and are pliant and flexible so as to allow perfect freedom of movement. But they are strong and only slightly extensible, so as not to yield readily to applied force.

The capsular ligament, or the articular capsule, is an envelope attached to the cranium on the circumference of the mandibular fossa and the articular tubercle, and to the neck of the condyle of the mandible. The capsular ligament encloses two articular cavities that are separated by the articular disc. The two cavities are filled with the synovial fluid.

The articular cavities contain only enough fluid to moisten and lubricate the joint and to provide viscous damping, which reduces the impact on the joint. It is generally

accepted that the articular capsule is load bearing under most normal conditions. This load is called the joint reaction force.

Ligaments are composed mainly of collagen fibers, which behave like a bundle of rubber bands. Therefore, they can sustain little compressive or shear loads, but can mainly sustain tensile load.

Constitutive relations have been experimentally determined for various ligaments by many authors, including, for example, R. L. Waters and J. M. Morris [5] for human spinal ligaments, S. L-Y. Woo et. al. [6] for canine medial collateral ligaments and D. L. Butler et. al. [7] for human knee ligaments. The elastic behavior has been shown to vary significantly for each individual and even for different ligaments in an individual. It also has been shown that the elastic behavior is highly nonlinear. Also, it is generally known that the maximum allowable elongation is about 10 % or less.

1.4 Muscles and Tendons of the Mandible

The muscles connecting the mandible to the cranium and giving the voluntary motion to the mandible are the masseter, the temporalis, the internal pterygoid, the external pterygoid and the opener or digastric, shown in Fig.1.1. The attachments of two ends of a muscle are called the origin and the insertion. It is customary to describe the muscle as arising from the origin and ending at the insertion. The origin is the more fixed and proximal end, the insertion the more movable and distal end. For the cranium and the mandible, the muscles arise or have their origins in the cranium and their insertions are into the mandible. Tendons are considered to be the most regular of the parallel-fibered collagenous structures. They connect the muscle fibers and bones at the origin and the insertion. One end of a tendon is inserted into bone; the other end is connected to the muscle fibers.

The muscle forces are known to be exerted by the contraction of muscles. It also is known that the opposite directional motion of any arbitrary motion caused by the contraction of a muscle or of a combination of muscles can be performed by the contraction of another muscle or a combination of other muscles called the antagonist or antagonists.

Although magnitudes of the muscle forces on the mandible cannot be directly measured, a number of attempts have been made to estimate the magnitudes of the forces during bite motion; these include, for example, Carlsoo(1952), Schumacher(1961), and Pruim et. al.(1980) [8]. Experimental evidence given by electromyography [9] indicates that the masseter, internal pterygoid and temporal muscles are definitely active and that the external pterygoid may be active during bite motion.

A theoretical prediction of muscle forces during bite motion was attempted by J. C. Barbenel [10] with a hypothesis of minimum muscle forces, but was concluded to be unacceptable. This will be discussed in section 4.2.

1.5 Scope of the Work

The main body of this study is divided into seven chapters. The contents of each chapter are summarized in this section. In chapter 2, the kinematic analysis of the mandible during normal opening is presented along with the strain analysis of ligaments. In chapter 3, a review of elastic and viscoelastic properties of ligaments measured by several authors along with their test methods is presented. Also, the mathematical modeling of the test results are carried out. In chapter 4, the analysis of bite motion is performed and the muscle forces working for the bite motion are predicted utilizing an optimization technique, and the results are compared with the experimental data measured by Pruim et. al. [8]. In chapter 5, muscle forces working for the normal

opening of the mandible are predicted using the same technique, and a method for theoretical prediction of the instantaneous center of rotation during normal opening of the mandible is proposed. In chapter 6, the stress relaxation behavior of ligaments of the mandible is predicted for a long period of time, and their creep behavior is predicted in chapter 7. A summary and discussion of results is given in chapter 8.

CHAPTER 2

KINEMATIC ANALYSIS OF THE MANDIBULAR MOTION

2.1 Normal Opening of the Mandible

The constraint of the ligaments of the temporomandibular joint causes the mandible to undergo complex movements during normal opening and closing. The locus of the instantaneous center of rotation [ICR] of the mandible has been determined by experimental observations. Since the center of the condyle is not the center of rotation, the mandible moves significantly relative to the cranium. To regenerate the mandibular motion from the measured ICR, the locus of the ICR was generated from six data points measured by R. E. Hall utilizing the cubic spline interpolation method [11], which is one of the well-known smooth curve fitting methods. As we do not know the mandibular motion for jaw opening angles less than 3°, the locus of ICR was extrapolated from the data measured by Hall. The range of the mandibular opening angle has been measured to be 0°~28°, and the 3° and 18° opened states are named as the rest and opened states respectively [11].

To regenerate the locations of the mandible during normal opening, a curvilinear coordinate system s with the scale of degree opening angle will be adopted so that each point on the locus corresponds to the ICR at that opening angle. Since $0^\circ \leq s \leq 28^\circ$, we will choose 29 discrete points S_0 to S_{28} on the locus of the ICR, such that the subscripts denote the corresponding opening angle from closed state to fully opened state with 1° interval, shown in Fig.1.1. To make the analysis simple, all the discrete points above will be assumed to be the average center of rotation for 1° of additional normal

opening. In other words, the point $S_0(x_0,y_0)$ is the center of rotation during $0^\circ\sim1^\circ$ normal opening, the point $S_1(x_1,y_1)$ during $1^\circ\sim2^\circ$, and so on.

Denoting an arbitrary point on the mandible at closed state $P^0(x^0,y^0)$, where the superscripts denote the corresponding opening angle in degrees, after 1° rotation about the point $S_0(x_0,y_0)$, the point will move to $P^1(x^1,y^1)$ such that

$$\begin{bmatrix} x^1 \\ y^1 \end{bmatrix} = \begin{bmatrix} \cos 1^\circ & \sin 1^\circ \\ -\sin 1^\circ & \cos 1^\circ \end{bmatrix} \begin{bmatrix} x^0 - x_0 \\ y^0 - y_0 \end{bmatrix} + \begin{bmatrix} x^0 \\ y^0 \end{bmatrix}$$

$$= \begin{bmatrix} x^0 + (x^0-x_0)\cos 1^\circ + (y^0-y_0)\sin 1^\circ \\ y^0 - (x^0-x_0)\sin 1^\circ + (y^0-y_0)\cos 1^\circ \end{bmatrix} \qquad (2.1)$$

By performing the transformation of all the points of interest, such as mandibular contour, the center of the condyle and the insertions of muscles and ligaments, the location of the mandible at 1°opened state will be generated. In the same manner, the location of the mandible at k° opened state will be expressed by

$$\begin{bmatrix} x^k \\ y^k \end{bmatrix} = \begin{bmatrix} x^{k-1} + (x^{k-1}-x_{k-1})\cos 1^\circ + (y^{k-1}-y_{k-1})\sin 1^\circ \\ y^{k-1} - (x^{k-1}-x_{k-1})\sin 1^\circ + (y^{k-1}-y_{k-1})\cos 1^\circ \end{bmatrix} \qquad (2.2)$$

where $P^k(x^k,y^k)$ is the new location of the point $P^0(x^0,y^0)$ after k° normal opening of the mandible and $S_{k-1}(x_{k-1},y_{k-1})$ is the average center of rotation for the jaw opening from $(k\text{-}1)^\circ$ to k°. Performing the procedure repeatedly until full opening of the jaw, we can determine the location of the mandible during normal opening from 0° to 28° with 1° interval , which is shown in Fig.2.1.

2.2 Stretch of the Ligaments – Normal Opening of the Jaw

To analyze the mandibular motion, the stretch of the related ligaments that constrain mandibular motion should be determined. To determine the ligamentous lengths, each ligament except the articular capsule was represented by a straight line between two end points, the origin on the cranium and the insertion on the mandible.

The capsular ligament, or the articular capsule, was represented by two fibers located at the anterior and posterior ends. Since part of the capsular ligament wraps around the condyle at some locations of the mandible, the lengths of two lines representing the capsular ligament was calculated along the mandibular contour on the contact surfaces, as shown in Fig.2.2. In doing this, the geometry of the condyle contour was interpolated from the geometric data measured in section 1.2, utilizing the cubic spline method, in the same fashion as of the ICR.

The ligamentous lengths due to normal opening of the mandible for an arbitrary opening angle can be determined by computing numerically the line integral along each line representing the ligament. These are shown in Fig.2.3 for the entire range of normal opening. The maximum allowable strain of a ligament is known to be approximately 10 %, we can conclude that each ligament at jaw closed state or at small opening angle is supposed to be slack and at the relaxed state, which will be discussed later in detail.

2.3 Translation Limit of the Mandible – Symmetric Motion

To secure maximum allowable space in TMJ for the penetration of arthroscopic tools, the mandible should be pulled to its allowable limit. The translation of the mandible is limited by the constraint brought about by the stretch of the ligaments. To account for this, we will assume that the maximum of a ligament length during normal opening of the mandible is the maximum allowable length of that ligament. Thus the

limit of translation of the mandible in x-y plane can be determined for any normal opening angle of the mandible. As an example, taking 4° opening angle, it is evident from Fig.2.3 that the length of any ligament being less than its available maximum, the mandible can be translated to any direction until one of the ligament lengths reaches its maximum allowable value. The locations of the mandible after 4° normal opening followed by translation to the limit, with 15° intervals are shown in Fig.2.4. The direction of the translation is limited between -120° to 0° with respect to positive x axis, to avoid the interference between the mandible and the cranium.

In the figure, the closed contour is the available range of translation of the mandible, represented by that of the center of the condyle on the mandible. The contour of translation limit is shown separately in Fig.2.5 together with the locus of the center of condyle during normal opening. The limit of translation of the mandible after normal opening represented by the locations of the center of the condyle for 0°~28° with 1° interval were generated and superposed along the path of the center of condyle during normal opening in Fig.2.6, which shows the totality of the translation limit of the mandible for symmetric motion. It should be noted that a possible location of the mandible is path-dependent. For example, the best way of locating the mandible so that the center of condyle is on the point (0.1″, -0.2″) is rotating the mandible to 12° by normal opening followed by translating it to that location, whereas at the opening angle less than 6°, the mandible can never reach that location by any translation to the limit. It is interesting that no translation is allowed for the jaw opening angle 18° to 21°. The only possible motion in this range is normal opening or closing of the jaw, which was expected from Fig.2.3.

Since these results are based on the assumption that the maximum allowable length of a ligament is its available maximum during normal opening of the mandible, it

is most conservative. Also it should be mentioned that the muscle effects were ignored in this analysis because the muscles are far less stiff than the ligaments. Furthermore, the free length of a muscle is much longer than that of a ligament on the mandible.

2.4 Nonsymmetric Motion of the Mandible

A three dimensional view of the mandible is shown schematically in Fig.2.7. In order to represent the mandible in three dimensional space, according to Wheeler [12], W. Bonwill (1889) described the mandible as adapting itself in part to an equilateral triangle, now called the Bonwill Triangle. The vertices of the triangle are placed at the center of each condyle and at the tip of the mandibular central incisors on the plane of symmetry.

For convenience in practical use, especially in analyzing the bite motion, efforts were taken to formulate the occlusal surface of the mandibular teeth by many authors, such as F. G. von Spee (1890) and G. S. Monson (1927). However, it seems that the occlusal surface does not fit any curved surface that can be formulated briefly by mathematical terms [12]. It is rather conventional that the occlusal plane, which is tangent to the contact points of the first and second molars, is used to represent the mandibular motion. The occlusal plane, in general, is known to be slanted 10° with respect to the horizontal plane when the jaw is at closed position.

Nonsymmetric or three dimensional motion of the mandible is composed of z directional translation and x and y directional rotations denoted by w, θ_x and θ_y respectively, as shown in Fig.2.7. The limit values of nonsymmetric translation can be determined in a similar fashion as the two dimensional case, and the results are plotted in Fig.2.8. In the figure, the closed region $ABDB'A'$ is the translation limit of the mandible on the x-z plane, taken for the positive z direction only. The negative z

direction is omitted for simplicity, since the shape is symmetric about the x-y plane. As an example, if the center of the condyle is located on the point A, B or C in the x-y plane, the z directional translation limit is $\overline{AA'}$, $\overline{BB'}$ or $\overline{CC'}$ respectively. The range of three dimensional translation for any opening angle can be built as shown, in the same way. These volumetric ranges were determined for all the discrete angles of rotation and were superposed from 0° to 28° with 1°interval, shown in Fig.2.9, which illustrates the totality of the translation of the mandible represented by the locus of the center of the condyle.

CHAPTER 3

MECHANICAL PROPERTIES OF LIGAMENTS

3.1 Overview

Ligaments, like most soft biological tissues, are composed of several different kinds of materials. Their major structural component is the collagen fiber, which is almost inextensible, but flexible. The other components consist of less stiff elastic fibers, fat and tissue fluid.

The mechanical properties of ligaments vary significantly, depending on relative composition, which is determined by their individual or local requirements. By their variety of shapes and mechanical behaviors, the tests for elastic or viscoelastic properties of soft tissues are not standardized yet, so the test scheme should be developed before each test. The emphasis is generally placed on the tensile tests because most soft tissues can sustain moderately large tensile loads but negligibly small compressive or shear loads.

The elastic and viscoelastic behavior of ligaments has been observed by many authors, including, for example, A. L. Nachemson and J. H. Evans [13], A. Viidik [14], R. L. Waters and J. M. Morris [5], S. L-Y. Woo et. al. [6], D. L. Butler et. al. [7], and G. A. Dumas et. al. [15]. However, quantitative evaluation of the mechanical properties of ligaments were performed for some limited cases only, and due to the variety of results, it is somewhat difficult to formulate their general behaviors.

3.2 Stress Relaxation of Ligaments

If a step increase in elongation is imposed on a viscoelastic material within its elastic limit, the stress developed in that material will be a function of time as well as of the strain ϵ. For a certain amount of strain imposed, a stress history is assumed of the form

$$\sigma(\epsilon,t) = \tilde{G}(\epsilon,t)\ \epsilon, \tag{3.1}$$

where the ratio of resultant stress to imposed strain is called the relaxation modulus and denoted by $\tilde{G}(\epsilon,t)$, which in general depends on both the time and imposed strain. If $\tilde{G}$ is dependent only on the strain, the material is called elastic, but if $\tilde{G}$ is dependent on time as well as on the strain, it is called viscoelastic. Most of soft biological tissues, including ligaments, display this behavior only up to a certain limit of strain or corresponding stress during any deformation process. If $\tilde{G}$ is a function of time only,

$$\sigma\ (\ \epsilon,t\ ) = \tilde{G}(t)\cdot\epsilon\ , \tag{3.2}$$

the material is called linearly viscoelastic. Most viscoelastic materials display this behavior only up to a certain critical value of stress or strain.

The most general type of viscoelastic behavior that is displayed by a material occurs when the stress σ is a function of strain history as well as of time, as expressed in eq.3.1. Provided that $\tilde{G}$ in eq.3.1 is separable with respect to t and ϵ, it will be expressed as

$$\sigma\ (\ \epsilon,\ t\ ) = G(t)\ \sigma^e(\epsilon)\ , \qquad G(0) = 1\ , \tag{3.3}$$

where G(t) is the reduced relaxation function, which, in general, is monotonically decreasing with time, and the time-independent term $\sigma^e(\epsilon)$ is the instantaneous elastic response. For a known strain history, the strain being expressed as a function of time,

$$\sigma(\epsilon(t),t) = \sigma(t)\ ; \tag{3.4}$$

thus eq.3.3 will be

$$\sigma(t)=G(t)\sigma^e(\epsilon(t)) \ . \tag{3.5}$$

Most viscoelastic materials display this type of nonlinearity as a result of a finite deformation within the elastic limit.

We take the stress response at time t to an infinitesimal step change in strain at time τ, which is less than t, as shown in Fig.3.1,

$$\Delta\sigma(t) = G\,(\,t - \tau\,)\cdot\Delta\sigma^e \ , \tag{3.6}$$

where $\Delta\sigma^e = \frac{d\sigma^e}{d\epsilon}\,\Delta\epsilon$, and assume that the superposition principle applies, so that

$$\sigma(t) = \int_{-\infty}^{t} G(t-\tau)\ \frac{d\sigma^e}{d\epsilon}\ \frac{d\epsilon}{d\tau}\ d\tau\ ; \tag{3.7}$$

that is, the stress at time t is the sum of contributions of all the fast changes, each governed by the reduced relaxation function. Provided the strain is applied at fully relaxed state, eq.3.7 will be replaced by

$$\sigma(t) = \int_{0}^{t} G(t-\tau)\ \frac{d\sigma^e}{d\epsilon}\ \frac{d\epsilon}{d\tau}\ d\tau \ . \tag{3.8}$$

Since the stress σ is a function only of time, it can be discussed in the framework of linear viscoelasticity, which is the quasi-linear viscoelastic model proposed by Y.C.Fung [16]. This model provides a useful tool for the description of the behavior of many soft tissues.

As is seen from eq.3.8 , to determine the stress relaxation behavior of a material, the reduced relaxation function G(t), the elastic stress response $\sigma^e(\epsilon)$, and the strain rate $\frac{d\epsilon}{dt}$ are the major parameters to be determined. Unlike general structural materials, these parameters can hardly be determined by a single test method. The

reduced relaxation function can be approximated by the stress relaxation test with relatively high strain rate in accordance with eq.3.2.

Since it is technically impossible to measure the time independent or instantaneous stress response in a tensile test, the test is performed using a moderately small strain rate measuring the time dependent response $\sigma(t)$. From the measured time dependent stress response $\sigma(t)$, the elastic stress response σ^e can be determined utilizing eq.3.8, which will be discussed in section 3.5.

3.3 Stress Relaxation Test

The measurement of the stress relaxation of a material is one of the simpler viscoelastic experiments. An Instron machine with special recording device can be used [5, 6, 17]. Basically, the sample to be tested is deformed to a fixed strain ϵ^* as rapidly as possible (in a few milliseconds), and the stress required to maintain that fixed strain is measured as a function of time.

3.3.1 Preparation of Specimens

Tissues to be tested should be removed as soon as possible after death. For a large part, the test specimen can be cut from the medial portion, but for a small part, bone-ligament-bone structure is cut to be used as the test specimen [5, 6, 7, 17]. Care should be taken to cut only along primary longitudinal fiber bundle directions.

Specimens generally are immersed in saline solution or in any other appropriate chemical solutions and kept at a low temperature or at body temperature. However, before testing, the specimen should be recovered to the body temperature [5, 7, 17, 18, 19] .

3.3.2 Cross Sectional Area

Cross sectional areas are usually measured by a special slot and plunger with dial gage [6, 7, 17]. The slot size should be selected by the width and thickness of the tissue.

3.3.3 Gripping

Isolated specimens are placed in the grip inserts, which have sinusoidal-shaped matching teeth with smooth surfaces [17]. To grip a bone-ligament-bone specimen, the bone block at each end is potted in the cavity of the grip body using synthetic adhesives, and to secure the grip, the bones are drilled and connected to the grip inserts by appropriate sized pins. Special ink is used to mark the gage points on the specimen [6, 17].

Care must be taken to ensure that the direction of applied force is kept parallel to the fiber direction.

3.3.4 Test Environment

Tests are usually performed at room temperature. In many cases, the specimens are fully submerged in saline-bath at body temperature to keep them wet and to mimic their mechanical behavior in vivo. It is recommended that variation of the room temperature and the saline-bath temperature should be kept within $\pm 1^{\circ}C$ and $\pm 0.1^{\circ}C$, respectively.

3.3.5 Stress Measurement

A load cell is most commonly used for the stress measurement. Since the stress relaxation experiment may cover the time range from a fraction of a millisecond to thousands of hours, the methods of recording the stress response will vary with the time range [20]. At very short time periods, it is necessary to use a high speed recorder [6, 17]. In the intermediate time range from a few seconds to a few hours, a strip-chart

recorder is satisfactory. For longer times, a non-recording instrument may be used.

The peak stress can be assumed to be the instantaneous elastic response $\sigma^{e*}(\epsilon^*)$.

3.3.6 Strain Measurement

The measurement of strain is considerably simpler than that of the stress simply because the sample strain remains constant throughout the experiment. Although only one strain measurement is necessary, it is desirable to make periodic measurements to assure that the strain is kept constant [20]. Simple tools, such as dial gages, are commonly used for the strain measurement.

3.4 Tensile Test

Tensile test can be performed with the same apparatus as the stress relaxation test. The sample to be tested is deformed at a certain strain rate and the corresponding stress is measured, either as a function of time or strain.

As shown in Fig.3.2, a load cell and a video dimensional analyzer(VDA), a linear variable differential transformer(LVDT), or any other appropriate device can be used to record the stress-strain relationship [5, 6, 7, 13, 15, 18].

3.5 Mathematical Modelling of the Reduced Relaxation Function

Phenomenologically, the relaxation behavior of soft tissues is similar to that of the generalized Maxwell Model [21], whose characteristics are shown briefly in Fig.3.3(a). From the stress relaxation test, the reduced relaxation function can be determined by utilizing eq.3.3,

$$G(t) = \frac{\sigma(t)}{\sigma^{e*}(\epsilon^*)} \quad , \qquad G(0) = 1, \tag{3.9}$$

where $\sigma(t)$ is the measured stress as a function of time and $\sigma^{e*}(\epsilon^*)$ is the peak stress measured at the time of full elongation.

For the reduced relaxation function, Y. C. Fung [16, 22] has proposed the empirical relation

$$G(t) = \frac{1 + C\,\{\,E_1\,(t/\tau_1) - E_1(t/\tau_2)\,\}}{1 + C \ln\,(\tau_2/\tau_1)}\,, \tag{3.10}$$

$$\text{with} \quad E_1 = \int_y^\infty \frac{e^{-x}}{x}\,dx\,, \tag{3,11}$$

where E_1 is the exponential integral whose values are tabulated in mathematical-tables such as "Handbook of Mathematical Functions" [23] and C, τ_1 and τ_2 are the viscoelastic parameters to be determined by experiments. C is the parameter which has the greatest influence on the total amount of relaxation after a long time interval. The time constant τ_1 influences the slope of the relaxation function just after the beginning of relaxation and the time constant τ_2 is determined for the time which is necessary to reach the maximum relaxation.

The reduced relaxation function expressed in eq.3.10 can be approximated to be

$$G(t) \simeq 1\,, \qquad 0 \le t < \tau_1$$

$$G(t) \simeq \frac{1 + C\,\gamma + C \ln \tau_1}{1 + C \ln\,(\tau_2/\tau_1)} - \frac{C}{1 + C \ln\,(\tau_2/\tau_1)} \ln t$$

$$= C_1 - C_2 \ln t\,, \qquad \tau_1 \le t < \tau_2 \tag{3.12}$$

$$G(t) \simeq \frac{1}{1 + C \ln\,(\tau_2\,/\tau_1)}\,, \qquad t \ge \tau_2$$

where $C_1 = \dfrac{1 + C\gamma + C \ln \tau_1}{1 + C \ln (\tau_2/\tau_1)}$,

$$C_2 = \frac{C}{1 + C \ln (\tau_2 / \tau_1)} \tag{3.13}$$

and γ is Euler's number defined as

$$\gamma = -\int_0^\infty e^{-x} \ln x \; dx \simeq 0.5772157 . \tag{3.14}$$

The asymptotic value of G(t) is

$$[\, G(t) \,]_{t=\infty} = \frac{1}{1 + C \ln (\tau_2 / \tau_1)} . \tag{3.15}$$

A typical shape of the reduced relaxation function is plotted in Fig.3.4.

The experimental results of canine medial collateral ligaments determined by S. L-Y. Woo et. al. are shown in Fig.3.5 [6], where it can be seen that the empirical function G(t) fit the experimental results very closely.

3.6 Mathematical Modelling of the Elastic Stress-Strain Relations

Since the elastic stress response σ^e is the instantaneous response, there is no direct way of measuring it. Even though it might be approximated from the test results of very high strain rate, in practice, it is not a simple method. However, it can be evaluated from the results of tensile tests with moderate strain rates [6]. From the tensile test results, $\sigma(t)$ is formulated as a known function of strain rate $\frac{d\epsilon}{dt}$ and time,

where $\frac{d\epsilon}{dt}$ was kept constant during the test. These results will be substituted into eq.3.8,

$$\sigma(t) = \int_0^t G(t-\tau)\ \frac{d\sigma^e}{d\epsilon}\ \alpha\ d\tau\ , \tag{3.16}$$

where $\alpha = \frac{d\epsilon}{d\tau}$ = constant, and G(t) and $\sigma(t)$ are known functions evaluated from test results. By inversion of eq.3.16, $\frac{d\sigma^e}{d\epsilon}$ can be evaluated.

It is a general behavior of soft biological tissues that the nonlinear behavior of stress-strain relation is followed by the linear one until it reaches the allowable maximum state.

Out of several different expressions, we choose an exponential one to represent the nonlinear part of stress-strain relation of the material [6]. Denoting the threshold stress and strain between the linear and nonlinear regions σ_r and ϵ_r respectively, the stress-strain relations were taken in the form :

$$\sigma^e(\epsilon) = A\ (e^{B\epsilon} - 1)\ , \qquad 0 \leq \epsilon \leq \epsilon_r$$

$$\text{and} \quad \sigma^e(\epsilon) = E\ (\epsilon - \epsilon_r) + \sigma_r\ , \qquad \epsilon > \epsilon_r \tag{3.17}$$

where A and B are constants to be determined for the nonlinear elastic range, and E is the tangent modulus in the linear elastic range. Differentiating eq.3.17 with respect to ϵ and substituting into eq.3.16,

$$\sigma(t) = A\ B\ \alpha \int_0^t G(t-\tau)\ e^{B\alpha\tau}\ d\tau\ , \qquad 0 \leq \epsilon \leq \epsilon_r \tag{3.18}$$

and $\sigma(t) = A\ B\ \alpha \int_0^{t_r} G(t-\tau)\ e^{B\alpha\tau}\ d\tau + E \int_{t_r}^{t} G(t-\tau)\ d\tau\ , \qquad \epsilon > \epsilon_r$

where t_r is defined as the time at which the strain reaches its threshold value between the linear and nonlinear ranges.

3.7 Creep Test and its Formulation

In a creep test, a certain tensile stress σ_0 is suddenly applied at time zero and held constant during the test. The corresponding strain is measured as a function of time. From the general behavior, it is known that the strain increases monotonically with time. This is phenomenologically similar to the generalized Kelvin Model [21] shown in Fig.3.3(b). Creep behavior can be easily formulated in the same context as the stress relaxation [16, 21, 22]. For a certain amount of instantaneous stress imposed, the strain history $\epsilon(t)$ is assumed to be of the form

$$\epsilon(\sigma_0, t) = \tilde{J}(\sigma_0,t)\ \sigma_0\ , \tag{3.19}$$

where $\tilde{J}(\sigma_0,t)$ is the creep compliance function and σ_0 is the instantaneous stress applied. As σ^e is a function of ϵ only, provided that $\tilde{J}(\sigma_0, t)$ is separable with respect to t and σ_0, it can be expressed as

$$\sigma^e(t) = J(t)\ \sigma_0\ , \qquad J(0) = 1 \tag{3.20}$$

where $J(t)$ is the reduced creep function. In the linearly elastic, linearly viscoelastic case, since $\sigma^e = E\ \epsilon$ and $\tilde{J} = \tilde{J}(t)$, we can easily deduce from eqs. 3.19 and 3.20 that $J(t) = E\ \tilde{J}(t)$, where E is Young's modulus.

We take the strain response and corresponding elastic stress response at time t correspond to an infinitesimal step change in applied stress at time $\tau \leq t$, as shown in Fig.3.6,

$$\Delta\sigma^e(t) = J(t - \tau) \cdot \Delta\sigma\ . \tag{3.21}$$

Provided the specimen is fully relaxed at the initial state, and assuming that the superposition principle applies,

$$\sigma^e(t) = \int_0^t J(t-\tau) \frac{d\sigma}{d\tau} d\tau . \tag{3.22}$$

That is , the tensile stress at time t is the sum of contributions of all changes in the past, each governed by the reduced creep function. From eq.3.22 and the elastic stress-strain relation given in eq.3.17, the elastic strain response will be formulated as

$$\begin{aligned} A(e^{B\epsilon(t)} - 1) &= \int_0^t J(t-\tau) \frac{d\sigma}{d\tau} d\tau , \quad \text{for} \quad 0 \le \epsilon \le \epsilon_r \\ E(\epsilon - \epsilon_r) + \sigma_r &= \int_0^t J(t-\tau) \frac{d\sigma}{d\tau} d\tau , \quad \text{for} \quad \epsilon > \epsilon_r . \end{aligned} \tag{3.23}$$

To determine the reduced creep function of a material, a creep test can be performed on the same apparatus as the stress relaxation test.

3.8 Interrelation of Stress Relaxation and Creep

Since the creep behavior is the inverse of the stress relaxation behavior, in principle they can be interconverted [21]. The reduced relaxation function G(t) and the reduced creep function J(t) can be interrelated by a convolution integral, denoted by $*$ [see Appendix(a)] ;

$$\begin{aligned} t &= G(t) * J(t) \\ &= \int_0^t G(\tau)\, J(t-\tau)\, d\tau \end{aligned} \tag{3.24}$$

Therefore the creep behavior can be analyzed with the stress relaxation data. The relation between the reduced relaxation function and the reduced creep function has been experimentally confirmed by Y. C. Fung [16] for rabbit mesentery.

3.9 Complex Modulus and Dynamic Test

If the material is subject to a cyclic stress of the form,

$$\sigma(t) = \sigma_A \, e^{i\omega t} \,, \tag{3.25}$$

and $\sigma^e(t) = \sigma^e_A \, e^{i\omega t}$,

relating eqs. 3.7 and 3.25,

$$\sigma_A \, e^{i\omega t} = \int_{-\infty}^{t} G(t-\tau) \;\; \sigma^e_A \;\; i\,\omega \;\; e^{i\omega\tau} \, d\tau \tag{3.26}$$

Changing $t - \tau = \theta$, and rearranging,

$$\frac{\sigma_A}{\sigma^e_A} \;=\; i\,\omega \int_0^{\infty} G(\theta)\, e^{-i\omega\theta} \, d\theta$$

$$=\; G^* \,, \tag{3.27}$$

where G^* is the complex modulus , or the dynamic modulus.

Rearranging eq.3.27,

$$G^* = \; i\,\omega \int_0^{\infty} G(\theta) \;\; \{ \;\; \cos(\omega\theta) - i\,\omega \sin(\omega\theta) \;\} \;\; d\theta$$

$$= \int_0^\infty G(\theta)\ \sin(\omega\theta)\ d\theta \ + \ i\,\omega \int_0^\infty G(\theta)\ \cos(\omega\theta)\ d\theta$$

$$= G' + i\,G'' . \tag{3.28}$$

Separating G^* into real and imaginary parts,

$$G'(\omega) = \int_0^\infty G(\theta)\ \sin(\omega\theta)\ d\theta \tag{3.29}$$

and $$G''(\omega) = \int_0^\infty G(\theta)\ \cos(\omega\theta)\ d\theta , \tag{3.30}$$

where $G'(\omega)$ and $G''(\omega)$ are generally referred to as the storage modulus and loss modulus respectively.

Alternatively,

$$G^* = G' + i\,G''$$
$$= G'\,(1 + i \tan\delta) , \tag{3.31}$$

where $\tan\delta = \dfrac{G''(\omega)}{G'(\omega)}$, which is sometimes referred to as internal friction and represents the phase shift between the cyclic stress and corresponding cyclic strain. A typical behavior of the complex modulus for various frequencies is shown in Fig.3.7.

Dynamic tests with sinusoidal cyclic strain can be performed with a fixture that is basically a variable amplitude scotch yoke. It has been observed that the sinusoidal test results were not in good agreement with the theoretical predictions [6,19]. In other words, the reduced relaxation function or the reduced creep function is too simple a mathematical model to explain the viscoelastic behavior of biological tissues.

CHAPTER 4

MUSCLE FORCES OF THE MANDIBLE

4.1 General Behavior of Muscles

Voluntary motion of the mandible is brought about by the contraction of muscles. The tendons are parts of the muscles, included in the description of a muscle as the ultimate attachments; that is, the origin and insertion of the muscle are the terminal attachments of the tendon to a bone.

In some muscles, the muscle fibers, composed of myosin and actin filaments, are parallel to the longitudinal axis and terminate at either end in tendons. In others the muscle fibers may converge from a broad surface to a narrow tendonous point, as is seen in the temporalis muscle, which is called a radiated muscle.

Muscle forces are known to be exerted by the contraction of muscles, which is brought about by the relative motion or sliding of myosin and actin filaments. The process of the muscle contraction involves a flood of calcium into the fluid inside muscle cells. To release muscle forces, these muscles must relax, which results when calcium flows back into storage sacs within muscle cells. While calcium's crucial role in muscle contraction was established more than a century ago, the mechanism that regulates calcium's movement within cells has only been discovered recently, and involves a tunnel shaped protein that acts as a gateway for the calcium. This protein, which can open and close to direct calcium flow, is believed to be a key factor regulating muscle contraction. In detail, the changes in the electrical potential, or the electric charge across the muscle cell membrane, act as a signal that opens the calcium pump protein

tunnels. This allows calcium to come out of storage and flow into the muscle cells, resulting in the contraction of muscles. When it is time for a muscle to relax, the protein pump sucks calcium back into the storage. Defects in these or other proteins are the underlying cause of a variety of muscular diseases.

4.2 Muscle Forces of the Mandible during Bite Motion

4.2.1 Major Muscle Forces of the Mandible

There are several muscle forces causing mandibular movement and equilibrating the external forces of the mandible, such as bite force. These are five major muscle forces exerted by the contraction of the muscles - the masseter, the temporalis, the internal pterygoid, the opener or digastric and the external pterygoid - and the joint reaction force , as shown in Fig.4.1.

Since the micromechanical behavior of the muscles gives no further information to determine the magnitude of muscle forces, macroscopic or structural tests of the mandible are often performed. Most of the tests have been performed for simple cases, such as the symmetric bite motion at rest position, where the system is considered to be free of ligamentous force. The most well-known technique for measuring muscle forces is the electromyography (EMG), which measures the electric potential of the active muscles at a set of two electrodes attached to the gage points on or near each muscle. It is generally known that the integrated electromyogrphy (EMGI) measured at a muscle is possibly, but not necessarily, proportional to the muscle force. To determine the stress at each muscle of the mandible, the physiological cross sectional areas of the muscles should be measured. They are usually measured by a special slot and plunger with dial gage, which is similar to the one used to measure the physiological cross sectional areas of ligaments. The appropriate slot size should be selected by the width

and the thickness of the muscle to be measured. Since in vivo measurements are not available, in vitro measurements are performed. The test specimens can be prepared in the same way as general biological soft tissues illustrated in section 3.3.1.

Physiological cross sectional areas of the mandibular muscles have been measured by several authors and are tabulated in Table 4.1. As seen from the table, the reported areas differ from author to author. However, their ratios are similar in all cases. This is due to the different methods of measuring used. We will take the data of Pruim et. al. [8], because they are the most recent ones, and they cover all the major muscles needed to analyze the mandibular motion.

Since the temporalis is widely radiated, most authors divided it into the posterior and anterior parts to obtain its physiological cross sectional area with accuracy. However, the method of dividing the temporalis into posterior and anterior parts is not clear, so the data vary significantly from one method to the other. But the total area of the temporalis is almost similar, within sufficient accuracy. We will consider the muscle force of the temporalis as the vectorial sum of all the individual muscle fiber forces. The effects of the radiation of the muscle fibers are discussed in the following section.

The maximum allowable stress of a muscle is known to differ from person to person and even from muscle to muscle in a given person; however, we will take the average value to make the analysis simple. Since there is significant difference in physiological cross sectional area of a muscle due to different measuring methods, the maximum allowable stress of a muscle also gives different values, as shown in Table 4.2. There are also siginificant differences among individuals due to individual variations. As we have taken the physiological cross sectional areas measured by Pruim et. al., we will take the average value of the maximum allowable muscle stress measured by them [8].

In Table 4.3, the predicted maximum allowable muscle forces of the mandible and

the experimentally measured data taken from Pruim et. al. were tabulated and were shown to be in fairly good agreement. It should be noted that since the masseter and the internal pterygoid are located very close to each other and run almost parallel, they can hardly be measured separately, and so they were added together.

4.2.2 Effective Area Reduction of the Temporalis Muscle

In each muscle except the temporalis, where the muscle fibers run parallel to each other, the maximum allowable value of each muscle force can be predicted by multiplying the cross sectional area by the maximum allowable muscle stress, as tabulated in Table 4.3. In the table, the measured total of the temporalis force is taken as the vectorial sum of the forces of the anterior and posterior parts as shown in Fig.4.1. However, since the muscle fibers are widely radiated in the temporalis, as seen from Fig.4.2(a), the total force of the temporalis should be corrected as the vectorial sum of all the muscle fiber forces in it. Therefore, from the figure, denoting $\vec{f}_i$, $\vec{F}_t$ and n as the individual muscle fiber force vector, the total resultant muscle force vector, and the total number of muscle fibers in the temporalis respectively, $\vec{F}_t$ will be expressed as

$$\vec{F}_t = \sum_{i=1}^{n} \vec{f}_i \quad , \tag{4.1}$$

where the vector $\vec{F}_t$ is assumed to run from the centroid of the insertion to that of the origin of the temporalis, denoted by points O and P, respectively.

By the rule of vector summation, rewriting eq.4.1 with scalar quantities,

$$F_t = \sum_{i=1}^{n} f_i \cos\theta_i \ , \tag{4.2}$$

where θ_i is the angle between i-th muscle fiber and the total muscle force. Denoting by s_i and σ_i the effective area of the physiological cross section possessed by one fiber and the corresponding stress, respectively, F_t will be

$$F_t = \sum_{i=1}^{n} s_i \sigma_i \cos\theta_i \quad . \tag{4.3}$$

We will assume that all the muscle fibers sustain the same amount of force in any circumstance and that the muscle fibers run with the same area density at any part of the cross section,

i.e., $\sigma_i = \text{constant}$

and $s_i = \frac{A_t}{n} = \text{constant}$, (4.4)

where A_t is the physiological cross sectional area of the temporalis.

Substituting eq.4.4 into eq.4.3,

$$F_t = \sum_{i=1}^{n} \sigma_i \frac{A_t}{n} \cos\theta_i \, . \tag{4.5}$$

Provided the number of muscle fibers n is large enough, eq.4.5 can be approximated in an integration form as follows :

$$F_t = \sigma_i \int_{A_t} \cos\theta \; dA$$

$$= \sigma_i \; (A_t)_{effective} \, , \tag{4.6}$$

where θ denotes the angle between the total muscle force vector and the differential area

dA measured with respect to the centroid of the insertion P.

Introducing the effective area reduction factor, denoted by ξ, and defined as

$$\xi = \frac{(A_t)_{effective}}{A_t}$$

$$= \frac{1}{A_t} \int_{A_t} \cos\theta \; dA \quad , \tag{4.7}$$

eq.4.6 will be rewritten as

$$F(t) = A_t \, \sigma_i \, \frac{1}{A_t} \int_{A_t} \cos\theta \; dA$$

$$= \xi \; A_t \; \sigma_i \; . \tag{4.8}$$

It is evident from the definition that $\xi \leq 1$, where the equal sign stands only for the case where all the muscle fibers run parallel.

To determine the factor ξ for the temporalis, it will be assumed that the origin of the temporalis and the centroid of the insertion of the temporalis, denoted by P, lie on the same plane, which we will call the reference plane of the temporalis. Also it will be assumed that the physiological cross section is located on the plane perpendicular to the reference plane, and that the muscle fibers arise with the same area density from any part of the origin of the temporalis, as shown in Fig.4.2(b). Then it can be approximated that

$$\xi \simeq \frac{(A_{to})_{effective}}{A_{to}} \quad , \tag{4.9}$$

where A_{to} denotes the area of the origin of temporalis and $(A_{to})_{effective}$ is defined by

$$(A_{to})_{effective} = \int_{A_{to}} \cos\theta \; dA \, . \tag{4.10}$$

Thus $$\xi = \frac{1}{A_{to}} \int_{A_{to}} \cos\theta \; dA \, , \tag{4.11}$$

which can be approximated by numerical integration. To perform the numerical integration, the origin was divided into 10 concentric sections of constant width, denoted by h, with the center of the concentric circle at point P. Therefore, we have

$$A_{to} \simeq \sum_{i=1}^{10} A_k$$

$$\simeq \sum_{i=1}^{10} h \; R_k \; (\theta_{k2} - \theta_{k1}) \, , \tag{4.12}$$

where subscript k denotes the serial number of the concentric section, A_k denotes the area of k-th section, R_k denotes the distance of the section measured from point P, and $(\theta_{k2} - \theta_{k1})$ is the angle of k-th section measured with respect to point P.

We also have

$$(A_{to})_{effective} \simeq \sum_{i=1}^{10} \int_{A_k} \cos\theta \; dA$$

$$\simeq \sum_{i=1}^{10} \int_{\theta_{k1}}^{\theta_{k2}} h \; R_k \cos\theta \; d\theta$$

$$= \sum_{i=1}^{10} h \; R_k \int_{\theta_{k1}}^{\theta_{k2}} \cos\theta \; d\theta$$

$$= \sum_{i=1}^{10} h\, R_k \sin(\theta_{k2}-\theta_{k1}) . \tag{4.13}$$

Thus it follows that

$$\xi \simeq \frac{\sum_{i=1}^{10} R_k \sin(\theta_{k2}-\theta_{k1})}{\sum_{i=1}^{10} R_k(\theta_{k2}-\theta_{k1})} . \tag{4.14}$$

By numerical calculations, it was found that

$$\xi \simeq 0.93 .$$

The effective area of the temporalis is given by

$$(A_t)_{effective} \simeq \xi \cdot A_t$$
$$= 3.9\ (cm^2) . \tag{4.15}$$

Thus the maximum allowable force of the temporalis will be

$$F_{t\ max} = (A_t)_{effective} \cdot \Gamma$$
$$= 3.9 \times 120$$
$$= 468.0\ \text{(Newton)}$$

4.2.3 The Directions of Muscle Forces

When the mandible is subjected to external loads, the system will be equilibrated by muscle forces and the joint reaction force. The direction of a muscle force can be determined by connecting its origin and insertion by a straight line. As the muscle forces are exerted only by the contraction of muscles, they always work as outward tensile loads to the mandible. However, since the external pterygoid is attached to the capsular ligament L_{c1}, as shown in Fig.4.1, it works on the mandible through the capsular ligament. Provided the ligament is initially in a relaxed state, the ligament L_{c1} will be stretched by the external pterygoidal force F_e, as shown in Fig.4.3(a). We

will assume that the length of L_{c1} stretched by the muscle force is approximated by L_{c10}, which we define as the free length of the ligament. Also, we will assume that the external pterygoidal muscle is connected to the capsular ligament L_{c1} at its midpoint.

From the geometry shown in Fig.4.3(b), we define T_1 and T_2 as the components of the external pterygoidal force working on the mandible and the cranium through the ligament, respectively. To obtain the effective force component T_1 working on the mandible in terms of the external pterygoidal force F_e, we will assume, in the figure, that the capsular ligament L_{c10} and the external pterygoid can be represented by line elements connected to each other at the midpoint of the ligament, and we denote it $A(x_A, y_B)$. Points $B(x_B,y_B)$ and $C(x_C,y_C)$ denote the insertion and the origin of the capsular ligament, point $E(x_E,y_E)$ denotes the origin of the external pterygoidal muscle, and the angles ζ_1, ζ_2 and ζ_3 denote the directions of the the force vectors T_1, T_2 and F_e with respect to positive x axis. Then point $A(x_A,y_A)$ can be expressed in terms of the known values $B(x_B,y_B)$, $C(x_C,y_C)$ and L_{c10} as follows,

$$x_A = \tfrac{1}{2}(x_B + x_C) + \tfrac{1}{2}(y_C - y_B)\left\{ \frac{L_{c10}^2}{(x_B - x_C)^2 + (y_B - y_C)^2} - 1 \right\}^{1/2}$$

$$y_A = \tfrac{1}{2}(y_B + y_C) + \tfrac{1}{2}(x_B - x_C)\left\{ \frac{L_{c10}^2}{(x_B - x_C)^2 + (y_B - y_C)^2} - 1 \right\}^{1/2} \qquad (4.16)$$

and the reference angles will be expressed as

$$\zeta_1 = \mathrm{Tan}^{-1}\left(\frac{y_A - y_B}{x_A - x_B}\right),$$

$$\zeta_2 = \mathrm{Tan}^{-1}\left(\frac{y_C - y_A}{x_C - x_A}\right), \qquad (4.17)$$

$$\zeta_e = \mathrm{Tan}^{-1}\left(\frac{y_E - y_A}{x_E - x_A} \right) .$$

Then the effective force of the external pterygoid working on the mandible T_1 will be determined from force equilibrium at point A as

$$T_1 = F_e \frac{\sin(\zeta_2 - \zeta_e)}{\sin(\zeta_2 - \zeta_1)}$$

$$= F_e \eta_e , \qquad (4.18)$$

where we define η_e, the efficiency of the external pterygoidal force, as

$$\eta_e = \frac{T_1}{F_e}$$

$$= \frac{\sin(\zeta_2 - \zeta_e)}{\sin(\zeta_2 - \zeta_1)} \qquad (4.19)$$

4.2.4 System of Equilibrium Equations during Bite Motion

For direct comparison of the theoretically predicted and experimentally measured muscle forces, we analyze the symmetric bite motion at the jaw opening angle 4°, at which the muscle forces have been experimentally measured by Pruim et.al.. As the mandible is near the rest position, it will be assumed that no ligamentous force work on the mandible.

From Fig.4.1, the system of equilibrium equations of the forces working on the mandible will be;

$$\sum F_x = F_{mx} + F_{tx} + F_{ix} + \eta_e F_{ex} + F_{ox} + R \cos\phi + L_x = 0 ,$$

$$\sum F_y = F_{my} + F_{ty} + F_{iy} + \eta_e F_{ey} + F_{oy} + R \sin \phi + L_y = 0 , \qquad (4.20)$$

$$\sum M_z = M_{mz} + M_{tz} + M_{iz} + \eta_e M_{ez} + M_{oz} + M_{L_z} = 0 ,$$

where the subscripts x, y, z denote the components of the vectors about the corresponding coordinate axes, F_m, F_t, F_i, F_e, F_o denote the muscle forces of the masseter, temporalis, internal pterygoid, external pterygoid and opener respectively, M_z denotes the moment about the center of condyle, R and ϕ denote the joint reaction force and its direction angle measured with respect to positive x axis respectively, L and M_L denote the external force or bite force and its moment about the center of condyle and η_e is the efficiency of the external pterygoidal force. As the joint reaction force works through the center of condyle, it always has zero moment.

Since we know the direction of all the muscle force vectors, their magnitudes are the unknowns to be determined from the system of equations. The system has three equations for seven unknowns - five magnitudes of muscle forces, R and ϕ ; it is a statically indeterminate system. To solve the statically indeterminate system of equations, we must introduce additional conditions, or an appropriate optimizing condition for the system. Out of several optimizing conditions proposed by many authors, the hypothesis of minimum muscle forces, which states, "the optimum equilibrium condition of the mandible subjected to the external loads is the one which the scalar sum of all the muscle forces is minimized," is one of the assumptions that is of interest to many people (see, for example, MacConail). However, computed results based on this hypothesis reveal that it is not an appropriate assumption for this system. The analysis based on this hypothesis predicts that the only muscle acting during the

beginning stage of bite motion would be the masseter, while the experimental observations indicate that at least two of the muscles, the masseter and the temporalis, are definitely active. A similar conclusion was found by J. C. Barbenel [10].

As an alternative trial, instead of the scalar sum of muscle forces, the scalar sum of muscle stresses has been minimized. But the result shows no significant difference with that of the hypothesis of minimum muscle forces, except that the magnitude of the muscle forces are a little different. There are some other hypotheses similar to this in the literature [24]. These include, for example, minimizing the sum of the cubes of each muscle force or each muscle stress. Though the results have demonstrated empirically improved muscle activity, they have fallen short of their physical interpretations.

4.2.5 Hypothesis of Minimum Muscle Stress

Here the hypothesis of minimum muscle stress, proposed by An et. al. [26], will be utilized to analyze the system. This states , "the optimum equilibrium condition of the mandible subjected to external loads is one in which the largest of all the muscle stress is minimized." Originally, it was proposed by the authors to analyze the flection of the human elbow and the results have been demonstrated to be well suited for two-dimensional as well as three-dimensional analyses. The same technique will be utilized for the mechanics of TMJ. This is based on the assumptions that the muscle fibers are distributed with an equal area density at any part of any muscle, that the physical properties of the muscle fibers are all the same for any muscle, and that the force exerted by a muscle is equally distributed among the muscle fibers in it. With this hypothesis, the force of an individual muscle fiber can then be represented by the muscle stress multiplied by the area possessed by the individual fiber. The hypothesis of minimum muscle stress can be interpreted as "the optimum condition is one in which

the force in a muscle fiber is kept its lowest value available [26]."

With this hypothesis, by utilizing a simplex technique [for the computational basis of the simplex technique, see Appendix(b)], which is one of the most common linear optimization methods, we suggest an optimizing procedure to solve the system of equations as follows.

(1) We give an appropriate value of external or bite force and corresponding moment in the system of equilibrium equations.

(2) Assuming that one muscle stress is the largest of all the muscle stresses, suppress it to the minimum.

(3) ϕ being taken as a parametric variable, for every value of ϕ, utilizing the simplex method, the muscle stresses will be obtained from the system of equilibrium equations for the condition given in procedure (2).

(4) By comparing the solution sets of stresses at each angle ϕ, one candidate of the optimum angle ϕ, at which the largest of the muscle stresses has minimum value, can be selected. The corresponding set of muscle stresses also is a candidate of the optimum solution set.

(5) Assuming one of the other muscle stresses is the largest, and repeating the procedure 1 to 3 , another candidate of ϕ_{opt} and a corresponding set of muscle stresses can be obtained.

(6) By sweeping through all five muscle stresses in the same procedure, five candidates for ϕ_{opt} and corresponding sets of muscle stresses can be obtained.

(7) By comparing five sets of muscle stresses, we can choose one set of optimum muscle stresses, the largest of which has its available minimum value, and the corresponding optimum angle ϕ_{opt} can be determined.

(8) By increasing the external load gradually and following the same

procedure, one can get a sequence of optimum solution sets for the increasing external load.

(9) When one of the muscle stresses reaches its maximum allowable value, the force of that muscle will be kept constant afterwards, and by following a similar procedure, sets of muscle stresses will be obtained, where one of them is kept constant at its maximum allowable state.

(10) When one or another muscle stresses reaches its maximum allowable value, it also will be kept constant afterwards, and the rest of the routine is similar to above.

(11) Finally, when it reaches the point that all the working muscle stresses reach their maximum, no further increase of the external load gives any appropriate answer to the system, and the corresponding external load is supposed to be the maximum allowable load the system can sustain.

The muscle forces for the symmetric bite motion were predicted theoretically through this procedure and plotted on Figs.4.4 and 4.5 for bite forces applied on the first and second molars, respectively, together with the experimentally measured data to compare them. The experimental data were taken from those measured by Pruim et.al., where the forces of the masseter and the internal pterygoid are added together because practically they cannot be measured separately, due to their close locations.

The predicted results of F_t and $(F_m + F_i)$ match fairly well with the experimental data measured by Pruim et. al., but the results of F_o and F_e do not appear satisfactory. Observing the experimental apparatus, muscle forces are measured by the electromyography [EMG], which measures the electric potentials between the electrodes attached on the skin close to each muscle [25]. Therefore, we can conclude that the measured data of the temporalis (F_t) and the masseter (F_m) are reliable, because their

magnitudes are large enough to be measured accurately, and also they run right beneath the skin. However, the internal pterygoid (F_i), the opener (F_o) and the external pterygoid (F_e) run further below the skin, and their magnitudes are small when compared with those of the former. As long as surface electrodes are used, there is no practical way of avoiding the interferences caused by other soft tissues near them, and accurate measuring is practically impossible. Thus, we can also conclude that the measured data of the latter are somewhat unreliable. Furthermore, it is generally accepted that there exists at least one muscle that is free of force at any state, which is reserved for the equilibration of the system with opposite directional external force. It is called the antagonist. Since a muscle can exert force in one direction only, this claim seems quite acceptable. In the theoretically predicted results, the opener was seen to play the role of the antagonist, but the measured results cannot support that claim.

Since surface electrodes do not give reliable EMG data, needle electrodes which use hypodermic needles to introduce fine wires into the belly of the muscles are widely used to improve the reliability. The bipolar hook type of electrode is the basic design for needle electrodes. This technique is very useful especially in the study of deeper muscles. For the muscles whose fibers run parallel, the electrodes should be placed midway between both the origin and insertion and the anterior and posterior borders of the muscles. On the other hand, the temporalis being a radiating muscle, three or more sets of needle electrodes are used to obtain the local variation of the muscle force. However, percutaneous insertion of needle electrodes always requires particular care for proper location of the electrodes and the likelihood of success depends on the skill of the operator.

CHAPTER 5

ANALYSIS OF NORMAL OPENING OF THE MANDIBLE

5.1 Introduction

In the previous chapter, an optimization procedure was proposed to determine the muscle forces working for the static bite motion of the mandible. It was assumed that the ligaments were free of stress for small opening angles. In this chapter, the procedure will be extended to analyze the opening motion of the mandible. The mandibular motion is brought about by the forces applied to the mandible exerted by the contraction of the muscles. Also the joint reaction forces will be exerted at the condyles of the mandible on both sides. The ligaments of the TMJ will give constraint to the motion of mandible.

Observing the motion of the mandible, its major portion is the normal opening or closing, which is symmetric, planar motion in the x-y plane. The three dimensional motion is composed of a relatively small amount of symmetric or nonsymmetric motions superposed on the normal opening or closing of the mandible. Here the analysis will emphasize the normal motion, and the optimized muscle forces and the joint reaction force along with the ligamentous forces will be determined. The analysis will be extended to include symmetric translation of the mandible to its allowable limits.

5.2 Elastic Properties of the Ligaments of the TMJ

We start with the ligamentous forces, which can be determined from the geometry and the constitutive relations of ligaments. The ligamentous forces can be expressed as

$$F_j = a_j \sigma_j \quad , \tag{5.1}$$

where F_j , a_j and σ_j denote the force, the physiological cross sectional area and the stress of a ligament, respectively. The physiological cross sectional areas of the ligaments can be approximated from the related figures in "Gray's Anatomy," [1] which shows various plane views of the ligaments.

The stresses of ligaments can be related with the ligamentous strains by the constitutive relations. The elastic behavior of ligaments has been determined by experimental observations performed by many authors, for various kinds of ligaments. For example, Waters and Morris [5] measured the elastic and viscoelastic behaviors of human spinal ligaments, S. L-Y. Woo et. al. [6] measured the elastic and viscoelastic behavior of canine medial collateral ligaments, and D. L. Butler et. al. [7] measured the elastic behavior of human knee joint ligaments. The test results show a wide variety of tensile properties of ligaments taken from different parts of the animal or the human body.

Since the elastic properties of human TMJ have not been reported yet, we take the elastic properties of human knee ligaments measured by D. L. Butler et. al. since they are closest to the widely known general properties of ligaments. The measured data, when fitted into the empirical relations given in eq.3.17 and shown in Fig.5.1, give us the values of the elastic coefficients. Eq.3.17, with the constants empirically determined, becomes

$$\sigma^e(\epsilon) = A\,(e^{B\epsilon} - 1) \qquad \text{for} \quad 0 \le \epsilon \le \epsilon_r$$

$$\text{and} \quad \sigma^e(\epsilon) = E\,(\epsilon - \epsilon_r) + \sigma_r \qquad \text{for} \quad \epsilon > \epsilon_r \,, \tag{5.2}$$

where $A \simeq 996.6 \quad psi$,

$$
\begin{aligned}
&B \simeq 19.8 \ , \\
&\epsilon_r \simeq 0.05 \ , \\
&\sigma_r \simeq 1687 \ \ psi \ , \\
&E \simeq 53100 \ \ psi \ , \\
&\epsilon_{max.allow.} \simeq 0.122 \ , \\
\text{and} \quad &\sigma_{max.allow.} \simeq 5500 \ \ psi \ .
\end{aligned}
\tag{5.3}
$$

At the state of maximum allowable strain or corresponding stress, it has been observed that failure of individual collagen fibers of the ligament initiates, and the stress drops drastically until structural failure occurs. This phenomenon is comparable to the necking of a classical structural material.

As is noted in section 2.3, the maximum ligamentous strain during normal opening of the mandible is assumed to be the maximum allowable strain, so that the strain of each ligament at any opening angle can be determined by inverse calculation. For example, from Fig.2.3, the maximum length of the sphenomandibular ligament is 1.48 inches at 21° opening angle, which will be assumed to be at the state of maximum allowable strain. Thus, the free length of the ligament is determined as 1.32 inches, which is the length at about 8° opening angle. The ligament is supposed to be slack and at the relaxed state when the opening angle is less than 8°. From the constitutive relation of ligaments given in eq.5.2, the ligamentous stresses during normal opening or translation of the mandible can be determined.

5.3 Combined Forces of Muscles and Ligaments — Normal Opening of the Mandible

To analyze the motion of the mandible, it will be modeled as a body supported by springs. The ligaments of the TMJ, acting like tension springs, will give constraint to

the motion of mandible, and the muscle forces and the joint reaction forces will act as the external forces on the system. The cranium and the mandible will be considered as a fixed boundary and moving rigid body, respectively. For simplicity, neglecting the inertia and gravity effects, from Figs.1.1 and 4.1, the equilibrium equations for planar motion of the system will be

$$\sum F_x = \sum_{j=1}^{5} (F_j)_x + \sum_{M=1}^{5} (F_M)_x + R_x = 0$$

$$\sum F_y = \sum_{j=1}^{5} (F_j)_y + \sum_{M=1}^{5} (F_M)_y + R_y = 0 \qquad (5.4)$$

$$\sum M_z = \sum_{j=1}^{5} h_j F_j + \sum_{M=1}^{5} h_M F_M = 0$$

where F and M denote the resultant force and the moment about the center of the condyle, respectively, the subscripts x, y and z denote the vectorial components along the corresponding coordinate axes. The variables F_j , F_M and R denote a ligamentous force, a muscle force and the joint reaction force, respectively.

Comparing the equilibrium equations of normal opening, eq.5.3, to those of bite motion, eq.4.20, the bite force does not appear in these equations. Instead, the ligamentous forces due to the stretch of ligaments appear. However, the system is basically the same as the equilibrium of the bite motion.

Since the only unknowns in eq.5.4 are the magnitudes of muscle forces, the hypothesis of minimum muscle stress will be used again and the optimization procedure given in section 4.5 will be modified to apply to the system of equations. The only modification of the procedure will be replacing the bite force by the ligamentous forces, which can be determined for any discrete opening angle. The rest of the procedure is

the same as in section 4.2.5.

Computed results are plotted in Fig.5.2, where it is shown that there exist negligibly small muscle forces for the opening angle less than 14°. Also it is worthwhile to note that the opener muscle works for normal opening, which was considered to be reserved as an antagonist in bite motion.

5.4 Analysis of Translation of the Mandible

When the mandible is pulled to a certain limit point, the required external force and moment can be easily determined by a similar procedure. In doing this, to eliminate the redundancy, it is assumed that there exists no muscle force or joint reaction force working on the system. Therefore, the procedure is an analysis of the equilibrium of the structure exerted by the ligamentous forces, and the external force given by the jaw fixing device will be determined. The resultant device force equilibrating the ligamentous forces will be easily determined by the static equilibrium of the system. As an example, for the case of 9° normal opening followed by the translation in the -60° direction with respect to the x-axis, the locations of the mandible were plotted in Fig.5.3.3 and corresponding ligamentous strains were determined. From the ligamentous strains obtained, corresponding ligamentous stresses, ligamentous forces, the resultant force and moment about the center of the condyle can be determined utilizing eqs. 5.1, 5.2 and 5.4. Four available limits of the mandibular translation after normal opening are selected, and the resultant force and moment required on the device are tabulated on Table 5.1. Also, the corresponding paths of the mandible during normal opening and translation are shown in Figs. 5.3.1 - 5.3.4.

Through this analysis, we can obtain insight into the behavior of the TMJ that provides significant guidance to the design of a suitable traction device that will open

the joint during arthroscopic surgery performed to treat the failure of the articular capsule. The purpose of the traction device is to hold the mandible securely during the surgery while giving maximum allowance for surgical tools to protrude into the articular capsule, which is drawn schematically in Fig.5.4.

5.5 Theoretical Prediction of the Normal Opening of the Mandible

The motion of the mandible during normal opening and closing is given by the contraction of the muscles, and is constrained by the ligaments. The locus of the ICR of the mandibular motion has been determined by experimental observations.

In this section, a method of predicting the locus of ICR will be proposed. The basis of the analysis is that the mandibular movement and its ICR will be such that they minimize the increment of total potential energy of the mandible. For the mandible at a certain location, the strains, stresses and forces of the ligaments and the muscle forces have been determined. A rigid body motion of the mandible can be generated by the superposition of the translation and the rotation of the mandible about any point on the mandible.

From Fig.5.5, denoting $P_0(x_0,y_0)$ and $P_2(x_2,y_2)$ as the center of the condyle and a point on the mandible, respectively, u, v and $\Delta\theta$ as the x and y directional components of translation of P_0 and the clockwise incremental rotation angle, respectively, the location of P_2 after incremental movement will be ;

$$\begin{bmatrix} x_2' - (x_0 + u) \\ y_2' - (y_0 + v) \end{bmatrix} = \begin{bmatrix} \cos \Delta\theta & \sin \Delta\theta \\ - \sin \Delta\theta & \cos \Delta\theta \end{bmatrix} \begin{bmatrix} x_2 + u - (x_0 + u) \\ y_2 + v - (y_0 + v) \end{bmatrix} \qquad (5.5)$$

where x_2' and y_2' are the coordinates of P_2 after the incremental movement of the mandible.

For small angle $\Delta\theta$,

$$\begin{bmatrix} x_2' \\ y_2' \end{bmatrix} \simeq \begin{bmatrix} 1 & \Delta\theta \\ -\Delta\theta & 1 \end{bmatrix} \begin{bmatrix} x_2 - x_0 \\ y_2 - y_0 \end{bmatrix} + \begin{bmatrix} x_0 - u \\ y_0 - v \end{bmatrix}$$

$$= \begin{bmatrix} x_2 + u + \Delta\theta\,(y_2 - y_0) \\ y_2 + v - \Delta\theta\,(x_2 - x_0) \end{bmatrix} . \qquad (5.6)$$

Denoting $x_2' - x_2 = \delta_x$ and $y_2' - y_2 = \delta_y$,

$$\delta_x = u + \Delta\theta\,(y_2 - y_0)$$

$$\text{and} \quad \delta_y = v - \Delta\theta\,(x_2 - x_0), \qquad (5.7)$$

where δ_x and δ_y are x and y directional displacement components of P_2 respectively.

Now we denote $P_1(x_1,y_1)$ as the origin of a ligament on the cranium and denote $P_2(x_2,y_2)$ and $P_2'(x_2',y_2')$ as the insertion of the ligament before and after the incremental movement, respectively. Then the ligamentous lengths before and after the movement will be

$$L = \overline{P_1P_2}$$

$$= \{ (x_2-x_1)^2 + (y_2-y_1)^2 \}^{1/2} \qquad (5.8)$$

$$\text{and} \quad L' = \overline{P_1P_2'}$$

$$= \{ (x_2'-x_1)^2 + (y_2'-y_1)^2 \}^{1/2}$$

$$= \{ (x_2-x_1+\delta_x)^2 + (y_2-y_1+\delta_y)^2 \}^{1/2}, \qquad (5.9)$$

where L and L' denote the ligamentous lengths before and after the movement respectively. The corresponding ligamentous strains will be

$$\epsilon_1 = \frac{L}{L_0} - 1$$

(5.10)

$$\text{and} \quad \epsilon_2 = \frac{L'}{L_0} - 1,$$

where L_0 is the free length of the ligament.

Denoting the variables of the j-th ligament with subscript j, the strain energy of the j-th ligament, denoted by U_j, will be

$$U_j = a_j L_{j0} \int_0^{\epsilon_{j2}} \sigma_j \, d\epsilon_j , \tag{5.11}$$

where a_j and L_{j0} are the physiological cross sectional area and the free length of the j-th ligament, respectively.

Using the same notations for the origin and insertion of a muscle, the work done by the muscle will be

$$W_m = (\vec{F_m} + \Delta \vec{F}_m) \cdot \vec{P_2P_2}' , \tag{5.12}$$

where F_m is the muscle force before the incremental movement, ΔF_m is the average incremental muscle force during the incremental movement of the mandible and $\cdot$ denotes the inner product of two vectors. This can be written as the scalar equation,

$$W_m = (F_m + \Delta F_m) \ \overline{P_2P_2'} \cos \alpha , \tag{5.13}$$

where α is the angle between muscle direction and displacement direction of the insertion of the muscle.

By definition of the inner product of two vectors,

$$\vec{P_2P_1} \cdot \vec{P_2P_2}' = L \ \overline{P_2P_2'} \cos \alpha .$$

$$\text{Thus } W_m = \frac{F_m + \Delta F_m}{L} \ \vec{P_2P_1} \cdot \vec{P_2P_2}' . \tag{5.14}$$

$$\text{Since } \quad \vec{P_2P_1} \cdot \vec{P_2P_2}' = \{x_1\text{-}x_2 \ \ y_1\text{-}y_2\} \begin{Bmatrix} \delta_x \\ \delta_y \end{Bmatrix}$$

$$= (x_1\text{-}x_2) \ \delta_x + (y_1\text{-}y_2) \ \delta_y, \tag{5.15}$$

from eq.5.14,

$$W_m = \frac{F_m + \Delta F_m}{L} \{ (x_1-x_2)\delta_x + (y_1-y_2)\delta_y \} . \quad (5.16)$$

Similarly, the work done by the joint reaction force is

$$\begin{aligned} W_R &= (\vec{R} + \Delta\vec{R}) \cdot \vec{P_0P_0'} \\ &= (R + \Delta R) \{ \cos\phi \quad \sin\phi \} \begin{Bmatrix} u \\ v \end{Bmatrix} \\ &= (R + \Delta R) (u \cos\phi + v \sin\phi) . \end{aligned} \quad (5.17)$$

Neglecting the inertia and gravity effects, the total potential energy, denoted by Π, is defined as

$$\Pi = \sum_j U_j - \sum_m W_m - W_R , \quad (5.18)$$

where subscripts j, m and R denote a ligament, a muscle and the joint reaction force, respectively.

The condition of minimizing the total potential energy will be

$$\frac{\partial \Pi}{\partial u} = 0 ,$$

$$\frac{\partial \Pi}{\partial v} = 0 , \quad (5.19)$$

and $$\frac{\partial \Pi}{\partial(\Delta\theta)} = 0 .$$

Arranging them term by term,

$$\sum_j \frac{\partial U_j}{\partial u} = \sum_m \frac{\partial W_m}{\partial u} + \frac{\partial W_R}{\partial u}$$

$$\sum_j \frac{\partial U_j}{\partial v} = \sum_m \frac{\partial W_m}{\partial v} + \frac{\partial W_R}{\partial v} \quad (5.20)$$

$$\sum_j \frac{\partial U_j}{\partial(\Delta\theta)} = \sum_m \frac{\partial W_m}{\partial(\Delta\theta)} + \frac{\partial W_R}{\partial(\Delta\theta)} \quad .$$

From eq.5.11,

$$\frac{\partial U_j}{\partial u} = \frac{\partial U_j}{\partial \epsilon} \frac{\partial \epsilon}{\partial u} \quad , \tag{5.21}$$

and $$\frac{\partial U_j}{\partial \epsilon} = a_j \; L_{j0} \; \sigma_{j2} \quad , \tag{5.22}$$

where σ_{j2} is the stress corresponds to the strain of the j-th ligament after incremental movement.

From eqs. 5.7, 5.9 and 5.10,

$$\left[\frac{\partial \epsilon}{\partial u} \right]_{\epsilon_2} = \frac{\partial \epsilon}{\partial \delta_x} \frac{\partial \delta_x}{\partial u}$$

$$= \frac{x_2 - x_1 + \delta_x}{L_0 L'} \quad . \tag{5.23}$$

From eqs. 5.21, 5.22 and 5.23, using subscript j for all the j-th ligamentous variables,

$$\frac{\partial U_j}{\partial u} = a_j \; \sigma_{j2} \; \frac{x_{j2} - x_{j1} + \delta_{jx}}{L_j'} \quad . \tag{5.24}$$

In the same way,

$$\frac{\partial U_j}{\partial v} = a_j \; \sigma_{j2} \; \frac{y_{j2} - y_{j1} + \delta_{jy}}{L_j'} \quad , \tag{5.25}$$

and $$\frac{\partial U_j}{\partial(\Delta\theta)} = \frac{a_j\,\sigma_{j2}}{L_j'}\left\{ (x_{j2}-x_{j1})(y_{j2}-y_0) + \delta_{jx}(y_{j2}-y_0) \right.$$

$$\left. -(y_{j2}-y_{j1})(x_{j2}-x_0) - \delta_{jy}(x_{j2}-x_0) \right\}. \qquad (5.26)$$

From eqs. 5.16 and 5.17, in the similar manner, using subscript m for the m-th muscle,

$$\frac{\partial W_m}{\partial u} = \frac{F_m + \Delta F_m}{L_m}(x_{m1}-x_{m2}) , \qquad (5.27)$$

$$\frac{\partial W_m}{\partial v} = \frac{F_m + \Delta F_m}{L_m}(y_{m1}-y_{m2}) , \qquad (5.28)$$

$$\frac{\partial W_m}{\partial(\Delta\theta)} = \frac{F_m + \Delta F_m}{L_m}\left\{ (x_{m1}-x_{m2})(y_{m2}-y_0) - (y_{m1}-y_{m2})(x_{m2}-x_0) \right\} \qquad (5.29)$$

and $$\frac{\partial W_R}{\partial u} = (R + \Delta R)\cos\phi , \qquad (5.30)$$

$$\frac{\partial W_R}{\partial v} = (R + \Delta R)\sin\phi , \qquad (5.31)$$

$$\frac{\partial W_R}{\partial(\Delta\theta)} = 0 . \qquad (5.32)$$

Substituting eqs. 5.24 - 5.32 into eq.5.20,

$$\sum_j a_j\,\sigma_{j2}\,\frac{x_{j2}-x_{j1}+\delta_{jx}}{L_j'} = \sum_m \frac{F_m + \Delta F_m}{L_m}(x_{m1}-x_{m2}) + (R + \Delta R)\cos\phi$$

$$\sum_j a_j\,\sigma_{j2}\,\frac{y_{j2}-y_{j1}+\delta_{jy}}{L_j'} = \sum_m \frac{F_m + \Delta F_m}{L_m}(y_{m1}-y_{m2}) + (R + \Delta R)\sin\phi \qquad (5.33)$$

$$\sum_j \frac{a_j\,\sigma_{j2}}{L_j'}\Big\{(x_{j2}-x_{j1})(y_{j2}-y_0)+\delta_{jx}(y_{j2}-y_0)-(y_{j2}-y_{j1})(x_{j2}-x_0)$$

$$-\delta_{jy}(x_{j2}-x_0)\Big\} = \sum_m \frac{F_m+\Delta F_m}{L_m}\Big\{(x_{m1}-x_{m2})(y_{m2}-y_0)-(y_{m1}-y_{m2})(x_{m2}-x_0)\Big\}$$

To linearize eqs.5.33, we take the Taylor expansion of the reciprocal of L_j with respect to δ_{jx} and δ_{jy},

$$\frac{1}{L_j'} \simeq \frac{1}{L_j} - \frac{x_{j2}-x_{j1}}{L_j^3}\delta_{jx} - \frac{y_{j2}-y_{j1}}{L_j^3}\delta_{jy} + \cdots\cdots . \qquad (5.34)$$

Substituting eqs. 5.7 and 5.34 into eqs. 5.33 and arranging them into matrix form,

$$\begin{bmatrix} A_{1,1} & A_{1,2} & A_{1,3} \\ A_{2,1} & A_{2,2} & A_{2,3} \\ A_{3,1} & A_{3,2} & A_{3,3} \end{bmatrix} \begin{bmatrix} u \\ v \\ \Delta\theta \end{bmatrix} = \begin{bmatrix} B_1 \\ B_2 \\ B_3 \end{bmatrix} \qquad (5.35)$$

where $A_{1,1} = \sum_j a_j\,\sigma_{j2}\,\frac{(y_{j2}-y_{j1})^2}{L_j^3}$

$$A_{1,2} = -\sum_j a_j\,\sigma_{j2}\,\frac{(x_{j2}-x_{j1})(y_{j2}-y_{j1})}{L_j^3}$$

$$A_{1,3} = \sum_j a_j\,\sigma_{j2}\,\frac{(y_{j2}-y_{j1})\Big\{(y_{j2}-y_{j1})(y_{j2}-y_0)+(x_{j2}-x_{j1})(x_{j2}-x_0)\Big\}}{L_j^3}$$

$$A_{2,1} = -\sum_j a_j\,\sigma_{j2}\,\frac{(x_{j2}-x_{j1})(y_{j2}-y_{j1})}{L_j^3}$$

$$= A_{1,2}$$

$$A_{2,2} = \sum_j a_j\,\sigma_{j2}\,\frac{(x_{j2}-x_{j1})^2}{L_j^3} \qquad (5.36)$$

$$A_{2,3} = - \sum_j a_j \sigma_{j2} \frac{(x_{j2} - x_{j1}) \left\{(y_{j2} - y_{j1})(y_{j2} - y_0) + (x_{j2} - x_{j1})(x_{j2} - x_0)\right\}}{L_j^3}$$

$$A_{3,1} = \sum_j a_j \sigma_{j2} \frac{(y_{j2} - y_{j1}) \left\{(y_{j2} - y_{j1})(y_{j2} - y_0) + (x_{j2} - x_{j1})(x_{j2} - x_0)\right\}}{L_j^3}$$

$$= A_{1,3}$$

$$A_{3,2} = - \sum_j a_j \sigma_{j2} \frac{(x_{j2} - x_{j1}) \left\{(y_{j2} - y_{j1})(y_{j2} - y_0) + (x_{j2} - x_{j1})(x_{j2} - x_0)\right\}}{L_j^3}$$

$$= A_{2,3}$$

$$A_{3,3} = \sum_j a_j \sigma_{j2} \frac{\left\{(x_{j2} - x_{j1})(x_{j2} - x_0) - (y_{j2} - y_{j1})(y_{j2} - y_0)\right\}^2}{L_j^3} \quad ,$$

and $$B_1 = - \sum_m \frac{F_m + \Delta F_m}{L_m} (x_{m2} - x_{m1}) + (R + \Delta R) \cos \phi - \sum_j a_j \sigma_{j2} \frac{x_{j2} - x_{j1}}{L_j}$$

$$B_2 = - \sum_m \frac{F_m + \Delta F_m}{L_m} (y_{m1} - y_{m2}) + (R + \Delta R) \sin \phi - \sum_j a_j \sigma_{j2} \frac{y_{j2} - y_{j1}}{L_j} \qquad (5.37)$$

$$B_3 = - \sum_m \frac{F_m + \Delta F_m}{L_m} \left\{(x_{m2} - x_{m1})(x_{m2} - x_0) - (y_{m2} - y_{m1})(y_{m2} - y_0)\right\}$$

$$- \sum_j a_j \sigma_{j2} \frac{(x_{j2} - x_{j1})(y_{j2} - y_0) - (y_{j2} - y_{j1})(x_{j2} - x_0)}{L_j}$$

Here the ligamentous stress σ_{j2} will be approximated as:

$$\sigma_{j2} = \sigma (\epsilon_{j2})$$

$$= \sigma (\epsilon_{j1} + \Delta \epsilon_j)$$

$$\simeq \sigma(\epsilon_{j1}) + \left[\frac{d\sigma}{d\epsilon}\right]_{\epsilon_{j1}} \Delta\epsilon_j \quad . \tag{5.38}$$

Also from eqs. 5.9 and 5.10, the incremental strain $\Delta\epsilon_j$ is,

$$\Delta\epsilon_j = \epsilon_{j2} - \epsilon_{j1}$$

$$\simeq \frac{1}{L_j L_{j0}} \{ (x_{j2} - x_{j1}) \delta_{jx} + (y_{j2} - y_{j1}) \delta_{jy} \} \quad . \tag{5.39}$$

Therefore,

$$\sigma_{j2} \simeq \sigma_{j1} + \sigma_{j1}' \frac{1}{L_j L_{j0}} \{ (x_{j2} - x_{j1}) \delta_{jx} + (y_{j2} - y_{j1}) \delta_{jy} \} \quad , \tag{5.40}$$

where $\sigma_{j1} = \sigma(\epsilon_{j1})$ and $\sigma_{j1}' = \left[\frac{d\sigma}{d\epsilon}\right]_{\epsilon_{j1}}$.

Substituting eq.5.40 into eqs. 5.35, 5.36 and 5.37 and rearranging,

$$\begin{bmatrix} A_{1,1} & A_{1,2} & A_{1,3} \\ A_{2,1} & A_{2,2} & A_{2,3} \\ A_{3,1} & A_{3,2} & A_{3,3} \end{bmatrix} \begin{bmatrix} u \\ v \\ \Delta\theta \end{bmatrix} = \begin{bmatrix} B_1 \\ B_2 \\ B_3 \end{bmatrix} \tag{5.41}$$

where $A_{1,1} = \sum_j a_j \left\{ \frac{(y_{j2} - y_{j1})^2}{L_j^3} \sigma_{j1} + \frac{(x_{j2} - x_{j1})^2}{L_j^2 L_{j0}} \sigma_{j1}' \right\}$

$$A_{1,2} = -\sum_j a_j \left\{ \frac{\sigma_{j1}}{L_j^3} + \frac{\sigma_{j1}'}{L_j^2 L_{j0}} \right\} (x_{j2} - x_{j1}) (y_{j2} - y_{j1})$$

$$A_{1,3} = \sum_j a_j \left\{ \frac{Q_2}{L_j^3} (y_{j2} - y_{j1}) \sigma_{j1} + \frac{Q_3}{L_j^2 L_{j0}} (x_{j2} - x_{j1}) \sigma_{j1}' \right\}$$

$$A_{2,1} = -\sum_j a_j \left\{ \frac{\sigma_{j1}}{L_j^3} - \frac{\sigma_{j1}'}{L_j^2 L_{j0}} \right\} (x_{j2} - x_{j1})(y_{j2} - y_{j1})$$

$$= A_{1,2}$$

$$A_{2,2} = \sum_j a_j \left\{ \frac{(x_{j2} - x_{j1})^2}{L_j^3} \sigma_{j1} + \frac{(y_{j2} - y_{j1})^2}{L_j^2 L_{j0}} \sigma_{j1}' \right\} \tag{5.42}$$

$$A_{2,3} = -\sum_j a_j \left\{ \frac{Q_2}{L_j^3} (x_{j2} - x_{j1}) \sigma_{j1} - \frac{Q_3}{L_j^2 L_{j0}} (y_{j2} - y_{j1}) \sigma_{j1}' \right\}$$

$$A_{3,1} = \sum_j a_j \left\{ \frac{Q_2}{L_j^3} (y_{j2} - y_{j1}) \sigma_{j1} + \frac{Q_3}{L_j^2 L_{j0}} (x_{j2} - x_{j1}) \sigma_{j1}' \right\}$$

$$= A_{1,3}$$

$$A_{3,2} = -\sum_j a_j \left\{ \frac{Q_2}{L_j^3} (x_{j2} - x_{j1}) \sigma_{j1} - \frac{Q_3}{L_j^2 L_{j0}} (y_{j2} - y_{j1}) \sigma_{j1}' \right\}$$

$$= A_{2,3}$$

$$A_{3,3} = -\sum_j a_j \left\{ \frac{Q_1 Q_2}{L_j^3} \sigma_{j1} - \frac{Q_3 Q_4}{L_j^2 L_{j0}} \sigma_{j1}' \right\}$$

and $$B_1 = -\sum_m \frac{F_m + \Delta F_m}{L_m} (x_{m2} - x_{m1}) + (R + \Delta R) \cos\phi - \sum_j a_j \sigma_{j1} \frac{x_{j2} - x_{j1}}{L_j}$$

$$B_2 = -\sum_m \frac{F_m + \Delta F_m}{L_m} (y_{m1} - y_{m2}) + (R + \Delta R) \sin\phi - \sum_j a_j \sigma_{j1} \frac{y_{j2} - y_{j1}}{L_j} \qquad (5.43)$$

$$B_3 = -\sum_m \frac{F_m + \Delta F_m}{L_m} \left\{ (x_{m2} - x_{m1})(y_{m2} - y_0) - (y_{m2} - y_{m1})(x_{m2} - x_0) \right\}$$

$$- \sum_j a_j \frac{Q_3}{L_j} \sigma_{j1} ,$$

where $$Q_1 = (x_{j2} - x_{j1})(x_{j2} - x_0) - (y_{j2} - y_{j1})(y_{j2} - y_0) ,$$

$$Q_2 = (x_{j2} - x_{j1})(x_{j2} - x_0) + (y_{j2} - y_{j1})(y_{j2} - y_0) ,$$

$$Q_3 = (x_{j2} - x_{j1})(y_{j2} - y_0) - (y_{j2} - y_{j1})(x_{j2} - x_0) , \qquad (5.44)$$

and $Q_4 = (x_{j2} - x_{j1}) (y_{j2} - y_0) + (y_{j2} - y_{j1}) (x_{j2} - x_0)$.

Taking ΔF_m and ΔR as parametric values, the system of equations 5.41 can be solved for u, v and $\Delta\theta$.

The center of rotation, denoted by (x_c,y_c), is related with u, v and θ as follows:

$$u\,x_c + v\,y_c = u\,x_0 + v\,y_0 + \frac{1}{2}u^2 + \frac{1}{2}v^2 ,$$

$$\delta_x\,x_c + \delta_y\,y_c = \delta_x\,x_0 + \delta_y\,y_0 + \frac{1}{2}\delta_x{}^2 + \frac{1}{2}\delta_y{}^2 , \qquad (5.45)$$

which can be solved for x_c and y_c .

The theoretical prediction cannot presently give physically meaningful results compared with the experimentally measured ones, because the physical properties and the physiological cross sections of ligaments are not known with sufficient accuracy, and the muscle forces and the joint reaction force are even less reliable. Therefore, it is not surprising that the predicted results based on these results are far from the measured ones. If the constitutive relation and the physiological cross sectional area of each ligament were given properly, this procedure could lead to a meaningful approach for determining the instantaneous center of rotation.

CHAPTER 6

STRESS RELAXATION OF LIGAMENTS OF THE TMJ

6.1 Overview

When the mandible is pulled to a certain location, the resultant stresses of the ligaments will be time dependent. The stress relaxation behavior of ligaments represented by the reduced relaxation function in section 3.5 was experimentally determined for the canine medial collateral ligament by S.L-Y. Woo et. al. [6] as shown in Fig.3.5, where G(t) is approximated as

$$
\begin{aligned}
G(t) &\simeq 1, && t < \tau_1 \\
G(t) &\simeq \frac{1 - C\,\gamma + C\,ln\,\tau_1}{1 + C\,ln\,(\tau_2/\tau_1)} - \frac{C}{1 + C\,ln\,(\tau_2/\tau_1)}\,ln\,t \\
&= C_1 - C_2\,ln\,t, && \tau_1 \le t < \tau_2 \\
G(t) &\simeq \frac{1}{1 + C\,\ln\,(\tau_2/\tau_1)}, && t \ge \tau_2
\end{aligned}
\tag{6.1}
$$

with the coefficients determined as

$$
\begin{aligned}
&C = 0.099, \\
&\tau_1 = 0.004833 \text{ minute}, \\
&\tau_2 = 3317 \text{ minutes}, \\
&C_1 = 0.749
\end{aligned}
\tag{6.2}
$$

and $C_2 = 0.042$.

The viscoelastic properties of human TMJ ligaments not being reported yet, these data will be used to analyze the behavior of ligaments of the human TMJ.

We will consider a general or realistic case of the stress relaxation behavior. That is, the strain of a ligament will increase with a known strain rate as a function of time until time t^*, and afterwards the ligamentous strain will be kept constant.

We will take the strain rate as :

$$\frac{d\epsilon}{dt} = \dot{\epsilon}(t) \qquad \text{for} \quad 0 \le t \le t^* ,$$

$$\text{and} \quad \frac{d\epsilon}{dt} = 0 \qquad \text{for} \quad t > t^* . \tag{6.3}$$

Now the stress relaxation behavior will be split into two different zones : the transient zone, which corresponds to the varying strain zone, and the relaxation zone, which corresponds to the constant strain zone, as shown in Fig.6.1. In the transient zone, the elastic stress build-up and the relaxation occur simultaneously in a ligament, while in the relaxation zone, only the relaxation occurs.

For the case of full relaxation at initial state, from eq.3.8, the stress of a ligament at time t will be

$$\sigma(t) = \int_0^t G(\, t - \tau \,) \, \frac{d\sigma^e}{d\epsilon} \, \dot{\epsilon}(\tau) \, d\tau \qquad \text{for} \quad 0 \le t \le t^*$$

$$\text{and} \quad \sigma(t) = \int_0^{t^*} G(\, t - \tau \,) \, \frac{d\sigma^e}{d\epsilon} \, \dot{\epsilon}(\tau) \, d\tau \qquad \text{for} \quad t > t^* , \tag{6.4}$$

where the latter equation might be called an extended convolution integral.

To make the analysis simple, taking a constant strain rate of a ligament,

$$\frac{d\epsilon}{dt} = \alpha = \text{constant} \quad \text{for} \quad 0 \le t \le t^* \tag{6.5}$$

the strain at time t will be

$$\epsilon(t) = \alpha\, t \qquad \text{for} \quad 0 \le t \le t^*$$

$$\text{and} \quad \epsilon(t) = \epsilon^* = \alpha\, t^* = \text{constant} \qquad \text{for} \quad t > t^* \ , \tag{6.6}$$

which were shown in Fig.6.1. Then, the stress in a ligament as a function of time will be :

$$\sigma(t) = \int_0^t G(t\text{-}\tau)\, \frac{d\sigma^e}{d\epsilon}\, \alpha\, d\tau \qquad \text{for} \quad 0 \le t \le t^*$$

$$\text{and} \quad \sigma(t) = \int_0^{t^*} G(t\text{-}\tau)\, \frac{d\sigma^e}{d\epsilon}\, \alpha\, d\tau \qquad \text{for} \quad t > t^* \ , \tag{6.7}$$

where $\frac{d\sigma^e}{d\epsilon}$ will be given by differentiating the elastic stress- strain relations in eqs. 5.2 and 5.3,

$$\frac{d\sigma^e}{d\epsilon} = A\, B\, e^{B\epsilon} \qquad \text{for} \quad 0 \le \epsilon \le \epsilon_r$$

$$\text{and} \quad \frac{d\sigma^e}{d\epsilon} = E \qquad \text{for} \quad \epsilon > \epsilon_r \tag{6.8}$$

The ligamentous stress will be discussed for two different cases in the following sections.

6.2 Behavior of the Ligamentous Stress under Constant Strain Rate

In the transient zone, where the elastic stress build-up and the relaxation occur simultaneously in a ligament, the time domain will be divided into four different subdivisions, denoted as regions (1) to (4) in Fig.6.1. Fig.6.1 represents the case $t^* > (t_r+\tau_1)$; the other cases can easily be carried out in the same manner.

Discussions will be perfomed for each different time region as follows :

6.2.1 For $0 \le t < \tau_1$;

Since $G(t-\tau) = 1$ for $t-\tau < \tau_1$,

$$\sigma(t) = \int_0^t A\,B\,e^{B\alpha\tau}\,\alpha\,d\tau$$

$$= A\,(e^{B\alpha t} - 1)\,. \tag{6.9}$$

6.2.2 For $\tau_1 \le t < t_r$, where $t_r = \frac{\epsilon_r}{\alpha}$;

$$\sigma(t) = \int_0^t G(t-\tau)\,A\,B\,e^{B\alpha\tau}\,\alpha\,d\tau\,. \tag{6.10}$$

Let $t-\tau = u$,

$$\sigma(t) = A\,B\,\alpha\,e^{B\alpha t}\int_0^t G(u)\,e^{-B\alpha u}\,du\,. \tag{6.11}$$

Since $G(u) = 1$ for $0 < u < \tau_1$,

and $G(u) = C_1 - C_2\,ln\,u$ for $u > \tau_1$,

$$\sigma(t) = A\,B\,\alpha\,e^{B\alpha t}\,[\int_0^{\tau_1} 1\cdot e^{-B\alpha u}\,du + \int_{\tau_1}^t (C_1 - C_2\,ln\,u)\,e^{-B\alpha u}\,du\,]$$

$$= A\,e^{B\alpha t}\,(1 - e^{-B\alpha\tau_1}) + A\,B\,\alpha\,e^{B\alpha t}\,I_1\,, \tag{6.12}$$

where $I_1 = \int_{\tau 1}^t (C_1 - C_2\,ln\,u)\,e^{-B\alpha u}\,du\,.$ (6.13)

Performing the integration,

$$I_1 = \frac{C_1}{B\alpha} \left(e^{-B\alpha\tau_1} - e^{-B\alpha t} \right) - C_2 I_2 \qquad (6.14)$$

where $I_2 = \int_{\tau_1}^{t} ln\, u\ e^{-B\alpha u}\, du$

$$= \frac{1}{B\alpha} \left(e^{-B\alpha\tau_1} ln\, \tau_1 - e^{-B\alpha t} ln\, t + \int_{\tau_1}^{\infty} \frac{e^{-B\alpha u}}{u} du - \int_{t}^{\infty} \frac{e^{-B\alpha u}}{u} du \right)$$

$$= \frac{1}{B\alpha} \left\{ e^{-B\alpha\tau_1} ln\, \tau_1 - e^{-B\alpha t} ln\, t + E_1(B\alpha\tau_1) - E_1(B\alpha t) \right\} , \qquad (6.15)$$

and E_1 is the exponential integral.

Therefore

$$I_1 = \frac{1}{B\alpha} \left[C_1 \left(e^{-B\alpha\tau_1} - e^{-B\alpha t} \right) + C_2 \left(e^{-B\alpha\tau_1} ln\, \tau_1 - e^{-B\alpha t} ln\, t \right) \right.$$

$$\left. - C_2 \left\{ E_1(B\alpha\tau_1) - E_1(B\alpha t) \right\} \right] \qquad (6.16)$$

and $\sigma(t) = A\, e^{B\alpha t} \left[1 + e^{-B\alpha\tau_1} \left(C_1 - C_2\, ln\, \tau_1 - 1 \right) - C_2 \left\{ E_1(B\alpha\tau_1) - E_1(B\alpha t) \right\} \right]$

$$- A \left(C_1 - C_2\, ln\, t \right) \qquad (6.17)$$

6.2.3 For $t_r \leq t < t_r + \tau_1$;

$$\sigma(t) = \int_0^t G(t-\tau) \frac{d\sigma^e}{d\epsilon} \alpha\, d\tau$$

$$= \int_0^{t_r} G(t-\tau) \frac{d\sigma^e}{d\epsilon} \alpha\, d\tau + \int_{t_r}^{t} G(t-\tau) \frac{d\sigma^e}{d\epsilon} \alpha\, d\tau$$

$$= A\,B\,\alpha \int_0^{t_r} G(t-\tau)\ e^{B\alpha\tau}\,d\tau + E\,\alpha \int_{t_r}^{t} G(t-\tau)\,d\tau$$

$$= A\,B\,\alpha\,I_3 + E\,\alpha\,I_4 \qquad (6.18)$$

where $I_3 = \int_0^{t_r} G(t-\tau)\ e^{B\alpha\tau}\,d\tau$ (6.19)

and $I_4 = \int_{t_r}^{t} G(t-\tau)\,d\tau$. (6.20)

Taking $u = t - \tau$,

$$I_3 = e^{B\alpha t}\int_{t-t_r}^{t} G(u)\ e^{-B\alpha u}\,du \qquad (6.21)$$

and $I_4 = \int_0^{t-t_r} G(u)\,du$. (6.22)

Since $t - t_r < \tau_1$,

$$I_3 = e^{B\alpha t}\left[\int_{t-t_r}^{\tau_1} 1\cdot e^{-B\alpha u}\,du + \int_{\tau_1}^{t} (C_1 - C_2\,ln\,u)\,e^{-B\alpha u}\,du\right.$$

$$= \frac{1}{B\alpha}\left\{ e^{B\alpha t_r} - e^{B\alpha(t-\tau_1)} \right\} + e^{B\alpha t}\,I_1 \ , \qquad (6.23)$$

where I_1 is defined in eq.6.13.

Rearranging ,

$$I_3 = \frac{1}{B\alpha}\left[e^{B\alpha(t-\tau_1)}(C_1 - C_2\,ln\,\tau_1 - 1) + e^{B\alpha t_r} - (C_1 - C_2\,ln\,t)\right.$$

$$+ C_2\, e^{B\alpha t} \{ E_1(B\alpha t) - E_2(B\alpha\tau_1) \}] \qquad (6.24)$$

and since $G(u) = 1$ for $t - t_r < \tau_1$,

$$I_4 = t - t_r . \qquad (6.25)$$

Therefore

$$\sigma(t) = A [e^{B\alpha(t - \tau_1)} (C_1 - C_2 \ln \tau_1 - 1) + e^{B\alpha t_r} - (C_1 - C_2 \ln t)$$

$$+ C_2 e^{B\alpha t} \{ E_1(B\alpha t) - E_1(B\alpha\tau_1) \}] + E \alpha (t - t_r) \qquad (6.26)$$

6.2.4 For $t_r + \tau_1 \leq t < t_{max}$, where $t_{max} = \frac{\epsilon_{max.\ allow}}{\alpha}$;

In a similar way as before,

$$\sigma(t) = A B \alpha \int_0^{t_r} G(t-\tau)\ e^{B\alpha\tau}\, d\tau + E \alpha \int_{t_r}^{t} G(t-\tau)\ d\tau$$

$$= A B \alpha e^{B\alpha t} \int_{t-t_r}^{t} G(u)\ e^{-B\alpha u}\, du + E \alpha \int_0^{t-t_r} G(u)\ du . \qquad (6.27)$$

Since $t - t_r > \tau_1$,

$$\sigma(t) = A B \alpha e^{B\alpha t} \int_{t-t_r}^{t} (C_1 - C_2 \ln u) e^{-B\alpha u}\, du$$

$$+ E \alpha \{ \int_0^{\tau_1} 1 \cdot du + \int_{\tau_1}^{t-t_r} (C_1 - C_2 \ln u)\, du \} .$$

$$= A [C_1(e^{B\alpha t_r} - 1) - C_2 \{ e^{B\alpha t_r} \ln (t - t_r) - \ln t \}$$

$$+ C_2\, e^{B\alpha t} \{ E_1(B\alpha t) - E_1(B\alpha(t-t_r)) \}] \qquad (6.28)$$

$$+ E\alpha [(C_1+ C_2) (t - t_r - \tau_1) + \tau_1 + C_2 \{\tau_1 \ln \tau_1 - (t - t_r) \ln (t - t_r) \}] .$$

Therefore, for a given strain rate α, the stress $\sigma(t)$ can be expressed as an explicit function of time.

6.3 Relaxation during Constant Strain Period

After pulling the ligament so that the ligamentous strain has reached a certain amount within the maximum allowable limit, the strain will be kept constant for a long period of time, and the stress relaxation will occur during this period.

From eq. 6.7 ,

$$\sigma(t) = \int_0^{t^*} G(t - \tau) \frac{d\sigma^e}{d\epsilon} \alpha \, d\tau , \qquad (6.29)$$

where the stress will be discussed for four different cases as below :

1. $0 \le t^* \le \tau_1$,
2. $\tau_1 < t^* \le t_r$,
3. $t_r < t^* \le t_r + \tau_1$,
4. $t_r + \tau_1 < t^* \le t_{max}$. (6.30)

For every case, when $t < t^*$, the resultant stress was determined in the previous section. Here we will consider $t > t^*$ only.

6.3.1 For $0 \le t^* \le \tau_1$

$$\sigma(t) = A\ B\ \alpha \int_0^{t^*} G(\ t - \tau\ )\ e^{B\alpha\tau}\ d\tau$$

$$= A\ B\ \alpha\ e^{B\alpha t} \int_{t-t^*}^{t} G(\ u\ )\ e^{B\alpha u}\ du \qquad (6.31)$$

We consider three subcases of time ranges.

6.3.1.1 For $t^* \leq t < \tau_1$,

$$\sigma(t) = A\ B\ \alpha\ e^{B\alpha t} \int_{t-t^*}^{t} 1 \cdot e^{-B\alpha u}\ du$$

$$= A\ (\ e^{B\alpha t^*} - 1\ ) \qquad (6.32)$$

6.3.1.2 For $\tau_1 \leq t < t^*+\tau_1$

$$\sigma(t) = A\ B\ \alpha\ e^{B\alpha t} [\ \int_{t-t^*}^{\tau_1} 1 \cdot e^{-B\alpha u}\ du + \int_{\tau_1}^{t} (\ C_1 - C_2\ ln\ u\ )\ e^{-B\alpha u}\ du\ ]$$

$$= A\ \{\ e^{B\alpha t^*} + e^{B\alpha(t-\tau_1)}\ (\ C_1 - C_2\ ln\ \tau_1 - 1\ ) - (\ C_1 - C_2\ ln\ t\ )$$

$$+ C_2\ e^{B\alpha t}\ \{\ E_1(B\alpha t) - E_1(B\alpha\tau_1)\ \}\ . \qquad (6.33)$$

6.3.1.3 For $t \geq t^*+\tau_1$

$$\sigma(t) = A\ B\ \alpha\ e^{B\alpha t} [\ \int_{t-t^*}^{t} (\ C_1 - C_2\ ln\ u\ )\ e^{-B\alpha u}\ du\ ]$$

$$= A\ [\ e^{B\alpha t^*}\ \{\ C_1 - C_2\ ln\ (t-t^*)\ \} - (\ C_1 - C_2\ ln\ t\ )$$

$$+ \quad C_2 \; e^{B\alpha t} \{ E_1(B\alpha t) \; - \; E_1(B\alpha\tau_1) \; \}] \; . \qquad (6.34)$$

6.3.2 For $\tau_1 \leq t^* < t_r$,

$$\sigma(t) = A \; B \; \alpha \int_0^{t^*} G(\; t - \tau \;) \; e^{B\alpha\tau} \; d\tau$$

$$= A \; B \; \alpha \; e^{B\alpha t} \int_{t-t^*}^{t} G(\; u \;) \; e^{-B\alpha u} \; du \; . \qquad (6.35)$$

We consider two subcases of time ranges.

6.3.2.1 For $t^* < t < t^* + \tau_1$,

$$\sigma(t) = A \; B \; \alpha \; e^{B\alpha t} \{ \int_{t-t^*}^{\tau_1} 1 \cdot e^{-B\alpha u} \; du \quad + \int_{\tau_1}^{t} (\; C_1 - C_2 \; ln \; u \;) \; e^{-B\alpha u} \; du \; \}$$

$$= A \; \{ \; e^{B\alpha(t-\tau_1)} \; (\; C_1 - C_2 \; \; ln \; \; \tau_1 - 1 \;) \; - \; (\; C_1 - C_2 \; \; ln \; \; t \;) \qquad (6.36)$$

$$+ \quad e^{B\alpha t^*} + \quad C_2 \; e^{B\alpha t} \{ \; E_1(B\alpha t) \; - \; E_1(B\alpha\tau_1) \; \}] \; .$$

6.3.2.2 For $t^* + \tau_1 < t$,

$$\sigma(t) = \; A \; B \; \alpha \; e^{B\alpha t} \; \int_{t-t^*}^{t} \; (\; C_1 - C_2 \; ln \; u \;) \; e^{-B\alpha u} \; du$$

$$= \; A \quad [\; e^{B\alpha t^*} \; \{ \; C_1 - C_2 \; ln \; (t-t^* \;) \; \} \; - \; (\; C_1 - C_2 \; \; ln \; \; t \;)$$

$$+ \quad C_2 \; e^{B\alpha t} \; \{ \; E_1(B\alpha t) \; - \; E_1(B\alpha(t-t^*) \; \} \;] \; . \qquad (6.37)$$

6.3.3 For $t_r \leq t^* < t_r + \tau_1$,

$$\sigma(t) = A\ B\ \alpha \int_0^{t_r} G(t-\tau)\ e^{B\alpha\tau}\, d\tau + E\ \alpha \int_{t_r}^{t^*} G(t-\tau)\, d\tau . \qquad (6.38)$$

Let $t - \tau = u$,

$$\sigma(t) = A\ B\ \alpha\ e^{B\alpha t} \int_{t-t_r}^{t} G(u)\ e^{-B\alpha u}\, du + E\ \alpha \int_{t-t^*}^{t-t_r} G(u)\, du . \qquad (6.39)$$

We consider three subcases of time ranges.

6.3.3.1 For $t^* \leq t < t_r + \tau_1$,

$$\sigma(t) = A\ B\ \alpha\ e^{B\alpha t} \{ \int_{t-t_r}^{t} 1 \cdot e^{-B\alpha u}\, du + \int_{\tau_1}^{t} (C_1 - C_2\ ln\ u)\ e^{-B\alpha u}\, du \}$$

$$+ E\ \alpha \int_{t-t^*}^{t-t_r} 1\, du$$

$$= A\ [\ e^{B\alpha(t-\tau_1)} (C_1 - C_2\ ln\ \tau_1 - 1) + e^{B\alpha t_r} - (C_1 - C_2\ ln\ t)$$

$$+ C_2\ e^{B\alpha t} \{ E_1(B\alpha t) - E_1(B\alpha\tau_1) \}] + E\ \alpha\ (t^* - t_r) . \qquad (6.40)$$

6.3.3.2 For $t_r + \tau_1 \leq t < t^* + \tau_1$,

$$\sigma(t) = A\ B\ \alpha\ e^{B\alpha t} \int_{t-t_r}^{t} (C_1 - C_2\ ln\ u)\ e^{-B\alpha u}\, du + E\ \alpha \int_{t-t^*}^{t-t_r} G(u)\, du$$

$$= A\ B\ \alpha\ e^{B\alpha t} \int_{t-t_r}^{t} (C_1 - C_2\ ln\ u)\ e^{-B\alpha u}\, du$$

$$+ \; E\,\alpha \left\{ \int_{t-t^*}^{\tau_1} 1 \, du \; + \; \int_{\tau_1}^{t-t_r} (C_1 - C_2 \, ln \, u) \, du \right\}$$

$$= A \left[\; e^{B\alpha t_r} \{ C_1 - C_2 \, ln \, (t-t_r) \} - (C_1 - C_2 \, ln \, t) \right.$$

$$\left. + \; C_2 \; e^{B\alpha t} \{ E_1(B\alpha t) - E_1(B\alpha(t-t_r)) \} \right]$$

$$+ E\,\alpha \; [t^* - t + \tau_1 + (C_1 + C_2) \; (t - t_r - \tau_1)$$

$$+ \; C_2 \{ (t - t_r) \ln (t - t_r) - \tau_1 \ln \tau_1 \}] \, . \qquad (6.41)$$

6.3.3.3 For $t^* + \tau_1 \leq t$,

$$\sigma(t) = A \, B \, \alpha \, e^{B\alpha t} \int_{t-t_r}^{t} (C_1 - C_2 \, ln \, u) \, e^{-B\alpha u} \, du + E \, \alpha \int_{t-t^*}^{t-t_r} (C_1 - C_2 \, ln \, u) \, du$$

$$= A \left[\; e^{B\alpha t_r} \{ C_1 - C_2 \, ln \, (t-t_r) \} - (C_1 - C_2 \, ln \, t) \right.$$

$$\left. + \; C_2 \; e^{B\alpha t} \{ E_1(B\alpha t) - E_1(B\alpha(t-t_r)) \} \right]$$

$$+ E\,\alpha \; [\; (C_1 + C_2) \; (t^* - t_r) + C_2 \{ (t - t^*) \ln (t - t^*)$$

$$- (t - t_r) \ln (t - t_r) \}] \, . \qquad (6.42)$$

6.3.4 For $t^* \geq t_r + \tau_1$,

$$\sigma(t) = A \, B \, \alpha \int_0^{t_r} G(t-\tau) \cdot e^{B\alpha\tau} \, d\tau + E \, \alpha \int_{t_r}^{t^*} G(t-\tau) \, d\tau \, . \qquad (6.43)$$

We consider two subcases of time ranges.

6.3.4.1 For $t^* \leq t < t^* + \tau_1$,

let $t-\tau = u$, then

$$\sigma(t) = A\,B\,\alpha\, e^{B\alpha t} \int_{t-t_r}^{t} (C_1 - C_2\, ln\, u)\, e^{-B\alpha u}\, du + E\,\alpha \int_{t-t^*}^{t-t_r} G(u)\, du .$$

$$= A\,B\,\alpha\, e^{B\alpha t} \int_{t-t_r}^{t} (C_1 - C_2\, ln\, u)\, e^{-B\alpha u}\, du$$

$$+ E\,\alpha \{ \int_{t-t^*}^{\tau_1} 1\, du + \int_{\tau_1}^{t-t_r} (C_1 - C_2\, ln\, u)\, du \}$$

$$= A [e^{B\alpha t_r} \{ C_1 - C_2\, ln (t-t_r) \} - (C_1 - C_2\, ln\, t)$$

$$+ C_2\, e^{B\alpha t} \{ E_1(B\alpha t) - E_1(B\alpha(t-t_r)) \}]$$

$$+ E\,\alpha [t^* - t + \tau_1 + (C_1 + C_2) (t - t_r - \tau_1)$$

$$+ C_2 \{ \tau_1 \ln \tau_1 - (t - t_r) \ln (t - t_r) \}] . \qquad (6.44)$$

6.3.4.2 For $t > t^* + \tau_1$,

in the same way as 6.2.3.2 ,

$$\sigma(t) = A\,B\,\alpha\, e^{B\alpha t} \int_{t-t_r}^{t} (C_1 - C_2\, ln\, u)\, e^{-B\alpha u}\, du$$

$$+ E\,\alpha \{ \int_{t-t^*}^{\tau_1} 1\, du + \int_{\tau_1}^{t-t_r} (C_1 - C_2\, ln\, u)\, du \}$$

$$= A \left[e^{B\alpha t_r} \{ C_1 - C_2 \ ln (t-t_r) \} - (C_1 - C_2 \ ln \ t) \right.$$

$$\left. + \ C_2 \ e^{B\alpha t} \{ E_1(B\alpha t) - E_1(B\alpha(t-t_r)) \} \right]$$

$$+ E \alpha [(C_1 + C_2) (t^* - t_r) + C_2 \{ (t-t^*) \ \ln (t-t^*) - (t - t_r) \ln (t- t_r) \}] . \quad (6.45)$$

Although the stress $\sigma(t)$ is governed by different equations for different regions, by physical observations, it should be continuous through the entire time region. By obtaining and comparing the threshold stresses of all the different ranges, the continuity can be verified without difficulty.

6.4 Numerical Examples

For each case of t^* shown in eq.6.30, the equations determining the stress will be selected from the previous sections and combined into a set of governing equations. For example, for $0<t^*<\tau_1$, the set of equations will be composed of equations in section 6.2.1 together with those of section 6.3.1, for $\tau_1<t^*<t_r$, those in sections 6.2.1, 6.2.2 and 6.3.2, for $t_r<t^*<(t_r+t_1)$, those in sections 6.2.1, 6.2.1, 6.2.3 and 6.3.3, and finally , for $t^*>(t_r+\tau_1)$, it will be composed of equations in sections 6.2.1, 6.2.2, 6.2.3, 6.2.4 and 6.3.4.

For numerical examples, the maximum applied strains were taken to be 0.002, 0.025, 0.05, 0.1 and 0.122 to cover all the different time ranges. Four different strain rates, ∞, 0.01, 0.001 and 0.0001 (/sec) were taken to compare the relaxation behaviors, where ∞ denotes the instantaneous elastic response. The resultant stresses

until 300 minutes of relaxation time were plotted in Fig.6.2.1 through Fig.6.2.5.

It should be noted that the short time scale t^*, drawn in the same scale in each figure, varies for different strain rates. For a specific example, from Fig.6.2.3, where $\epsilon^*=0.050$, since $t^*=\epsilon^*/\alpha$, $t^*=$ 0, 5, 50 and 500 seconds for $\alpha=\infty$, 0.01, 0.001 and 0.0001(/sec), respectively. They show that the maximum stress of a ligament is dependent on the strain rate, the major portion of relaxation occurs in a few minutes of relaxation time, and the asymptotic value of the stress, or the infinitely long time behavior, is dependent only on the magnitude of the maximum applied strain and independent of the strain rate.

The results can be extended to the structural behavior, such as the force applied by a device to keep the mandible in a fixed position for a long period of time. Thus, it can be concluded that there exists no significant difference in the device force to pull the mandible to a certain limit point for varying strain rates as long as the strain rate remains moderately large, and that the long time behavior of the device force depends on the ligamentous strains and the relaxation time only.

CHATER 7

CREEP OF LIGAMENTS OF THE TMJ

7.1 Determination of the Reduced Creep Function

When the mandible is acted on by a known external force as a function of time, each ligament of the TMJ will be in a state of stress as a function of time, which is governed by the reduced creep function of the ligament. Although the reduced creep function can be determined from the given reduced relaxation function in principle, as shown in section 3.8, due to the complexity of the mathematical formulation of the reduced relaxation function, it is not an easy task to determine it in a straightforward way. However, in this section a numerical procedure approximating the reduced creep function from the known reduced relaxation function will be introduced.

Since they are related with each other as expressed in eq.3.24, we will derive the reduced creep function as an explicit form of the reduced relaxation function. From the relation of resultant stress and the reduced relaxation function, eq.3.8,

$$\sigma(t) = \int_0^t G(t - \tau) \frac{d\sigma^e}{d\tau} d\tau . \qquad (7.1)$$

Integrating by parts,

$$\sigma(t) = [G(t - \tau) \sigma^e(\tau)]_0^t + \int_0^t \dot{G}(t - \tau) \sigma^e(\tau) d\tau , \qquad (7.2)$$

where $\dot{G}(t - \tau) = [\frac{dG (t)}{d(t)}]_{t=t-\tau}$

$$= - \frac{dG\,(t-\tau)}{d\tau} \quad . \tag{7.3}$$

Provided the initial condition is

$$\sigma^e(0) = 0 \ ,$$

since $G(0) = 1$,

$$\sigma(t) = \sigma^e(t) + \int_0^t \dot{G}(t-\tau)\ \sigma^e(\tau)\ d\tau \ . \tag{7.4}$$

Rearranging,

$$\sigma^e(t) = \sigma(t) - \int_0^t \dot{G}(t-\tau)\ \sigma^e(\tau)\ d\tau \ . \tag{7.5}$$

For the reduced relaxation function given in the form of eq.3.12 in section 3.5, $\dot{G}(t-\tau)$ can be determined for three different time domains.

Rewriting the reduced relaxation function $G(t)$,

$$G(t) \simeq 1, \qquad 0 \le t < \tau_1$$

$$G(t) \simeq C_1 - C_2 \ln t, \qquad \tau_1 \le t < \tau_2 \tag{7.6}$$

$$G(t) \simeq \frac{1}{1 + C \ln (\tau_1/\tau_2)} , \qquad t \ge \tau_2$$

we obtain $\dot{G}(t-\tau)$ for three different time domains .

(1) For $0 \le t < \tau_1$,

since $0 \leq (t - \tau) < \tau_1$,

$$\dot{G}(t - \tau) = 0 . \tag{7.7}$$

(2) For $\tau_1 < t < \tau_2$,

$$\dot{G}(t - \tau) = - \frac{C_2}{t - \tau} \qquad \text{for} \qquad 0 \leq \tau < (t - \tau_1) ,$$

$$\dot{G}(t - \tau) = 0 \qquad \text{for} \quad (t - \tau_1) \leq \tau < \tau_2 . \tag{7.8}$$

(3) For $t \geq \tau_2$,

$$\dot{G}(t - \tau) = 0 \qquad \text{for} \qquad 0 \leq \tau < (t - \tau_2) ,$$

$$\dot{G}(t - \tau) = - \frac{C_2}{t - \tau} \qquad \text{for} \qquad (t - \tau_2) \leq \tau < (t - \tau_1) , \tag{7.9}$$

$$\dot{G}(t - \tau) = 0 \qquad \text{for} \quad (t - \tau_1) \leq \tau < t .$$

$\dot{G}(t - \tau)$ for different time domains determined above are plotted in Fig.7.1.

To obtain σ^e by a numerical approximation from eq.7.5, we take the applied stress as

$$\sigma(t) = \sigma_0 \, u(t), \tag{7.10}$$

where σ_o is the magnitude of applied stress and $u(t)$ is the unit step function defined as

$$u(t) = 0 \quad \text{for} \quad t < 0 ,$$

$$= 1 \quad \text{for} \quad t \geq 0 . \tag{7.11}$$

Taking discrete time steps as $0, t_1, 2t_1, 3t_1, \cdots\cdots nt_1, \cdots\cdots$, where t_1 is an appropriately small time increment greater than τ_1, as shown in Fig.7.2, the elastic

response of the stress corresponding to the time dependent resultant strain at the k-th time interval will be approximated by the linear interpolations as follows :

$$\sigma^e(\tau) = \sigma_{k-1} + \frac{\tau - (k-1)\,t_1}{t_1}\,(\sigma_k - \sigma_{k-1})$$

$$= \frac{\tau}{t_1}(\sigma_k - \sigma_{k-1}) + k\,\sigma_{k-1} - (k-1)\,\sigma_k \quad \text{for} \quad (k\text{-}1)\,t_1 \leq \tau < k t_1, \quad (7.12)$$

where $\sigma_k = \sigma^e(k\,t_1)$. By eq.7.12, the elastic stress response at any time τ can be expressed as a function of the elastic stress responses at discrete time steps.

From eq. 7.5, we can calculate the elastic stress response σ^e and corresponding reduced creep function at the n-th discrete time step.

i) When $n = 0$ or $t=0$,

$$\sigma_0^e = \sigma_0$$

or $J_0 = 1$. (7.13)

ii) When $n = 1$ or $t=t_1$,

since $\sigma^e(\tau) = \frac{\tau}{t_1}(\sigma_1 - \sigma_0) + \sigma_0$ for $0 \leq \tau < t_1$, (7.14)

$$\sigma_1 = \sigma^e(t_1)$$

$$= \sigma_0 + \int_0^{t_1-\tau_1} \frac{C_2}{t_1 - \tau}\left\{\frac{\tau}{t_1}(\sigma_1 - \sigma_0) + \sigma_0\right\} d\tau$$

$$= \sigma_0 + \frac{C_2}{t_1}(\sigma_1 - \sigma_0)\left(\tau_1 - t_1 - t_1 \ln \frac{\tau_1}{t_1}\right) - C_2\,\sigma_0 \ln \frac{\tau_1}{t_1} . \quad (7.15)$$

Rearranging for σ_1,

$$\sigma_1 = \frac{1 + C_2 \left(1 - \frac{\tau_1}{t_1} \right)}{1 + C_2 \left(1 - \frac{\tau_1}{t_1} + \ln \frac{\tau_1}{t_1} \right)} \sigma_0 \qquad (7.16)$$

or $J_1 = \frac{\sigma_1}{\sigma_0}$

$$= \frac{1}{1 + \frac{C_2 \ln \frac{\tau_1}{t_1}}{1 + C_2 \left(1 - \frac{\tau_1}{t_1} \right)}} \qquad (7.17)$$

where J_1 is the discrete value of the reduced creep function $J(t)$ at time $t=t_1$.

iii) When $n \geq 2$ or $t \geq 2\, t_1$,

$$\sigma_n = \sigma_0 + \sum_{k=1}^{n-1} \int_{(k-1)t_1}^{kt_1} \frac{C_2}{nt_1 - \tau} \sigma^e(\tau)\, d\tau + \int_{(n-1)t_1}^{nt_1 - \tau_1} \frac{C_2}{nt_1 - \tau} \sigma^e(\tau)\, d\tau$$

$$= \sigma_0 + \sum_{k=1}^{n-1} \int_{(k-1)t_1}^{kt_1} \frac{C_2}{nt_1 - \tau} \left\{ \frac{\tau}{t_1}(\sigma_k - \sigma_{k-1}) + k\sigma_{k-1} - (k-1)\sigma_k \right\} d\tau$$

$$+ \int_{(n-1)t_1}^{nt_1 - \tau_1} \frac{C_2}{nt_1 - \tau} \left\{ \frac{\tau}{t_1}(\sigma_n - \sigma_{n-1}) + n\sigma_{n-1} - (n-1)\sigma_n \right\} d\tau$$

$$= \sigma_0 + \sum_{k=1}^{n-1} C_2 \left[-\sigma_k + \sigma_{k-1} + \left\{ (n-k+1)\sigma_k - (n-k)\sigma_{n-k} \right\} \ln \left(\frac{n-k+1}{n-k} \right) \right]$$

$$+ C_2 \left[(-\sigma_n + \sigma_{n-1}) \left(1 - \frac{\tau_1}{t_1} \right) + \sigma_n \ln \frac{\tau_1}{t_1} \right] . \qquad (7.18)$$

Arranging for σ_n ,

$$\sigma_n = \frac{\sigma_0 + C_2 \left(1 - \ln \frac{\tau_1}{t_1} \right) \sigma_{n-1} + C_2 S}{1 + C_2 \left(1 - \frac{\tau_1}{t_1} - \ln \frac{\tau_1}{t_1} \right)}$$

$$= J_n \sigma_0 , \tag{7.19}$$

where $S = \sum_{k=1}^{n-1} [-\sigma_k + \sigma_{k-1} + \{ (n - k + 1) \sigma_k - (n - k) \sigma_{k-1} \} \ln (\frac{n - k + 1}{n - k})]$

and J_n , the reduced creep function $J(t)$ evaluated at $t = n\, t_1$ is

$$J_n = \frac{\sigma_0 + C_2 (1 - \ln \frac{\tau_1}{t_1}) \sigma_{n-1} + C_2 S}{\sigma_0 \{ 1 + C_2 (1 - \frac{\tau_1}{t_1} - \ln \frac{\tau_1}{t_1}) \}} . \tag{7.20}$$

Therefore, the reduced creep function can be evaluated by eqs. 7.13, 7.17 or 7.20 for any discrete step of time and also it can be interpolated for any arbitrary time by eq.7.12. As a numerical example, for a given reduced relaxation function given by eqs. 6.1 and 6.2 in section 6.1, the corresponding reduced creep function was evaluated for 0 - 300 minutes with 0.5 minute intervals. It is plotted together with the reduced relaxation function in Figs.7.3(a) and 7.3(b) .

Since the strain response can be directly related to the elastic stress response, it can be determined from the elastic stress-strain relations given in eq.3.17 for both linear and nonlinear ranges.

7.2 Creep Behavior of Ligaments for the Time Dependent Stress History

In a real case, the applied force or stress is given as a function of time, and the corresponding strain response will also be a function of time, which will be governed by the reduced creep function $J(t)$ as expressed in eq.3.22 in section 3.7.
Rewriting it,

$$\sigma^e(t) = \int_0^t J(t - \tau) \frac{d\sigma}{d\tau} d\tau . \tag{7.21}$$

We take the applied stress in the form

$$\sigma(t) = f(t) \quad \text{for} \quad 0 \le t \le t^* ,$$

$$\sigma(t) = \sigma^* \quad \text{for} \quad t \ge t^*, \tag{7.22}$$

where $\sigma^* = \sigma(t^*) = f(t^*)$, as shown in Fig.7.3. Provided $f(t)$ is a well defined function such that $\frac{df(t)}{dt}$ exists, the elastic stress response $\sigma^e(t)$ can be determined by numerical integration. As we have evaluated the reduced creep function only for the discrete time steps, for ease of calculation the same time steps will be used to evaluate the elastic response.

Differentiating eq.7.20 with respect to time,

$$\frac{d\sigma(\tau)}{d\tau} = \dot{f}(\tau) \quad \text{for } 0 \le t \le t^*$$

$$\text{and} \quad \frac{d\sigma(\tau)}{d\tau} = 0 \qquad \text{for} \quad t \ge t^* \ ; \tag{7.23}$$

thus eq.7.21 will be

$$\sigma^e(t) = \int_0^t J(t - \tau) \ \dot{f}(\tau) \ d\tau \qquad \text{for} \quad 0 \le t \le t^*$$

$$\text{and} \quad \sigma^e(t) = \int_0^{t^*} J(t - \tau) \ \dot{f}(\tau) \ d\tau \qquad \text{for} \quad t \ge t^* . \tag{7.24}$$

Therefore, $\sigma^e(t)$ can be determined by an appropriate numerical integration.

As an example, let the applied stress be a linear function of time,

$$\sigma(t) = a\,t \qquad \text{for} \quad 0 \le t \le t^*$$

$$\text{and} \quad \sigma(t) = a\,t^* = \text{constant} \qquad \text{for} \quad t \ge t^* , \tag{7.25}$$

where a is a constant and t^* is the time at which the applied stress will remain constant, which will be taken as $t^* = nt_1$.

The time derivative of the applied stress will be

$$\frac{d\sigma(t)}{dt} = a \qquad \text{for} \quad 0 \leq t \leq t^*$$

$$\text{and} \quad \frac{d\sigma(t)}{dt} = 0 \qquad \text{for} \quad t \geq t^* , \tag{7.26}$$

so eq.7.23 will be replaced by

$$\sigma^e(t) = a \int_0^t J(t - \tau) \, d\tau \qquad \text{for} \quad 0 \leq t \leq t^*$$

$$\text{and} \quad \sigma^e(t) = a \int_0^{t^*} J(t - \tau) \, d\tau \qquad \text{for} \quad t \geq t^* , \tag{7.27}$$

which can easily be integrated for the discrete values of J(t) obtained.

CHAPTER 8

SUMMARY AND CONCLUSIONS

In this study, analytic and numerical procedures and algorithms have been developed to predict the mechanics of the human TMJ. This investigation was initiated as a first step in determining the design data for a jaw traction device to aid arthroscopic surgery of TMJ. The intention of this study is to utilize from the field of published data some simple rules that seem to apply in the in vivo behavior of the human mandibular structure.

The translation of the mandible limited by the allowable maximum strain of the related ligaments has been discussed in chapter 2. Here the allowable maximum strain of a ligament is assumed to be the maximum available strain of the ligament during normal opening, so the analysis is marginally safe.

As discussed in chapter 3, one of the main complicating features of the solution of a biomechanical problem is that the properties of biological tissues may vary from one individual to the other, from one skeletal element to another within the same individual, and even from one region to another within the same skeletal element. Therefore, one cannot expect a simple formula to account exactly for all the experimental data. In particular, although most authors make some effort to justfy in-vitro test data as comparable to in-vivo characteristics, one cannot be absolutely sure. Nevertheless, it is assumed in this study that the elastic and viscoelastic behaviors of the soft tissues are governed by simple formulae.

The viscoelastic behavior of ligaments is formulated by the reduced relaxation

function measured for finite time domain and extrapolated to infinite time. Thus, it is inevitable that there exists some discrepancies in the long time behaviors predicted by the different mathematical models, as shown in Fig.3.4. However, as C. Lanczos commented [16], it would be idle to hope that some other modified mathematical procedure could give better results, since the difficulty lies not with the manner of evaluation but with the extraordinary sensitivity of the exponents and amplitudes to very small changes of the data, which no amount of least-square or other form of statistics could remedy. Realizing these facts, it can be concluded that for a living tissue, a viscoelastic law based on the fully relaxed elastic response, $G(t)$ as $t \to \infty$, is not realistic. In fact, a formulation based on $G(\infty)$ may run into a true difficulty because it seems that the relaxation will last until the specimen will be free of stress.

The viscoelastic behavior represented by the reduced relaxation function can be deduced to analyze the creep or the dynamic behavior. The relation between the reduced relaxation function and the reduced creep function has been confirmed by experimental observations [16]. But for the dynamic behavior it has been indicated that the discrepancies between predicted and measured are not negligible [6,19]. Thus it can be concluded that the physics of the viscoelastic behavior of soft tissue is much too complicated to be expressed in a mathematical model such as the reduced relaxation function, the reduced creep function or the dynamic modulus.

In chapter 4, muscle forces working during bilateral static bite motion have been predicted at different bite force levels and the results have been shown to be in excellent comparison with the experimentally measured data. It should be noted that there exist some uncertain factors in measuring muscle forces by electromyography, due to complex human physiology. Therefore it is virtually impossible to improve the accuracy in measuring the muscle forces beyond a certain extent.

The joint reaction force has been determined on the basis that it works so as to equilibrate the system of optimized muscle forces and the ligamentous forces of the mandible. Thus its variation depends on the craniomandibular geometry and corresponding forces of muscles and ligaments, which has been discussed by G. S. Throckmorton and L. S. Throckmorton [28,29].

In chapter 5, the mechanics of normal opening and the symmetric translation of the mandible has been discussed. In reality, the jaw motion or the motion of any other skeletal system is highly complicated to model, and the theoretical prediction cannot fully explain the real phenomena. In other words, the analysis can only be limited in methodological approach. However, since the analysis has been performed with marginal safety, it may be the preliminary guideline to the design of the jaw traction device for arthroscopic surgery of the TMJ.

In chapter 6, the stress relaxation of ligaments of the TMJ is analyzed. It should be noted that the parameters C, τ_1 and τ_2 in eq.6.2 are determined on the basis that the initially applied strain is assumed to be a step function of time. In reality, it is physically impossible to realize a true step change in the strain, so it is assumed that the stress response to a fast steplike change in the strain can be used as a fair approximation of the response to a true step change. As L. Dortmant et. al. discussed [30], considering the time lags due to the steplike change of strain and its stress response, the parameters C, τ_1 and τ_2 may vary from a few percent to several hundred percent. However, it is evident that even though the values of parameters may vary significantly, the corresponding variations of the values of the reduced relaxation function are negligibly small. In this regard, the reduced relaxation function G(t) approximated in the form of eq.6.1 is much more convenient to use than that of eq.3.10 proposed by Y. C. Fung [16,22].

From the time dependent stress response predicted and plotted in figs.6.2.1 to 6.2.5, it can be concluded that the peak stress depends on both the maximum applied strain and the strain rate and that the stress at the fully relaxed state depends only on the magnitude of the maximum applied strain and is independent of the strain rate. Also the structural behavior of the mandible depends on the ligamentous strains and the relaxation time, while it does not depend on the strain rate of the ligaments except for a few minutes of transient period.

In chapter 7, a procedure for determining the reduced creep function from the reduced relaxation function is proposed and utilized to predict the creep behavior of ligaments for the applied stress varying with time.

As is mentioned, due to the lack of test data for the physical properties of the components of the human TMJ, most other parts of this study have been limited to the methodological approach. However, it has been shown to be quantitatively or qualitatively comparable to the test results obtained by many authors.

TABLES

Author / Muscle force	Carlsoo (year) (ratio)	Schumacher (1961) (ratio)	Grant (1977) cm^2	Grant (1977) (ratio)	Pruim et.al. (1980) cm^2	Pruim et.al. (1980) (ratio)
masseter	(1.0)	(1.0)	2.53	(1.0)	3.4	(1.0)
internal pterygoid	(0.5)	(0.5)	1.43	(0.57)	1.9	(0.56)
anterior temporalis	-	-	1.65	(0.65)	2.6	(0.76)
posterior temporalis	-	-	1.65	(0.65)	1.6	(0.47)
temporalis total	(1.3)	(1.2)	3.3	(1.3)	4.2	(1.24)
opener	-	-	-	-	1.0	(0.29)
external pterygoid	-	-	-	-	2.1	(0.62)

Table 4.1 Physiological cross sectional areas of muscles

Maximum allowable muscle stress MN/m^2	Maximum allowable muscle stress psi	Author	(year)
1.0	145.0	Johnson	(1930)
0.9	130.5	Morris	(1948)
		Hettinger	(1961)
0.4 - 0.7	58.0 - 101.5	Ikai et. al.	(1968)
0.9 - 1.8	130.5 -271.0		
(average 1.2)	(average 174.0)	Pruim et. al.	(1980)

Table 4.2 Maximum allowable muscle stress

muscle	cross sectional area of muscle (cm^2)	F_{max}, measured (Pruim et. al.) Newton (lb)	F_{max} predicted Newton (lb)
masseter	3.4		408 (91.7)
int. pterygoid	1.9	640 (143.9)	228 (51.3)
ant. temporalis	2.6	362 (81.4)	312 (70.1)
post. tempoalis	1.6	198 (44.5)	192 (43.2)
temporalis total	3.9*	526 (118.2)	467 (105.0)
opener	1.0	115 (26.9)	120 (27.0)
ext. pterygoid	2.1	379 (85.2)	365 (82.1)

Table 4.3 Maximum allowable muscle forces

(* denotes effective cross sectional area)

opening angle (°)		3.	5.	9.	12.
direction of translation (°)		-90.	-75.	-60.	-45.
location of the center of the condyle (Ref. ; Fig.2.6)		P_1	P_2	P_3	P_4
amount of available translation (inch)		0.164	0.140	0.093	0.062
ligament at the limit length		L_l	L_{st}	L_l	L_l , L_{st}
length of the capsular ligament (inch)	L_{c1}	0.484	0.491	0.513	0.533
	L_{c2}	0.638	0.642	0.645	0.656
device force components	F_x (lb)	-16.2	-11.7	-13.1	-10.3
	F_y (lb)	-120.7	-120.9	-128.0	-131.4
	M_z^*(in-lb)	-14.6	-12.8	-10.6	-4.2
reference figure number		Fig.5.3.1	Fig.5.3.2	Fig.5.3.3	Fig.5.3.4

Table 5.1 Translation of the mandible after normal opening and corresponding device force (M_z^* denotes the moment about the center of condyle)

FIGURES

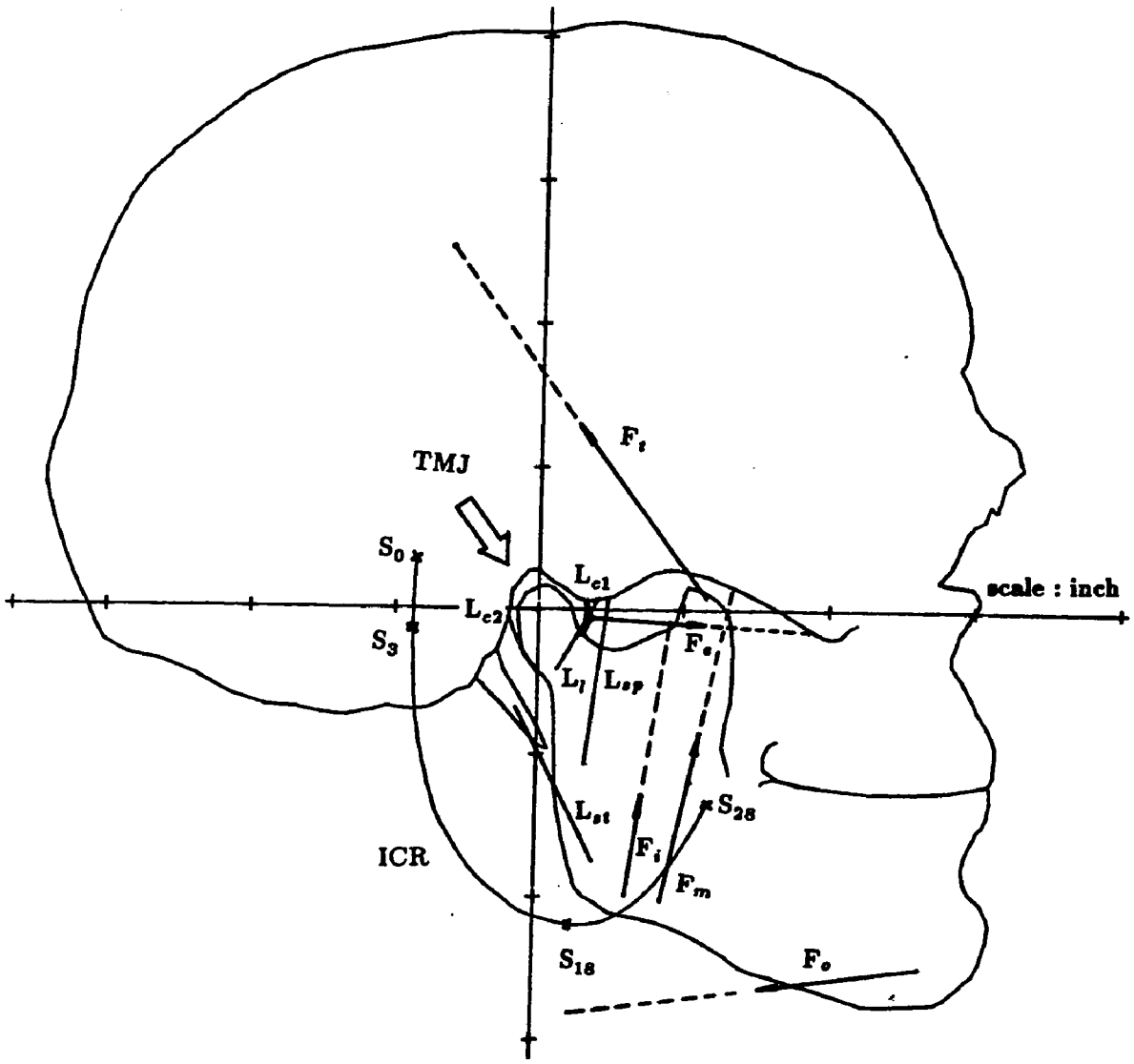

Ligaments

L_{c1} , L_{c2} : the capsular ligament

L_{sp} : the sphenomandibular ligament

L_{st} : the stylomandibular ligament

L_l : the lateral ligament

Muscle forces

F_m : the masseter

F_t : the temporalis

F_i : the internal pterygoid

F_e : the external pterygoid

F_o : the opener

Fig.1.1 Human TMJ with ligaments, muscles and the locus of ICR of the mandible

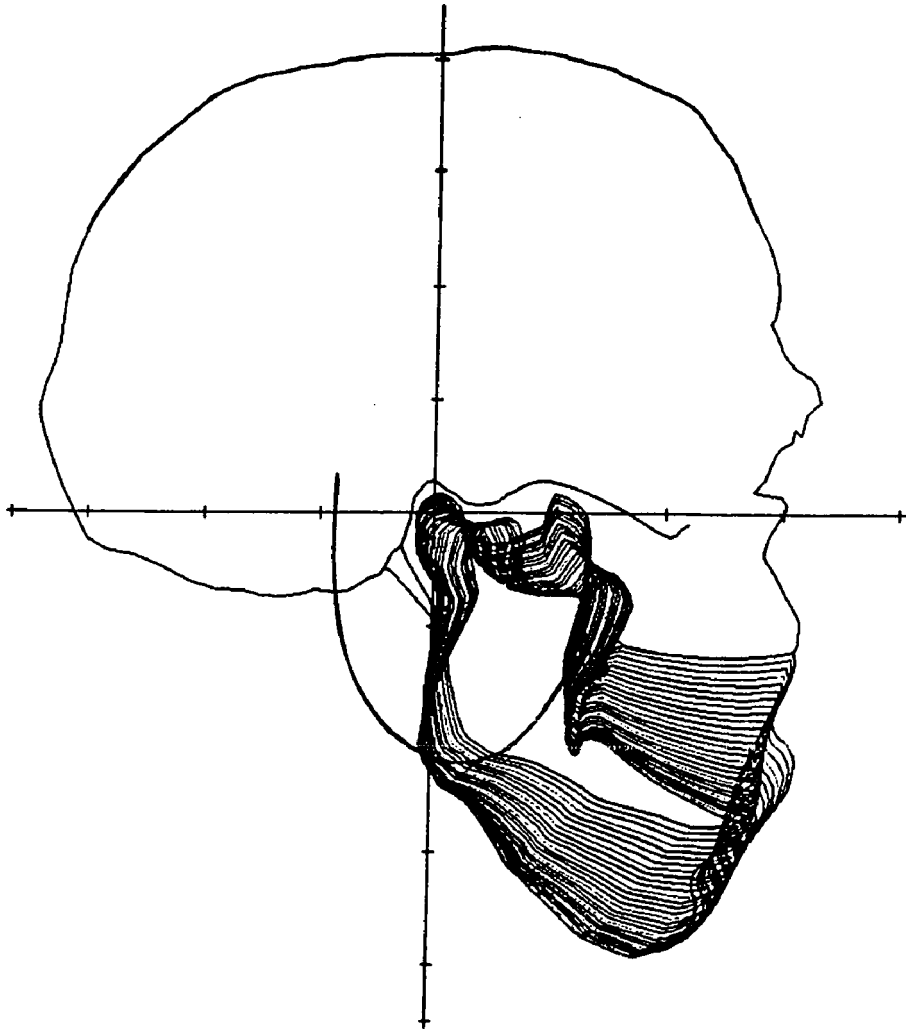

Fig.2.1 Location of the mandible during normal opening

(jaw opening angle 0° - 28° with 1° interval)

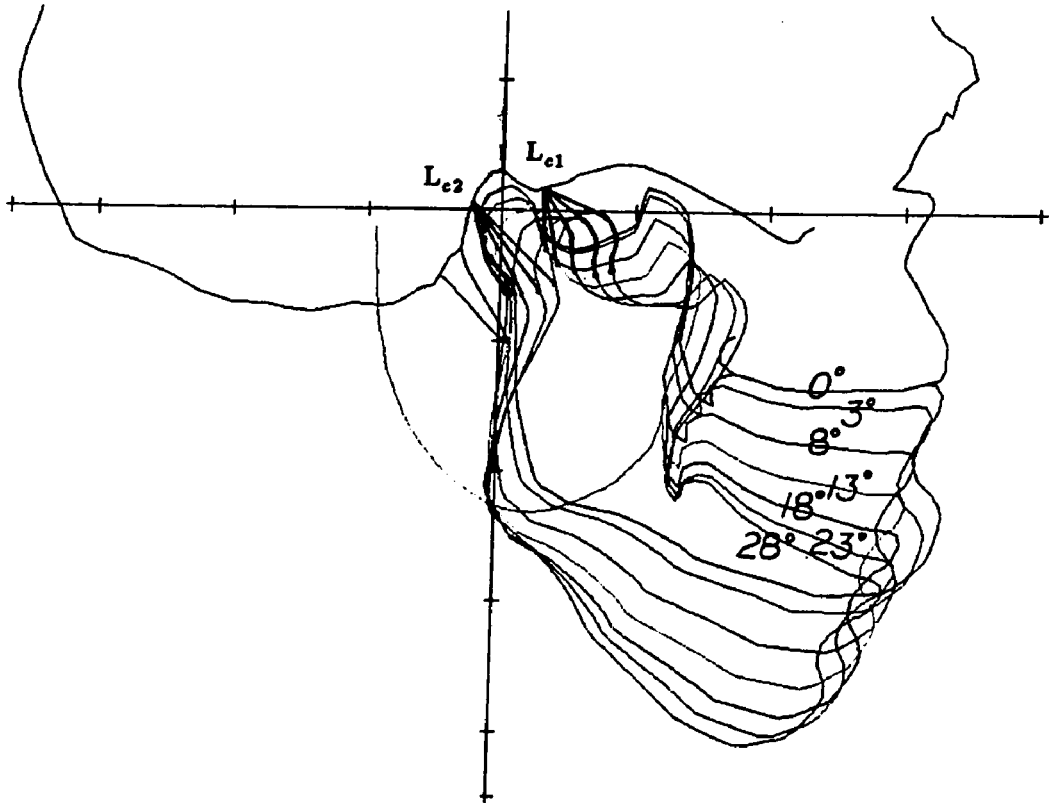

Fig.2.2 Stretch of the capsular ligament

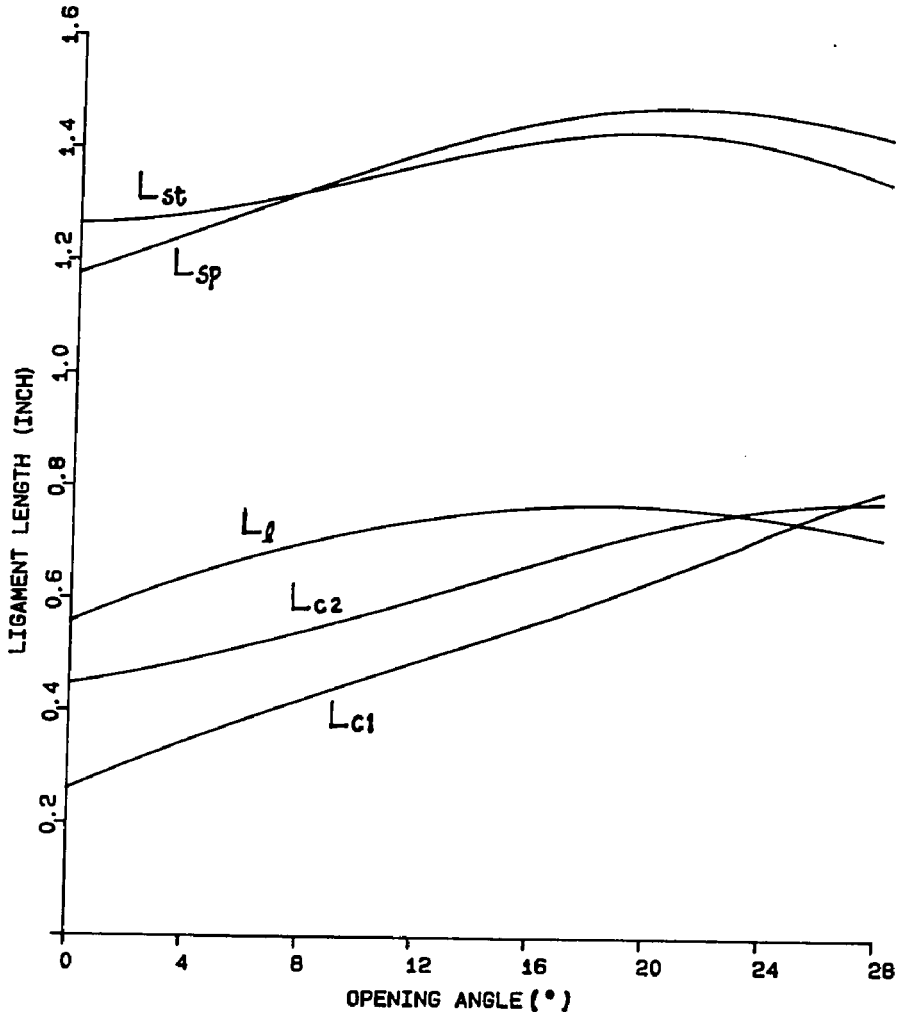

Fig.2.3 Ligamentous lengths during normal opening of the mandible

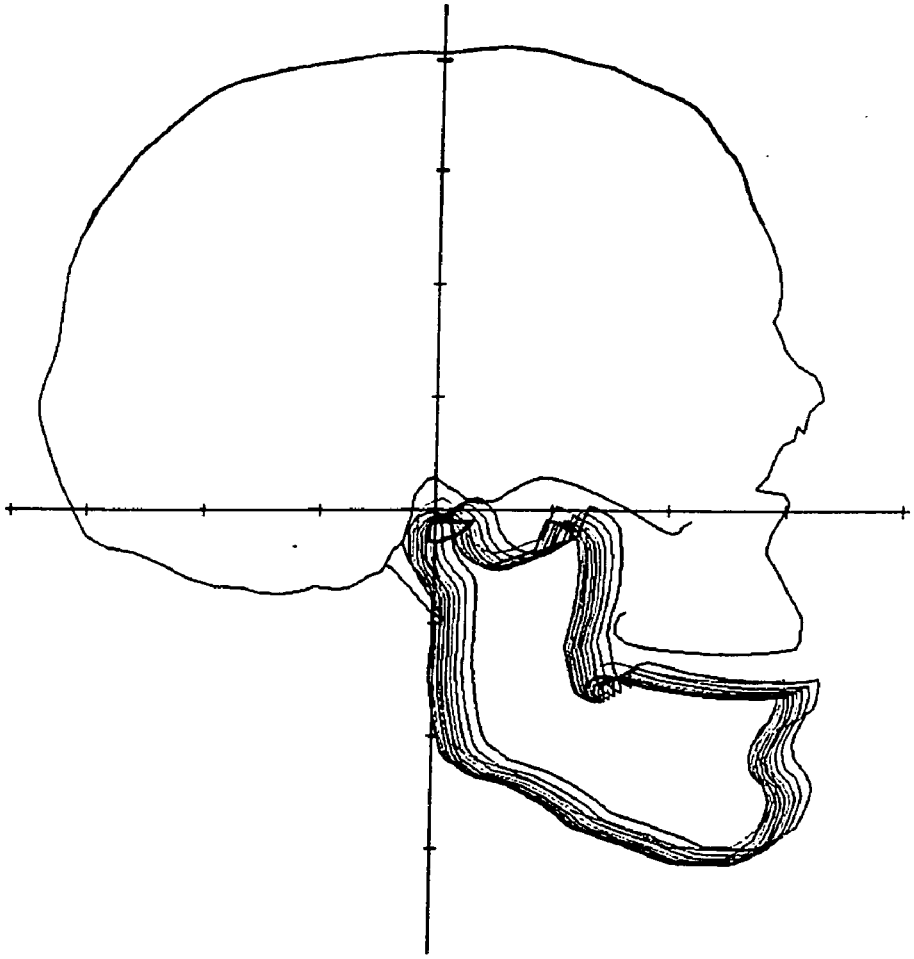

Fig.2.4 Jaw translations to the limit after 4° opening — symmetric case

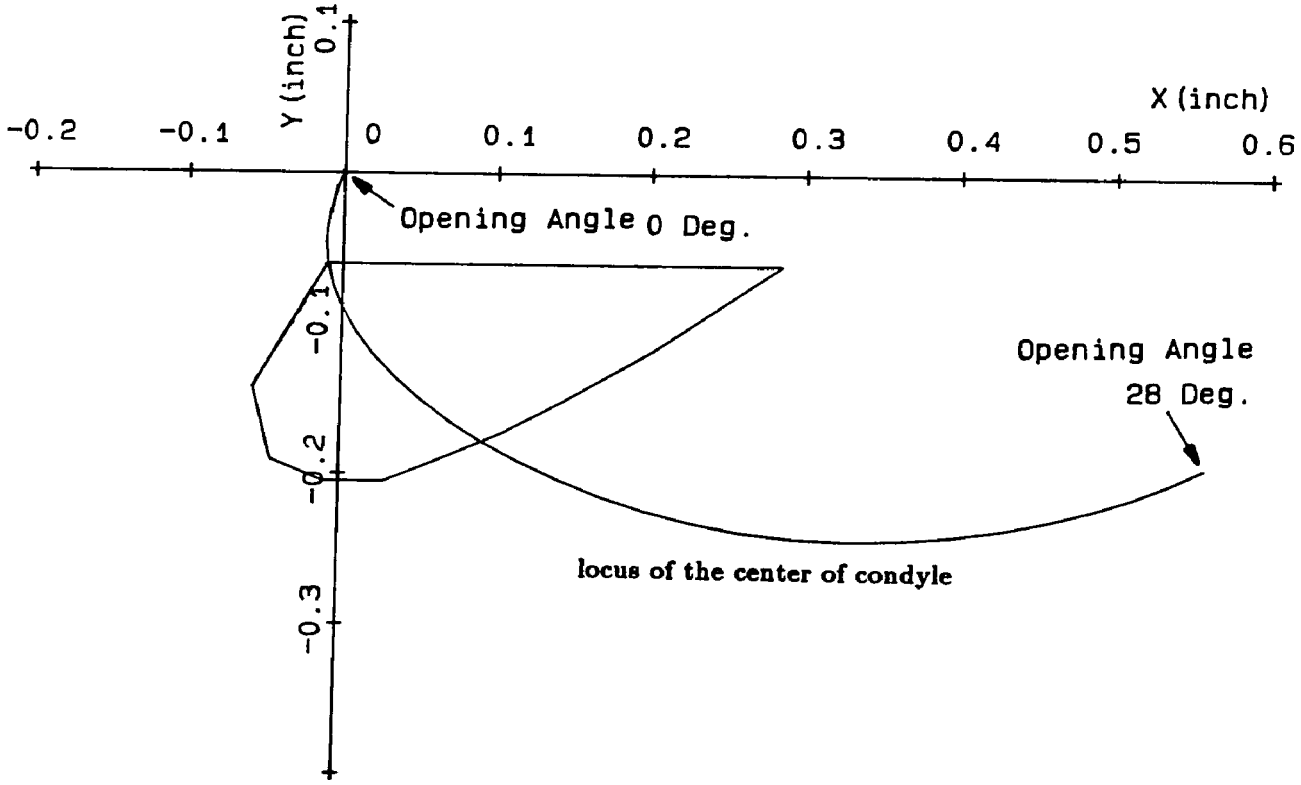

Fig.2.5 Translation limit of the mandible represented by the locus of the center of condyle — 2 dimensional case, opening angle 4°

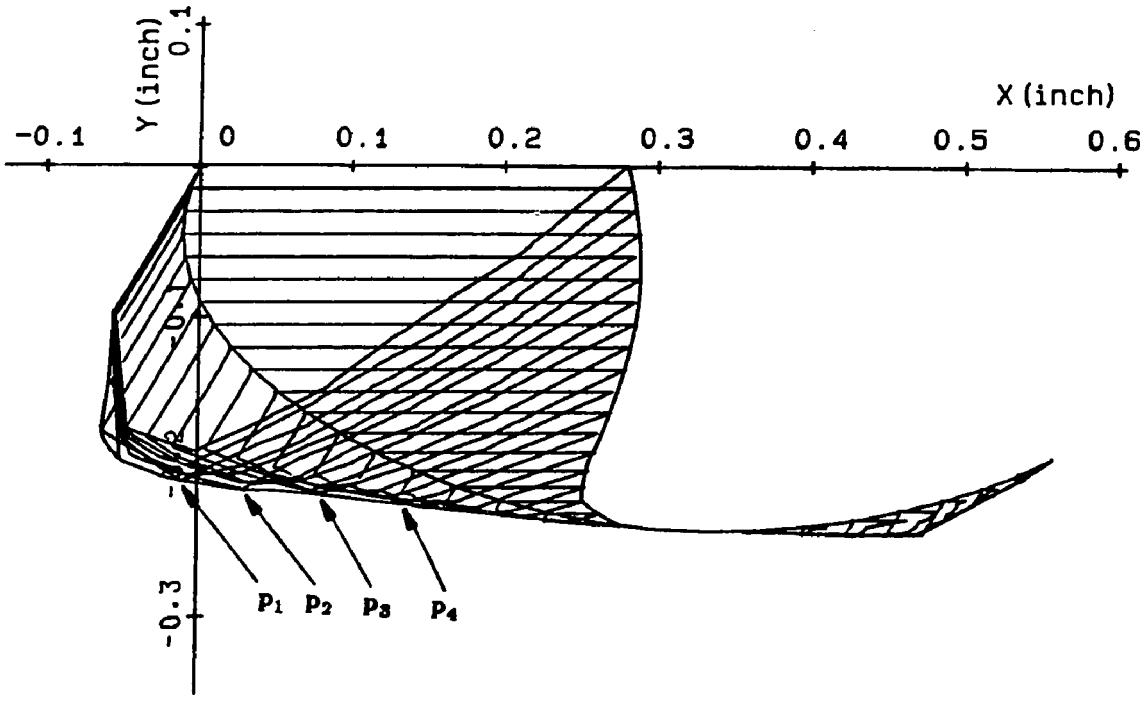

Fig.2.6 Totality of the translation limit of the mandible represented by the locus of the center of condyle — 2 dimensional case, opening angle $0^{\circ} \sim 28^{\circ}$

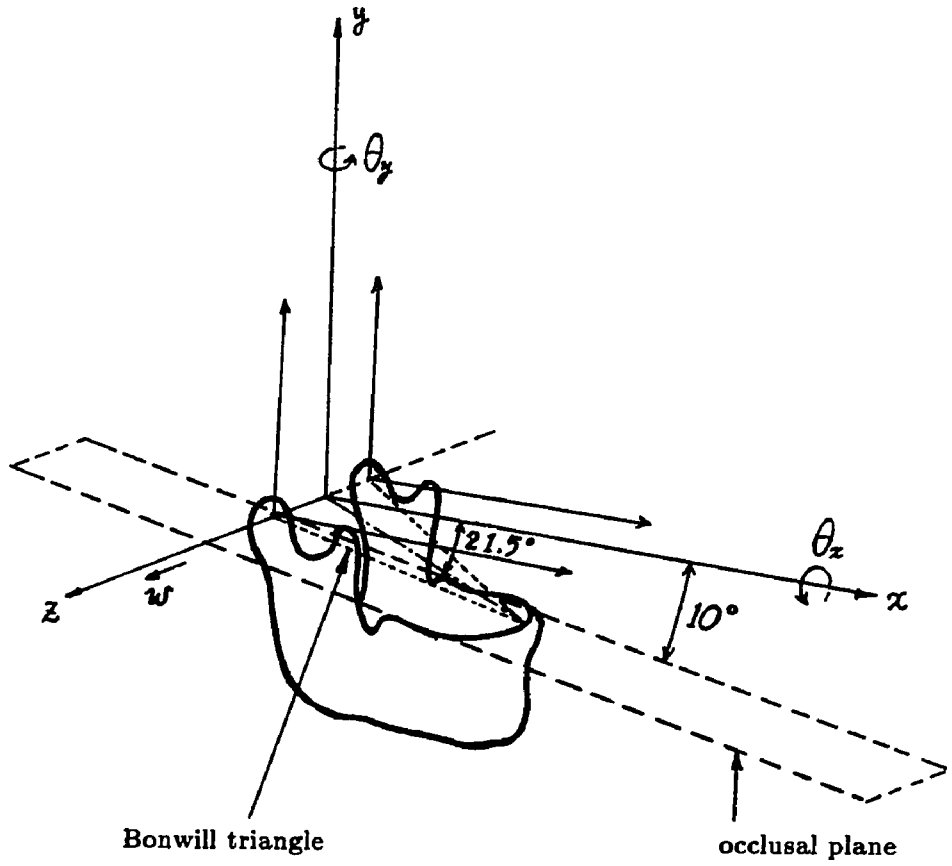

Fig.2.7 Mandible in 3 dimensional view

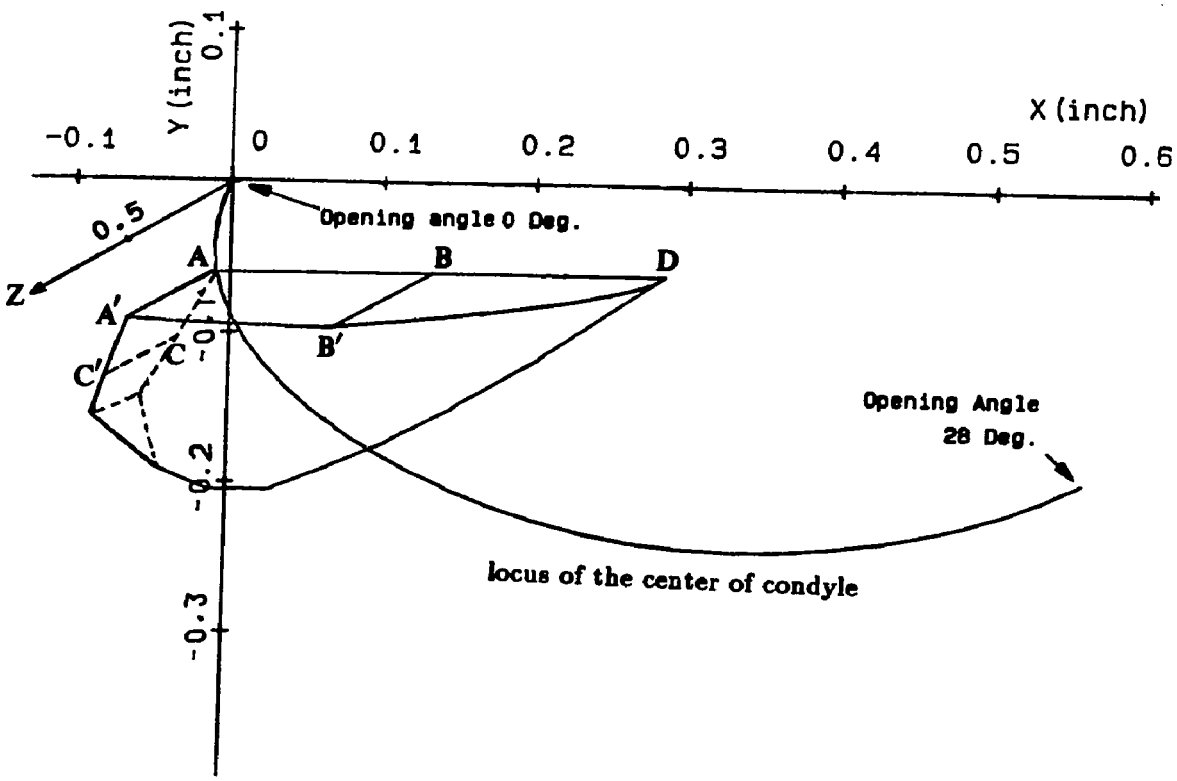

Fig.2.8 Translation limit of the mandible represented by the locus of the center of condyle — 3 dimensional case, opening angle 4°

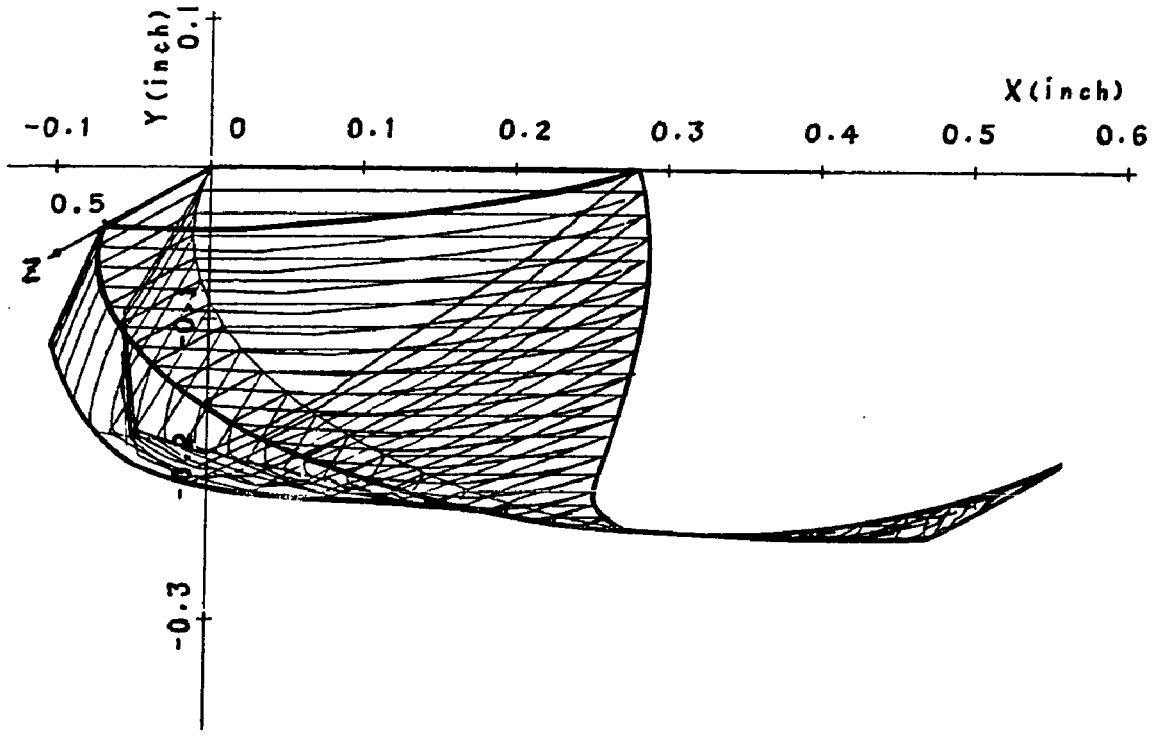

Fig.2.9 Totality of the translation limit of the mandible represented by the locus of the center of condyle — 3 dimensional case, opening angle $0^{\circ} \sim 28^{\circ}$

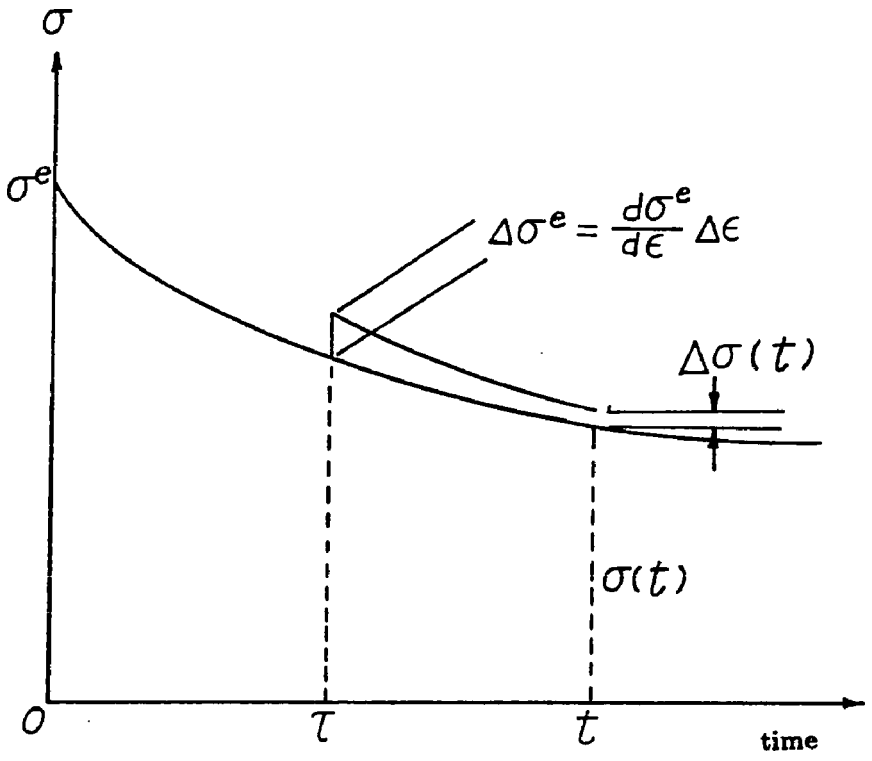

Fig.3.1 Stress relaxation superposed by an incremental step strain

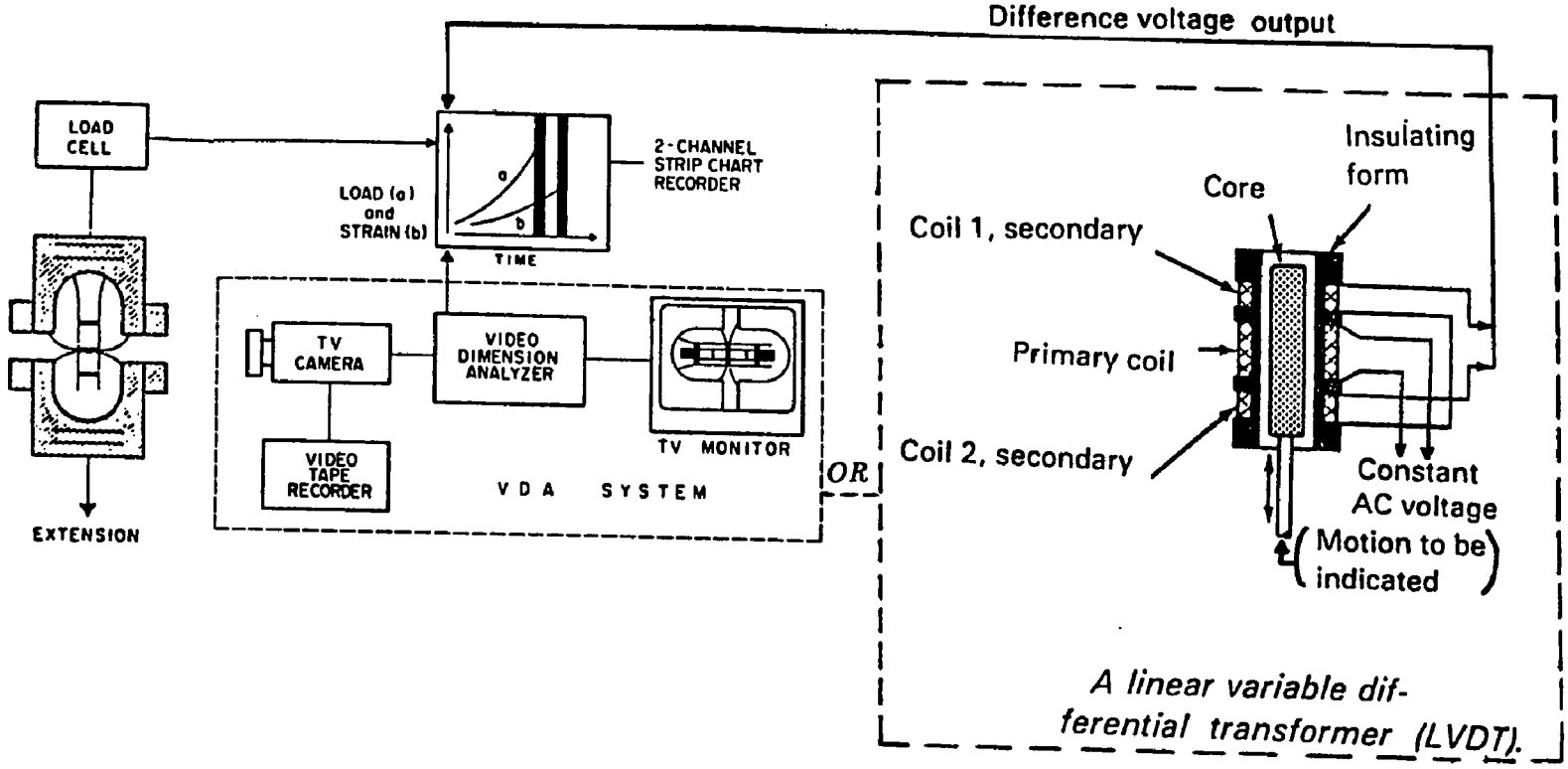

Fig.3.2 A flow chart detailing the apparatus used to obtain the tensile properties of the soft tissue [6, 18]

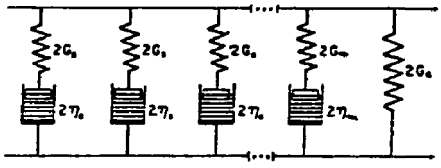

Generalized Maxwell model representation.

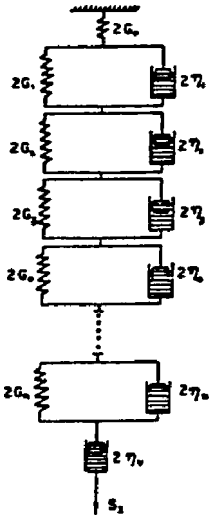

Generalized Kelvin model representation.

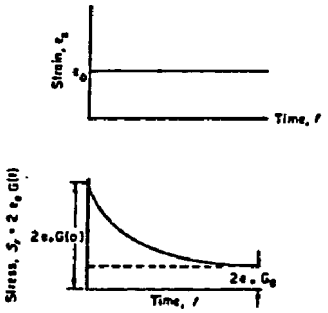

Stress and strain as a function of time for a Maxwell model.

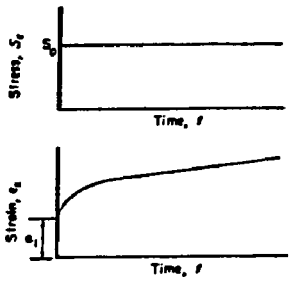

Stress and strain as a function of time for the three element Kelvin model.

(a) (b)

Fig.3.3 Modeling of viscoelastic behavior of soft tissues

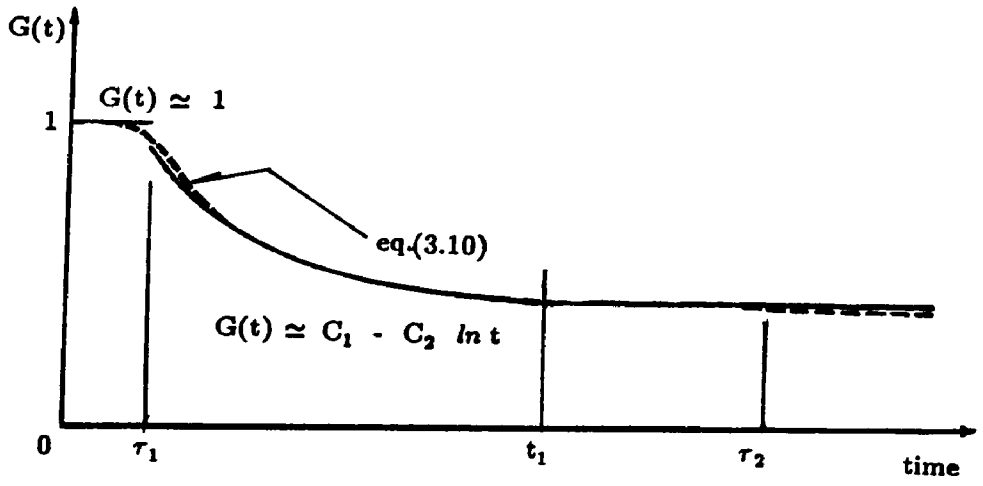

Fig.3.4 Typical shape of the reduced relaxation function

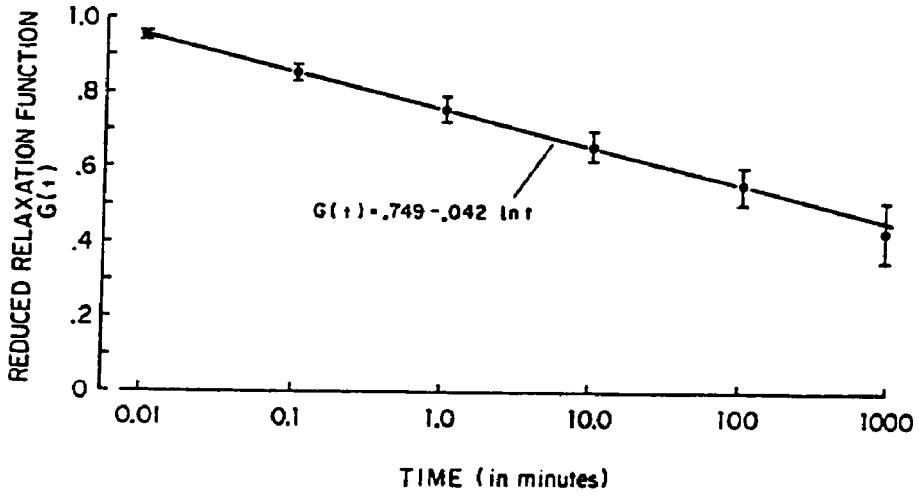

Fig.3.5 Long-term relaxation behavior of canine MCL. [6]

(The experiments were carried to 16 hr at 37°C and data are expressed in mean ± standard error. The straight line is reduced relaxation function as predicted by theory.)

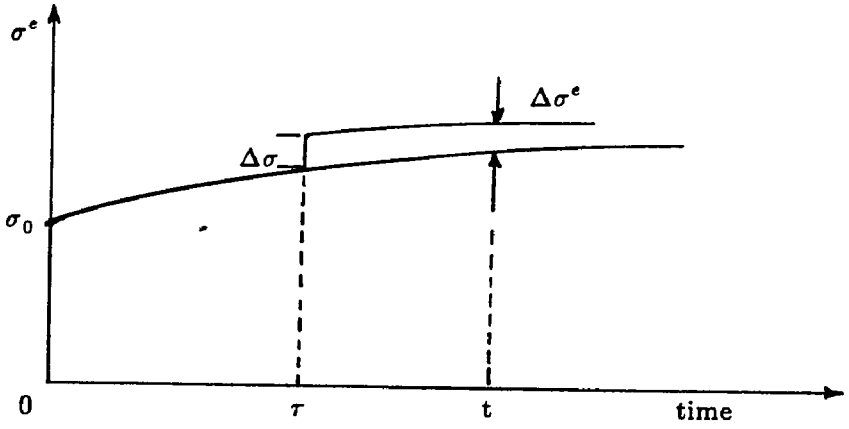

Fig.3.6 Elastic stress response corresponds to creep strain superposed with incremental step stress

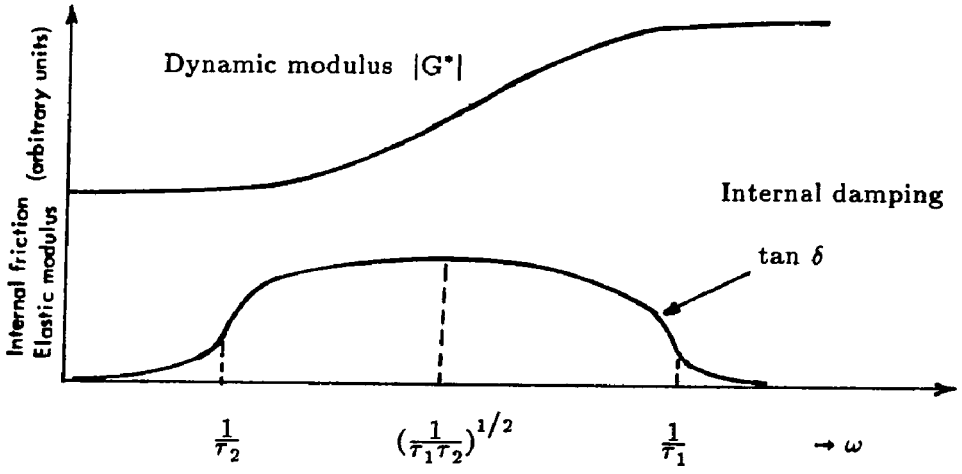

Fig.3.7 Typical shape of the dynamic modulus |G*| and the internal damping tan δ plotted as a function of the logarithm of the frequency ω

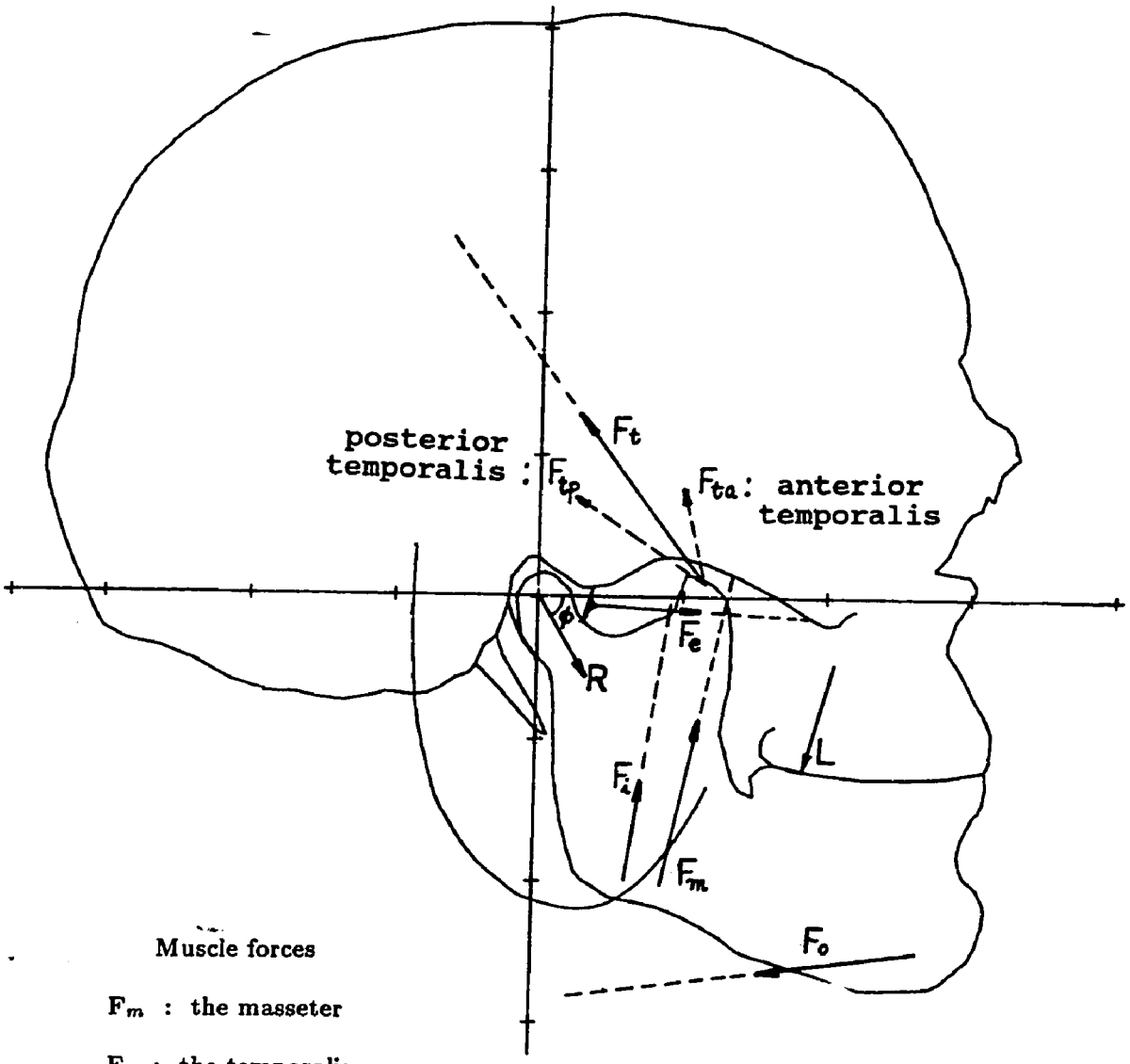

Muscle forces

F_m : the masseter

F_t : the temporalis

F_i : the internal pterygoid

F_e : the external pterygoid

F_o : the opener

R : Joint reaction force

L : Bite force

Fig.4.1 Muscle forces in the mandible

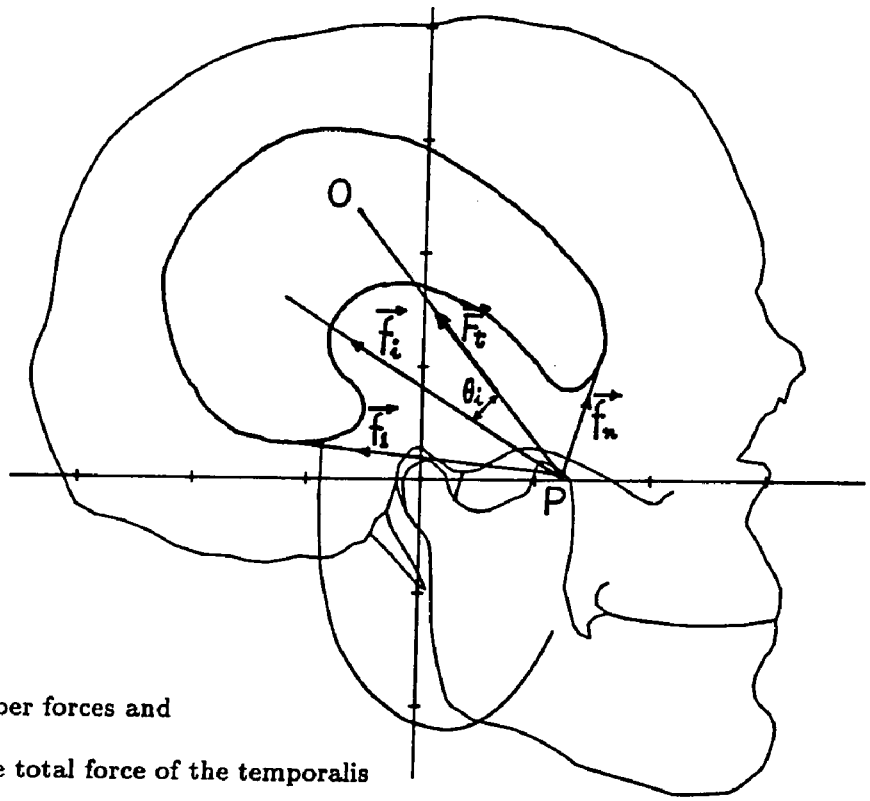

(a) Fiber forces and the total force of the temporalis

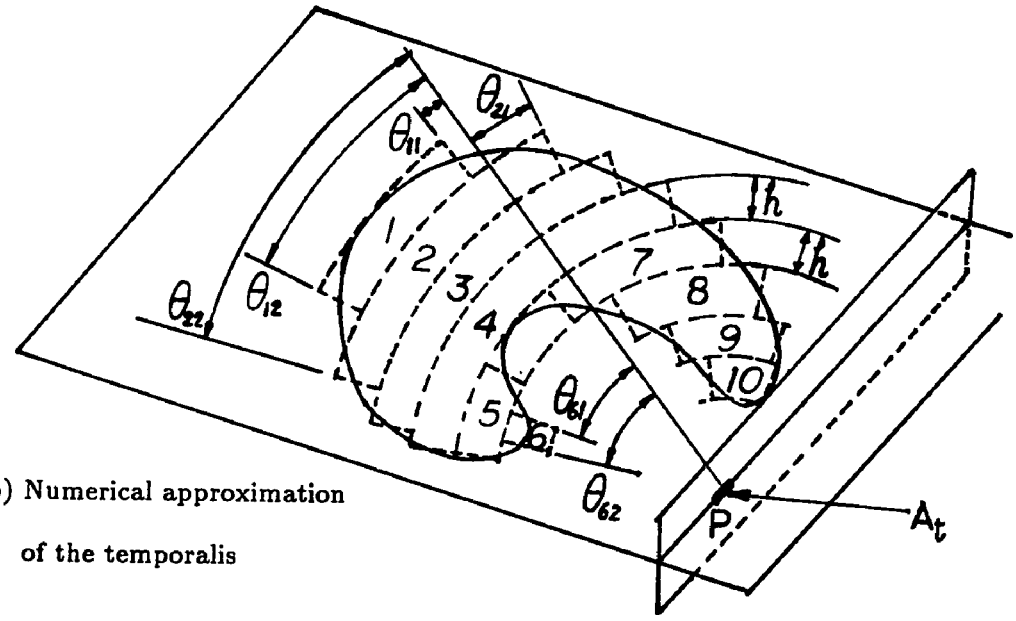

(b) Numerical approximation of the temporalis

Fig.4.2 The geometry of the temporalis

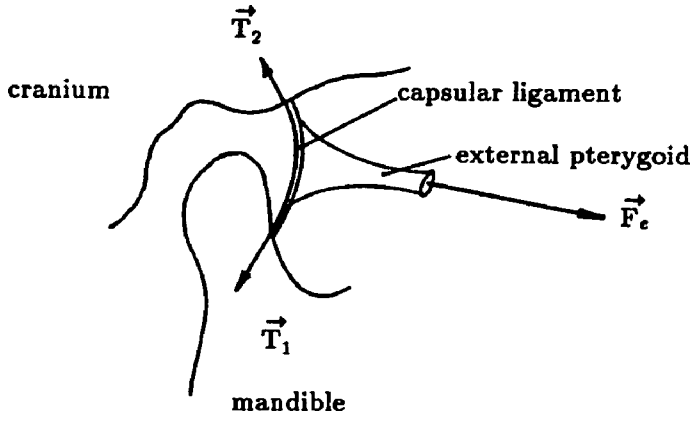

(a) The external pterygoid and the capsular ligament L_{c1}

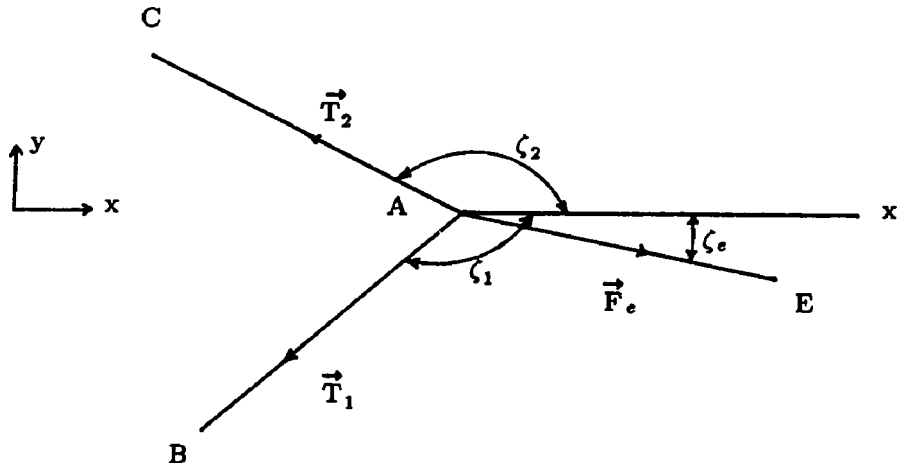

(b) Vector diagram of the external pterygoidal force

Fig.4.3 The external pterygoidal force

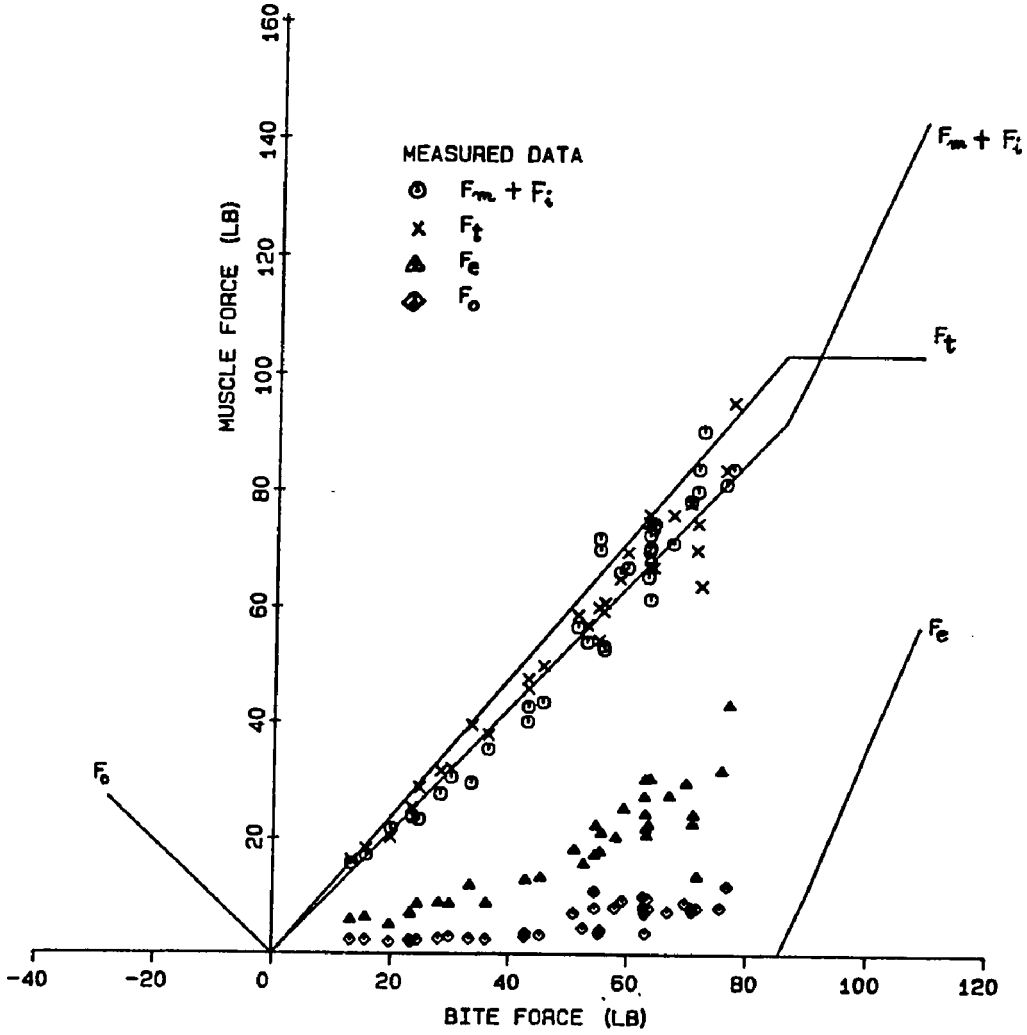

Fig.4.4 Bite force - muscle force relations

(Jaw opening angle 4°, bite position; 1-st molar)

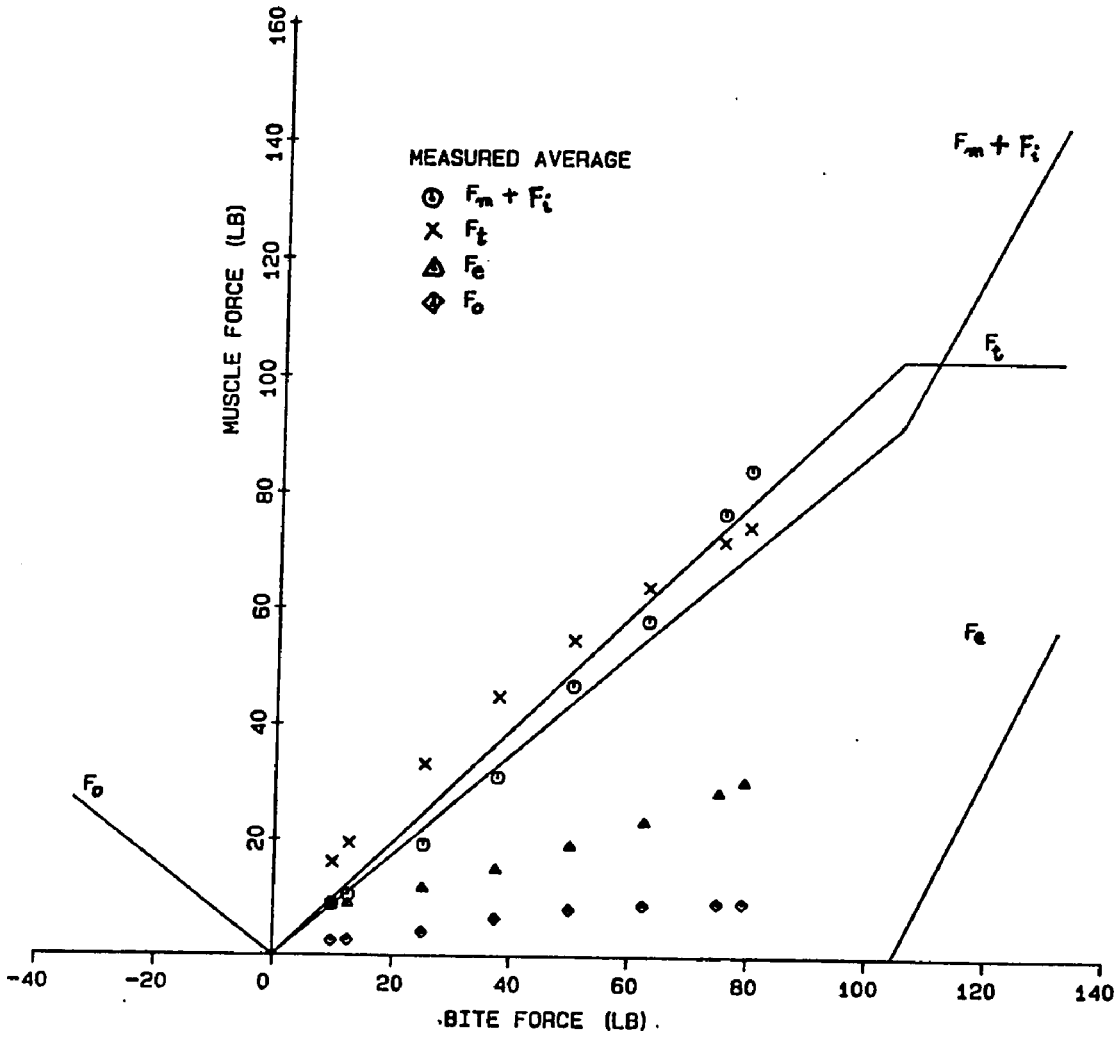

Fig.4.5 Bite force - muscle force relations

(Jaw opening angle 4°, bite position; 2-nd molar)

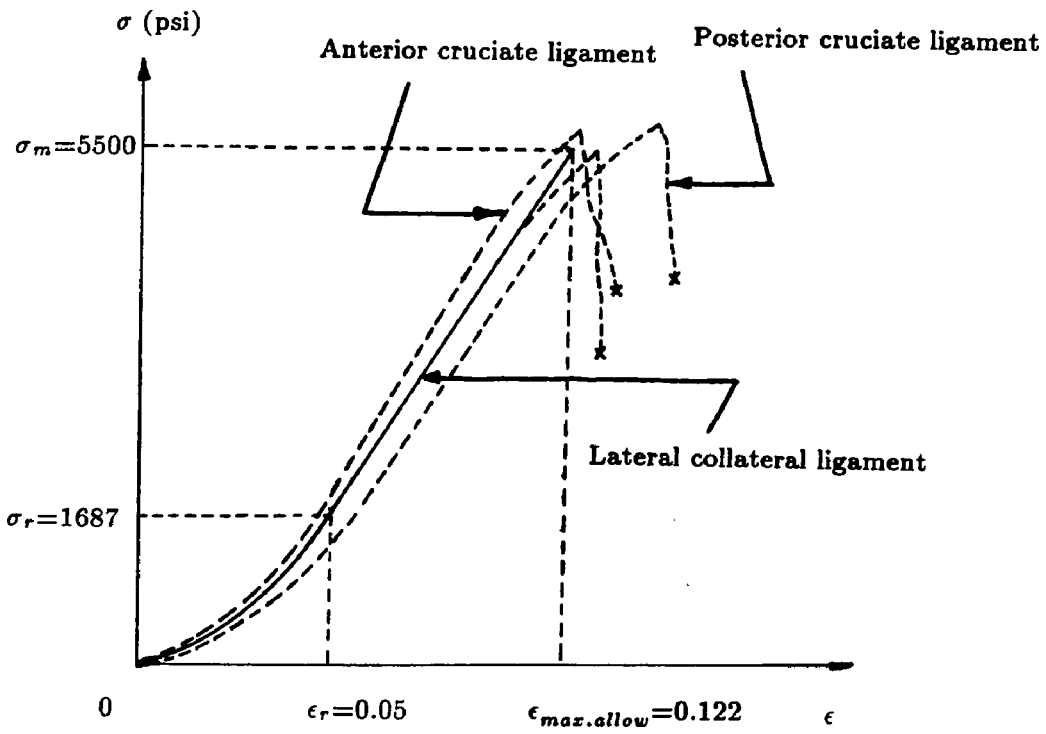

Fig.5.1 Stress - strain relation of human knee ligament

(Ref. ; Butler et. al. [7])

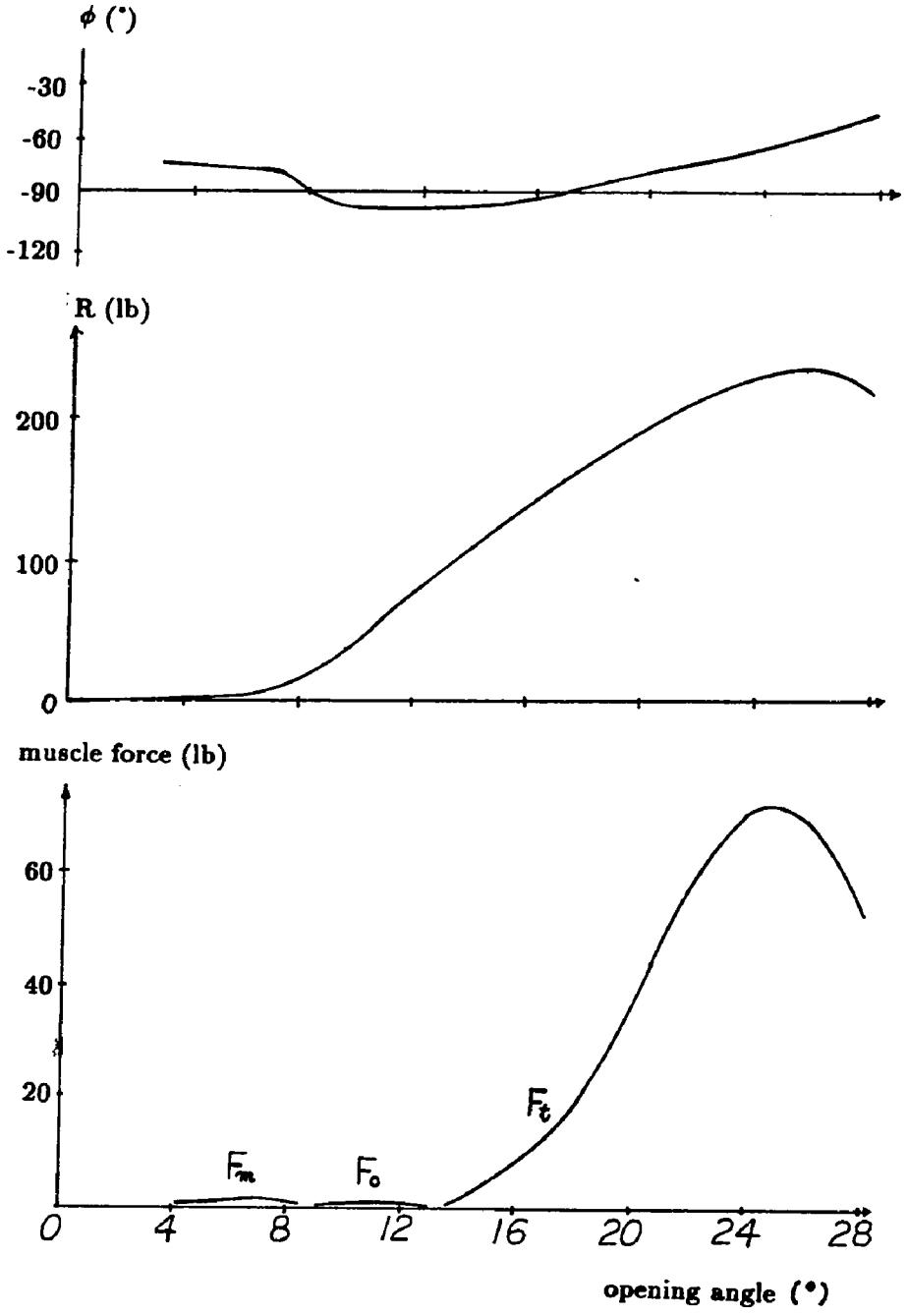

Fig.5.2 Prediction of muscle forces and joint reaction force with the direction along the normal opening of the jaw

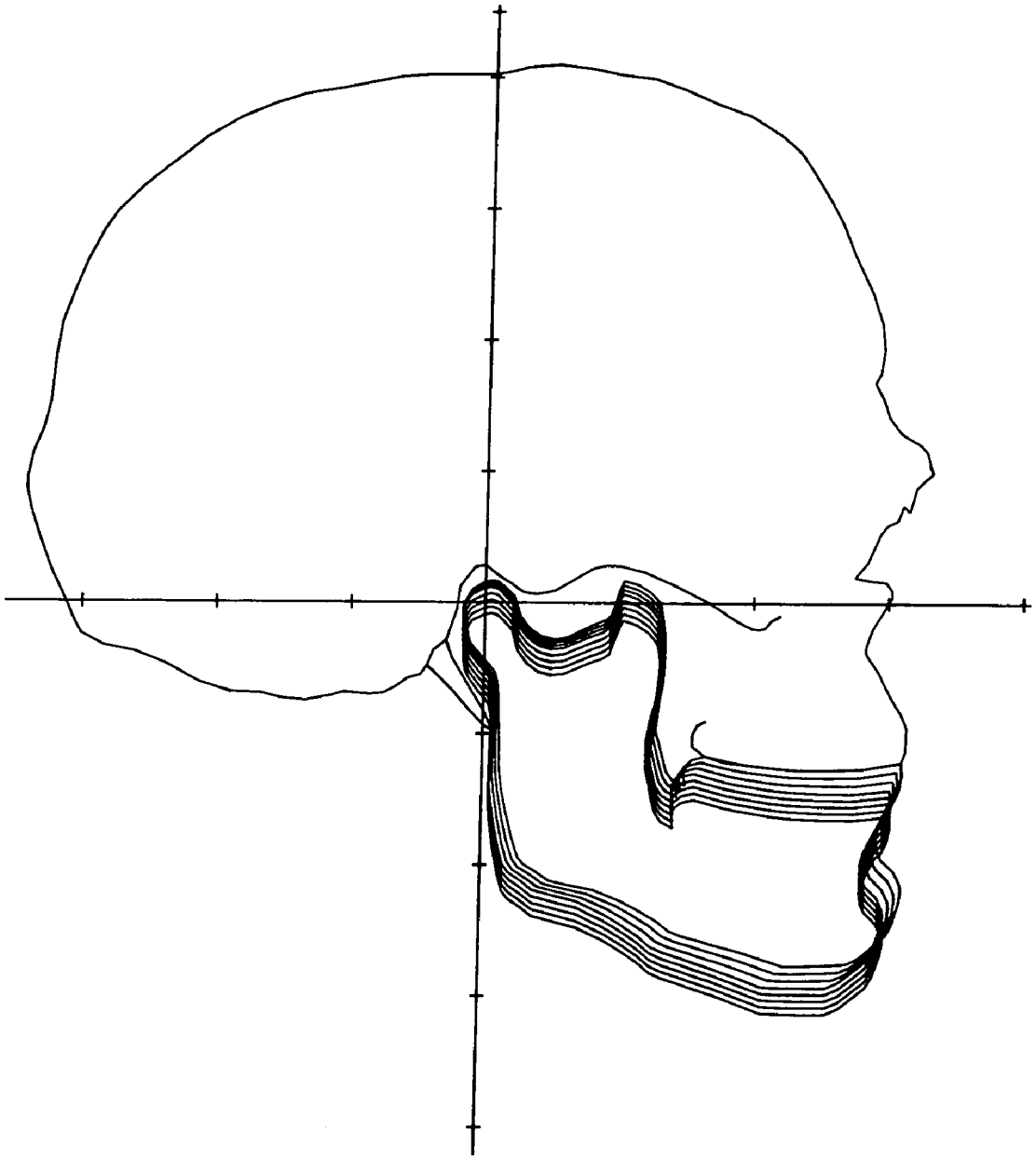

Fig.5.3.1 Translation of the mandible after normal opening

(opening angle 3°, direction of translation -90°)

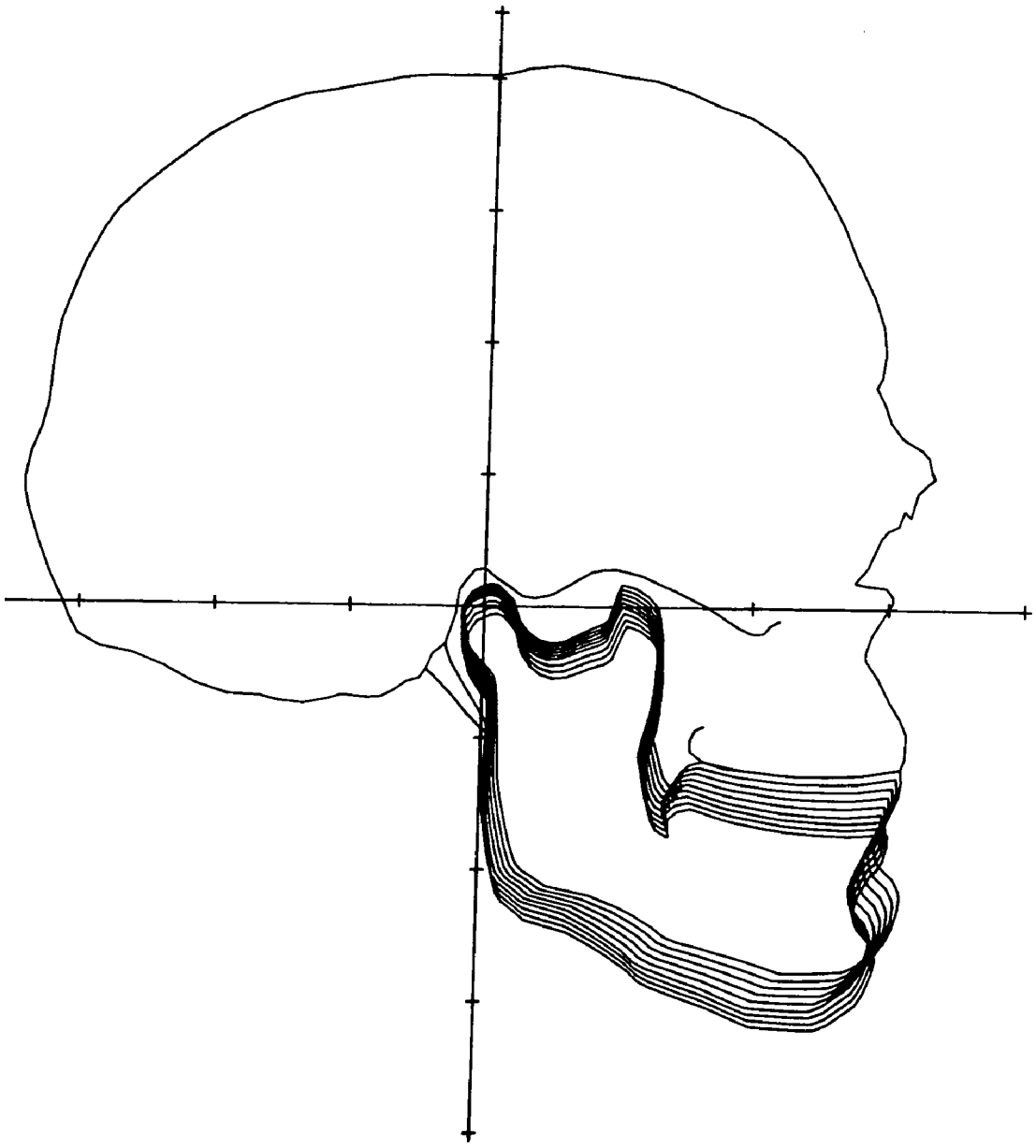

Fig.5.3.2 Translation of the mandible after normal opening

(opening angle 5°, direction of translation -75°)

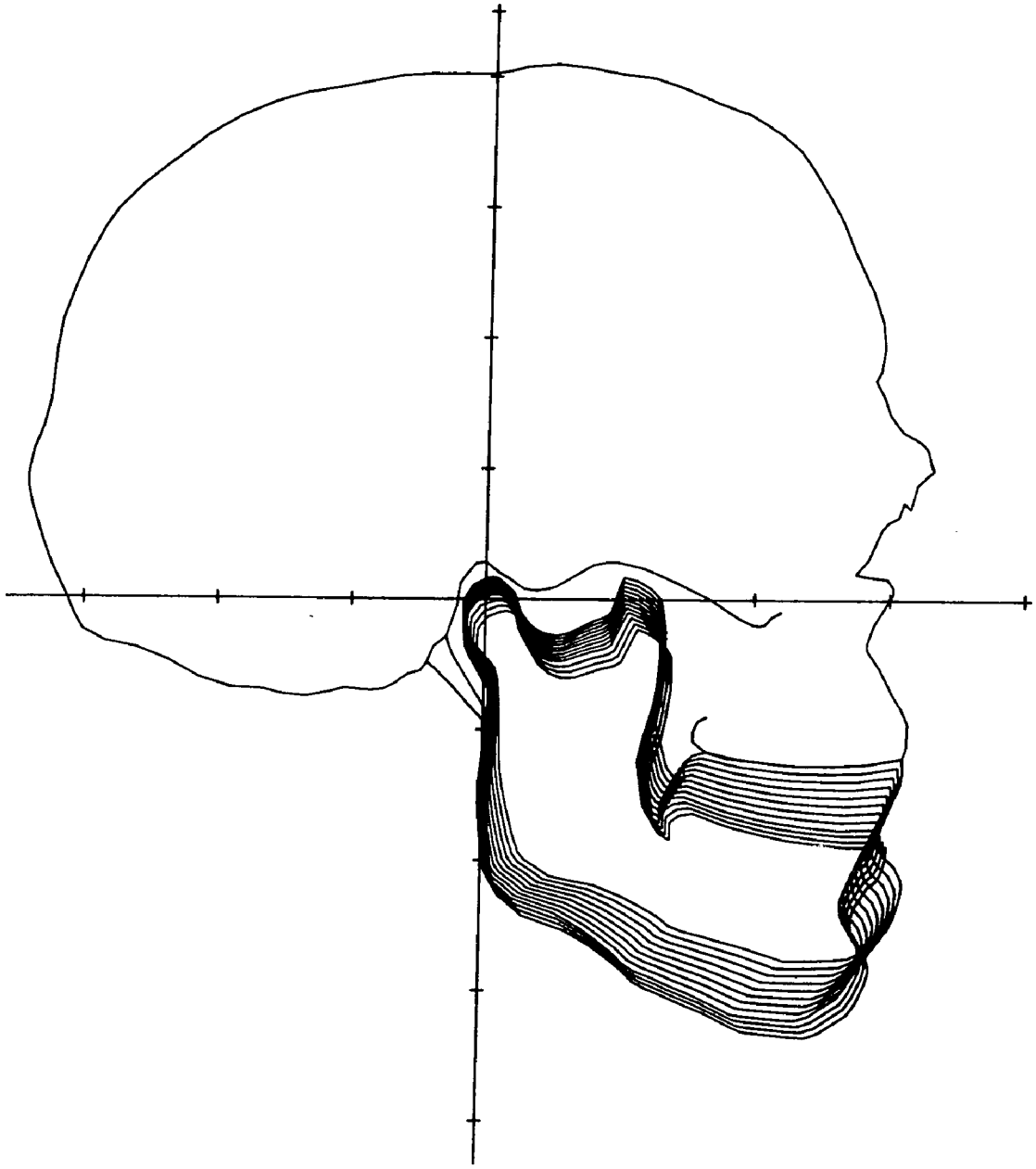

Fig.5.3.3 Translation of the mandible after normal opening

(opening angle 9°, direction of translation -60°)

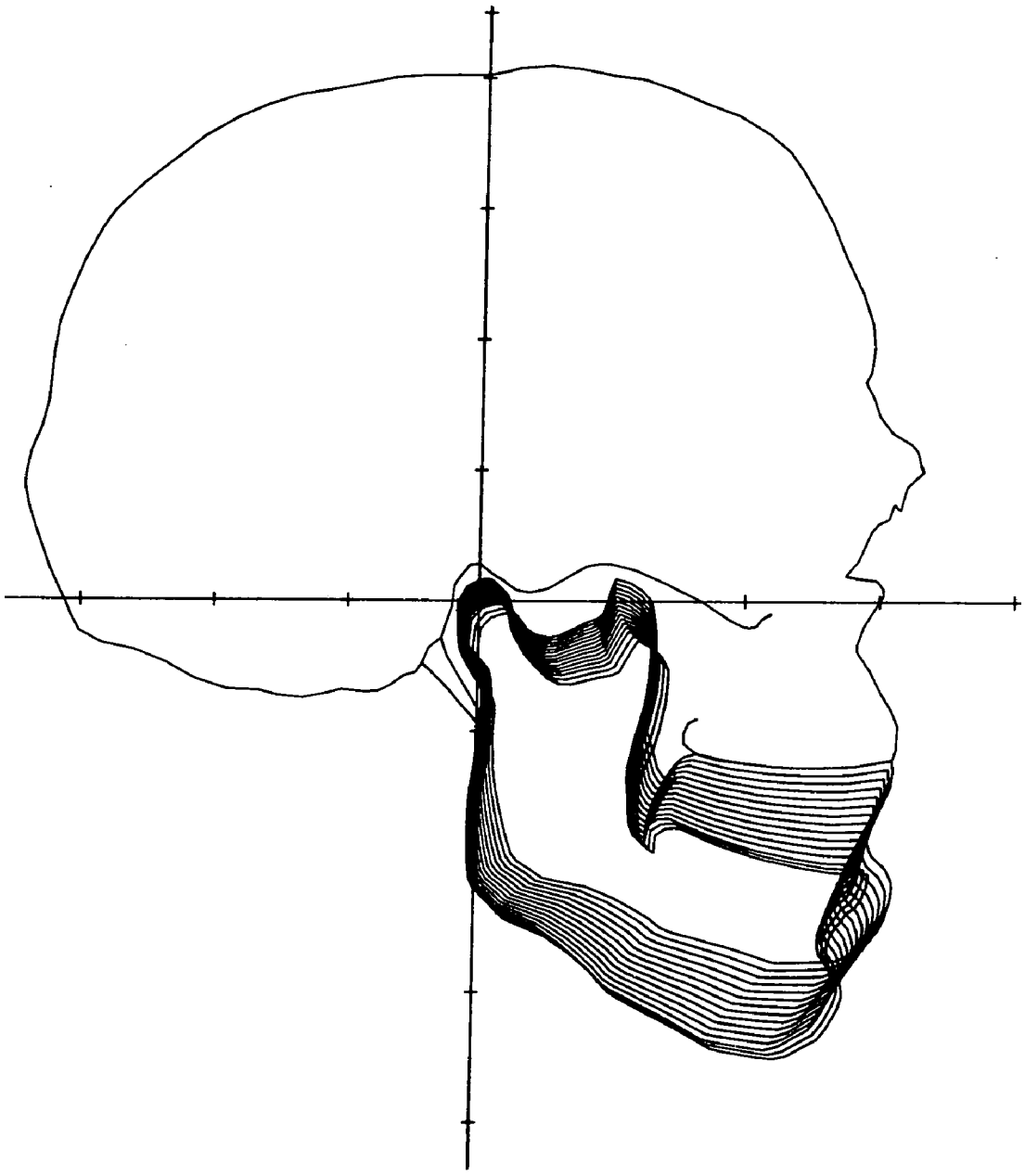

Fig.5.3.4 Translation of the mandible after normal opening

(opening angle 12°, direction of translation -45°)

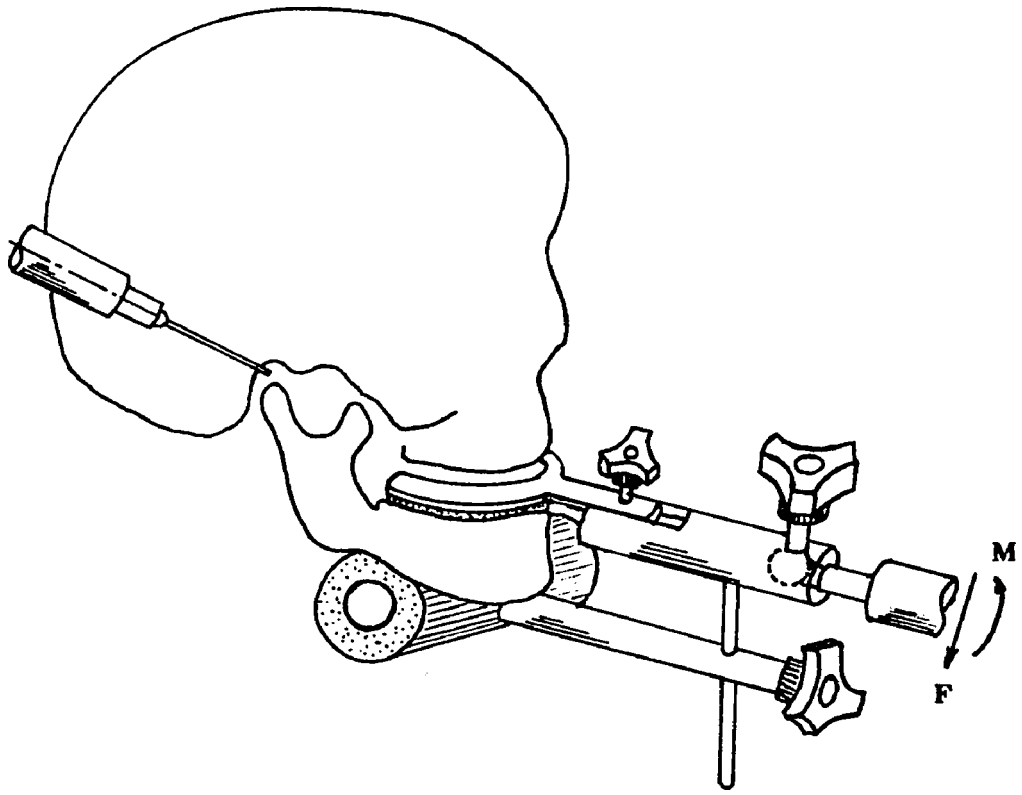

Fig. 5.4 Scheme of arthroscopic surgery of TMJ

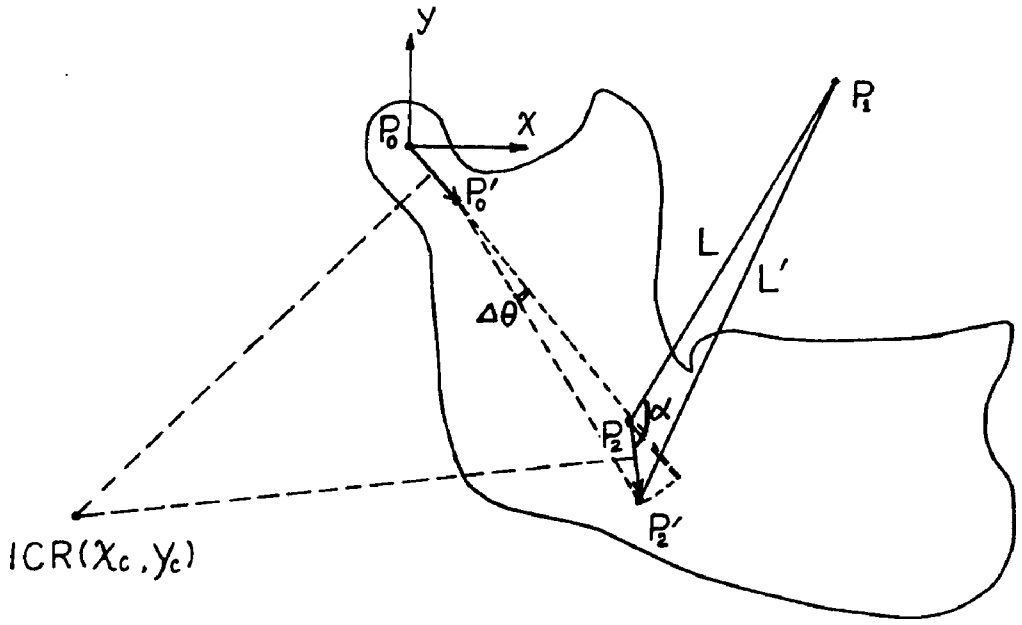

Fig. 5.5 Incremental motion of the mandible and corresponding ICR

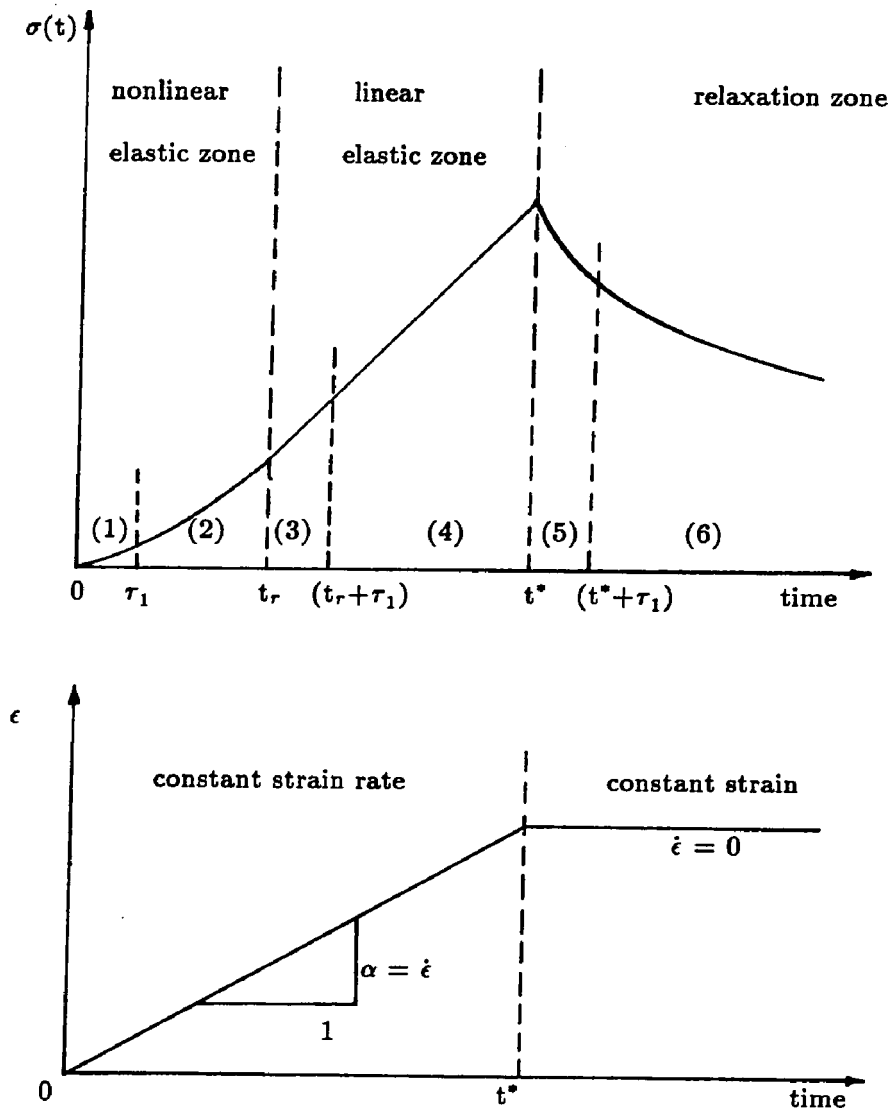

Fig.6.1 Stress relaxtion behavior corresponds to finite strain rate drawn schematically along time scale

[(1)~(6) denote different time domain for relaxation behavior]

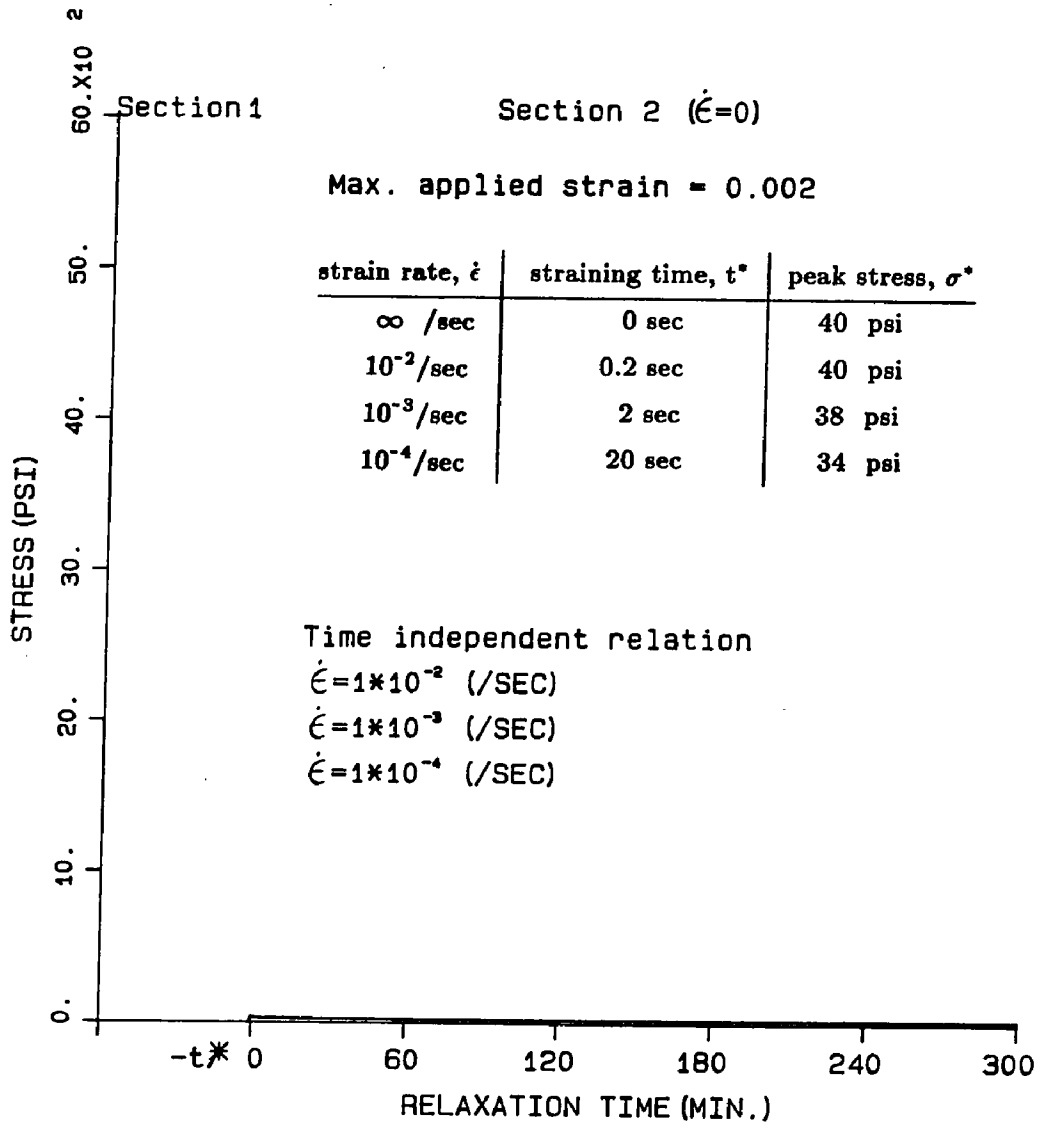

Fig.6.2.1 Stress relaxation of a ligament for finite strain rate

($\epsilon^* = 0.002$)

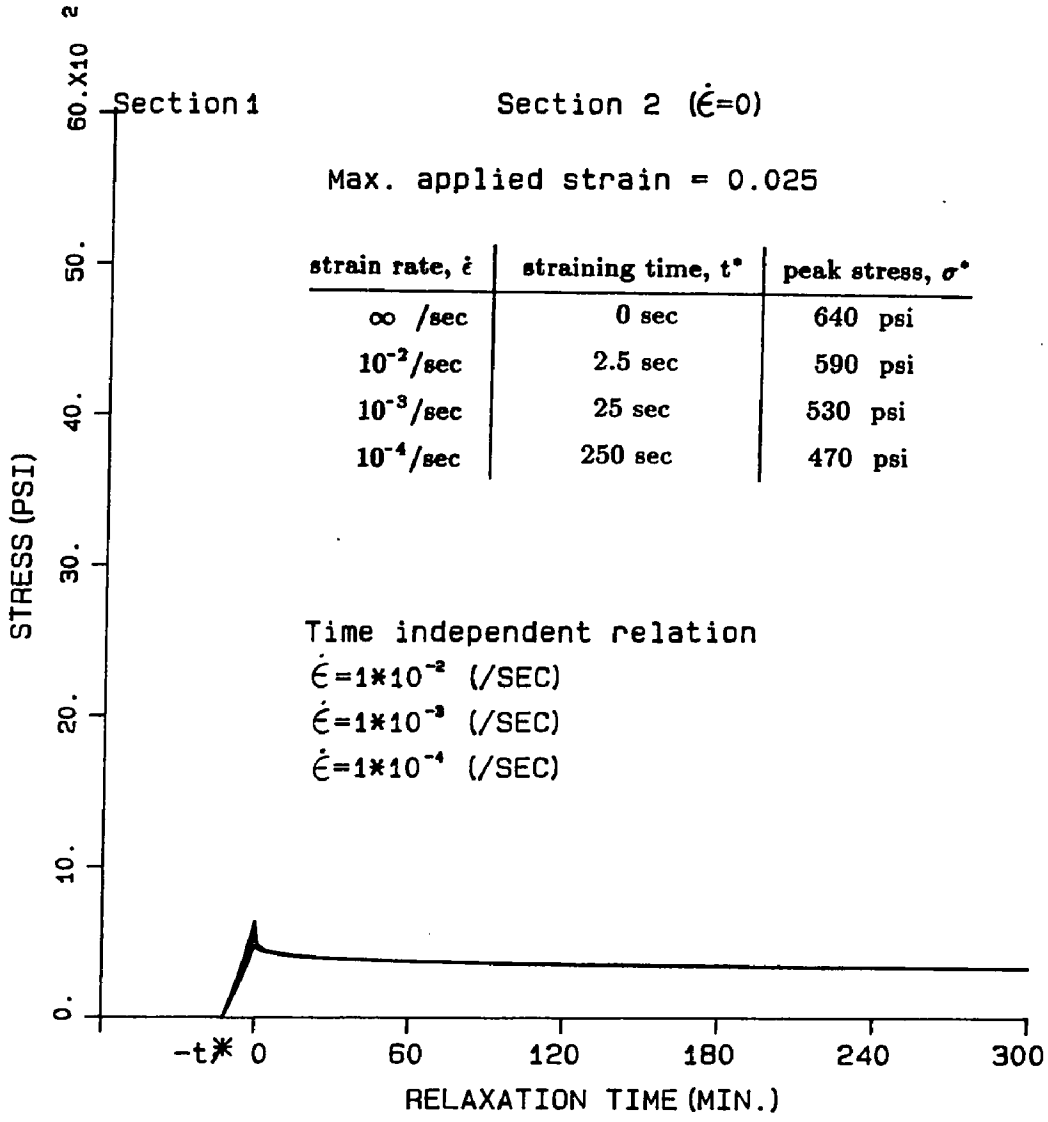

Fig.6.2.2 Stress relaxation of a ligament for finite strain rate

($\epsilon^* = 0.025$)

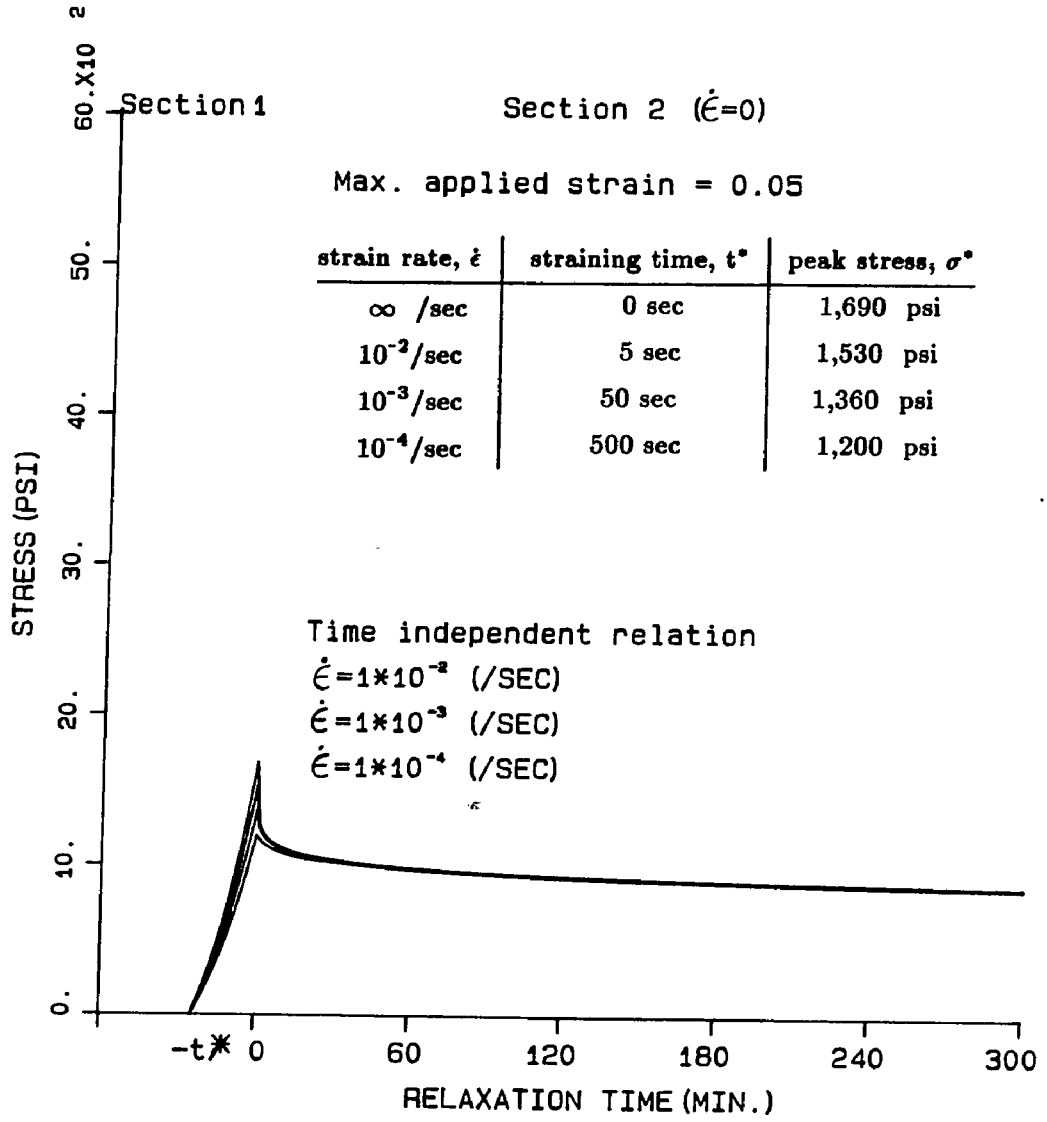

Fig.6.2.3 Stress relaxation of a ligament for finite strain rate

($\epsilon^* = 0.050$)

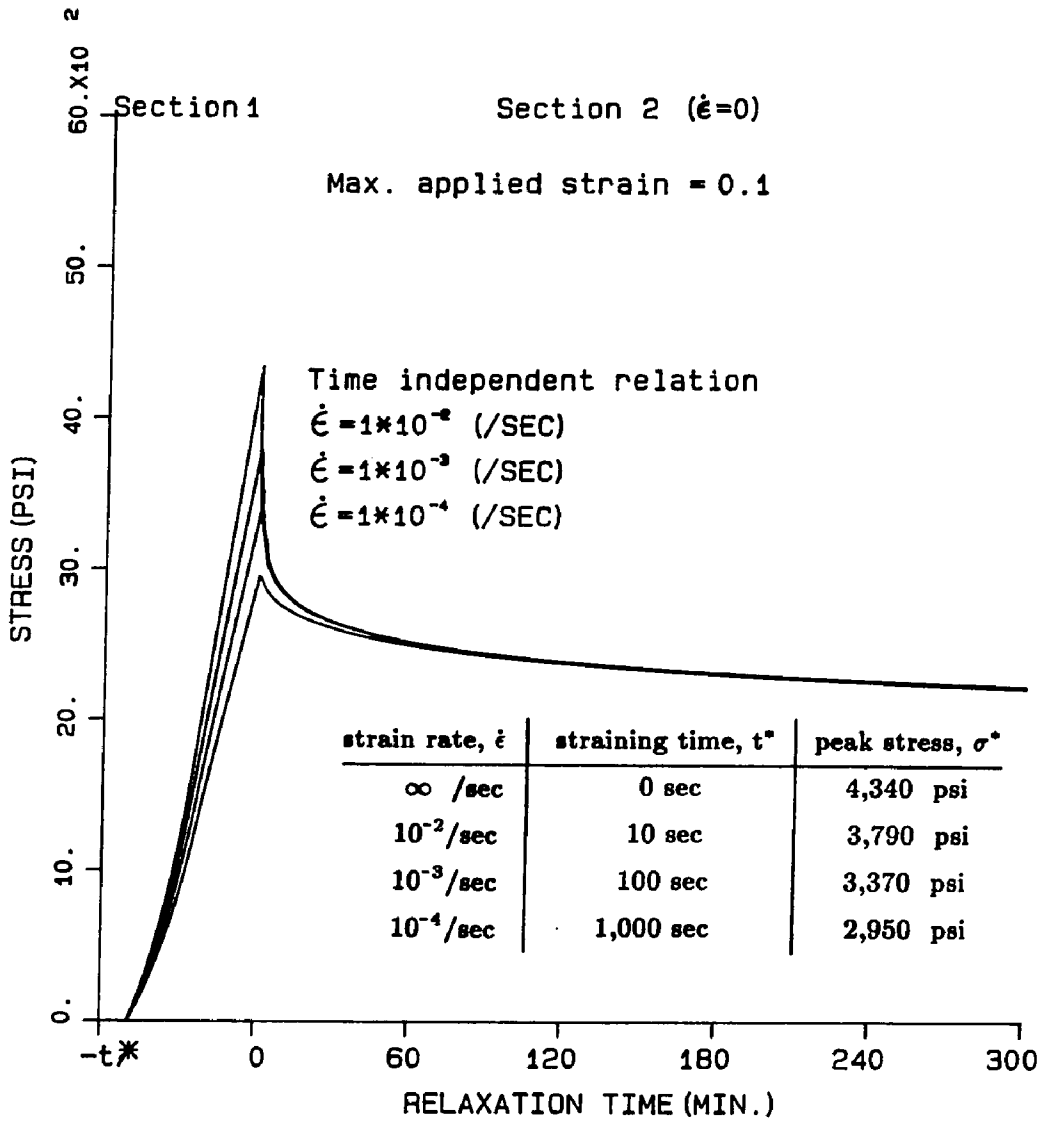

strain rate, $\dot{\epsilon}$	straining time, t^*	peak stress, σ^*
∞ /sec	0 sec	4,340 psi
10^{-2}/sec	10 sec	3,790 psi
10^{-3}/sec	100 sec	3,370 psi
10^{-4}/sec	1,000 sec	2,950 psi

Fig.6.2.4 Stress relaxation of a ligament for finite strain rate

($\epsilon^* = 0.100$)

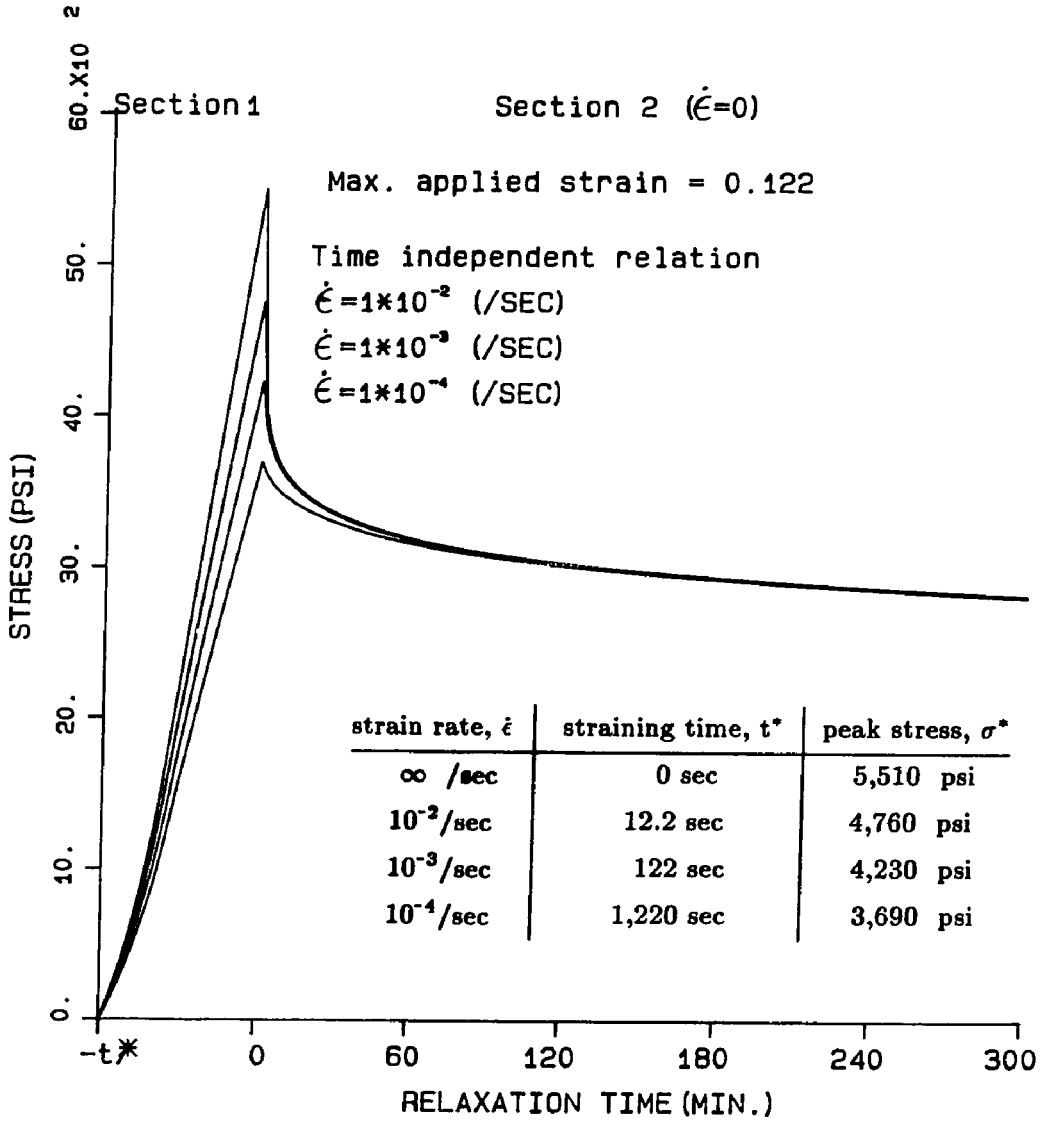

strain rate, $\dot{\epsilon}$	straining time, t^*	peak stress, σ^*
∞ /sec	0 sec	5,510 psi
10^{-2}/sec	12.2 sec	4,760 psi
10^{-3}/sec	122 sec	4,230 psi
10^{-4}/sec	1,220 sec	3,690 psi

Fig.6.2.5 Stress relaxation of a ligament for finite strain rate

($\epsilon^* = 0.122$)

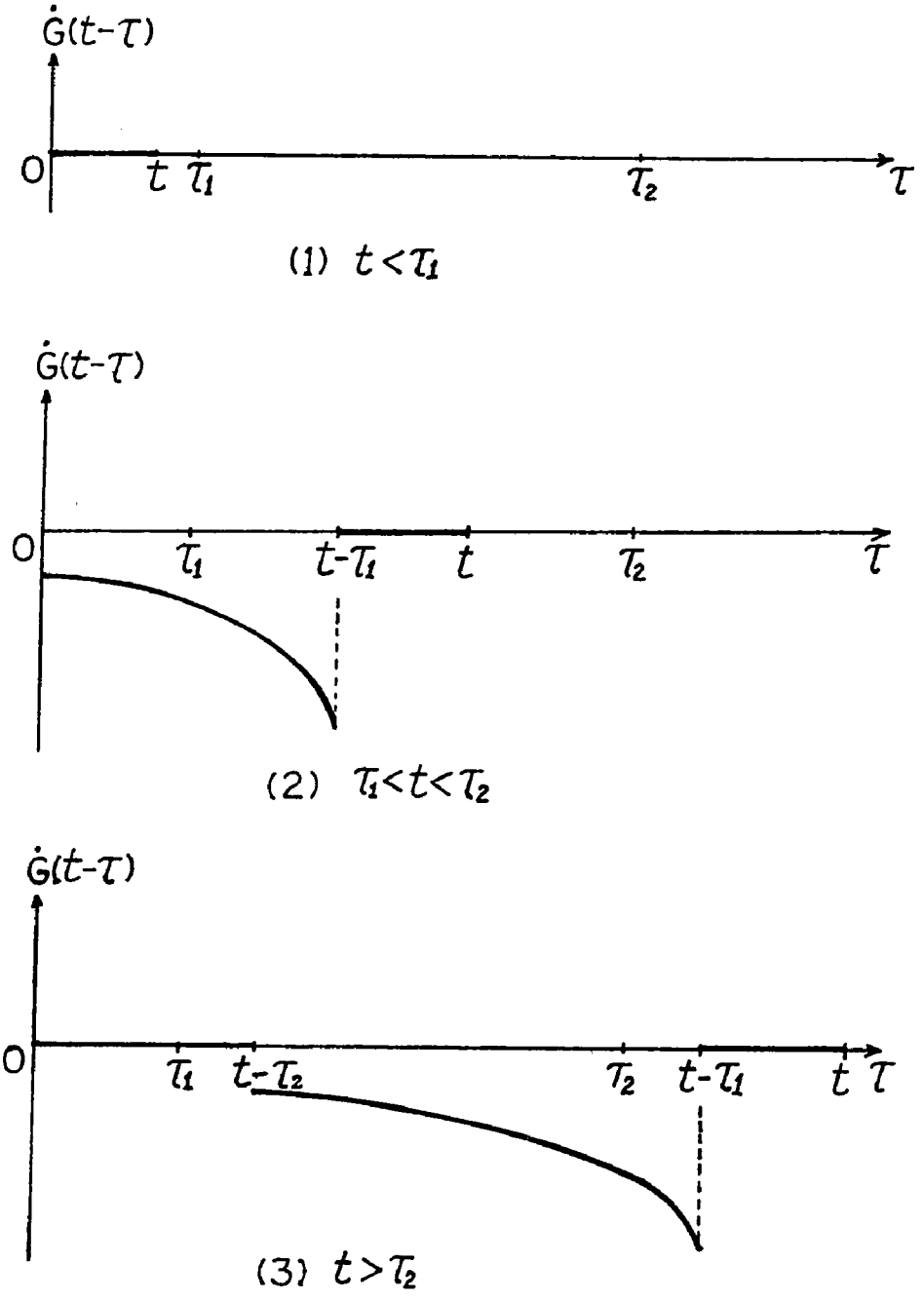

Fig.7.1 Shape of $\dot{G}(t-\tau)$

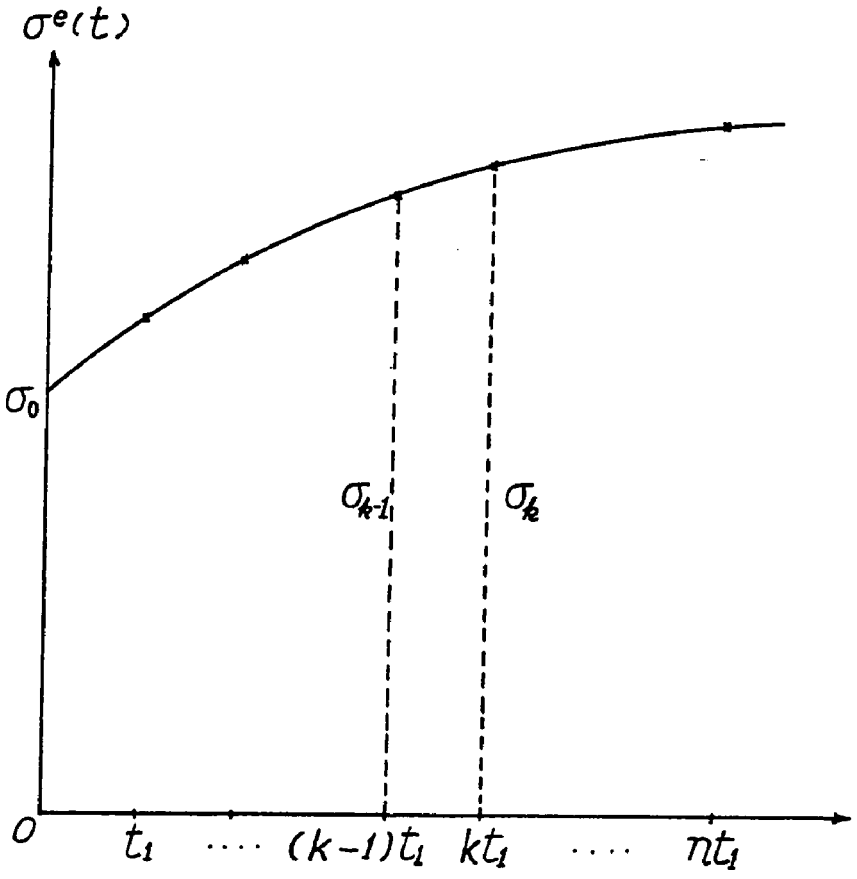

Fig.7.2 Creep stress at discrete time steps

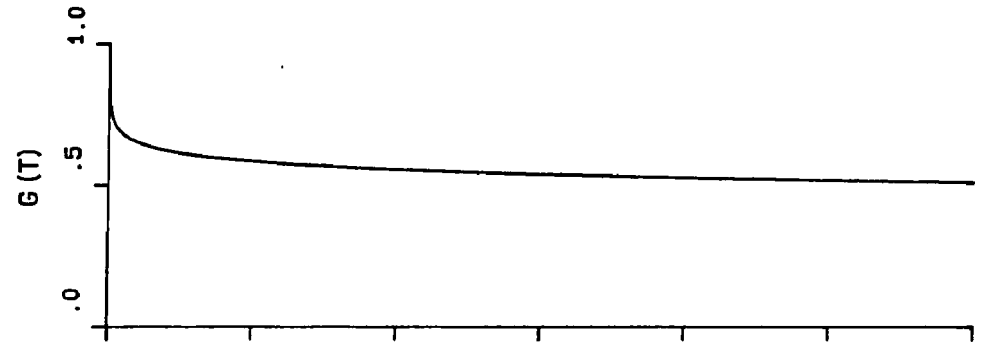

REDUCED RELAXATION FUNCTION

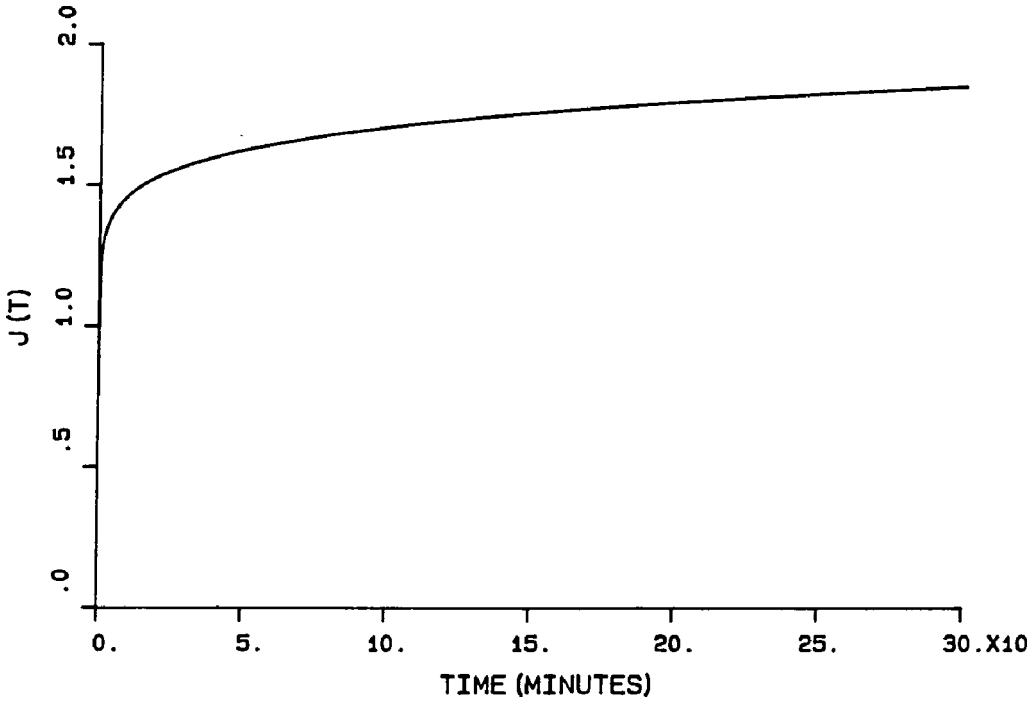

REDUCED CREEP FUNCTION

Fig.7.3 Reduced creep function corresponds to reduced relaxation function

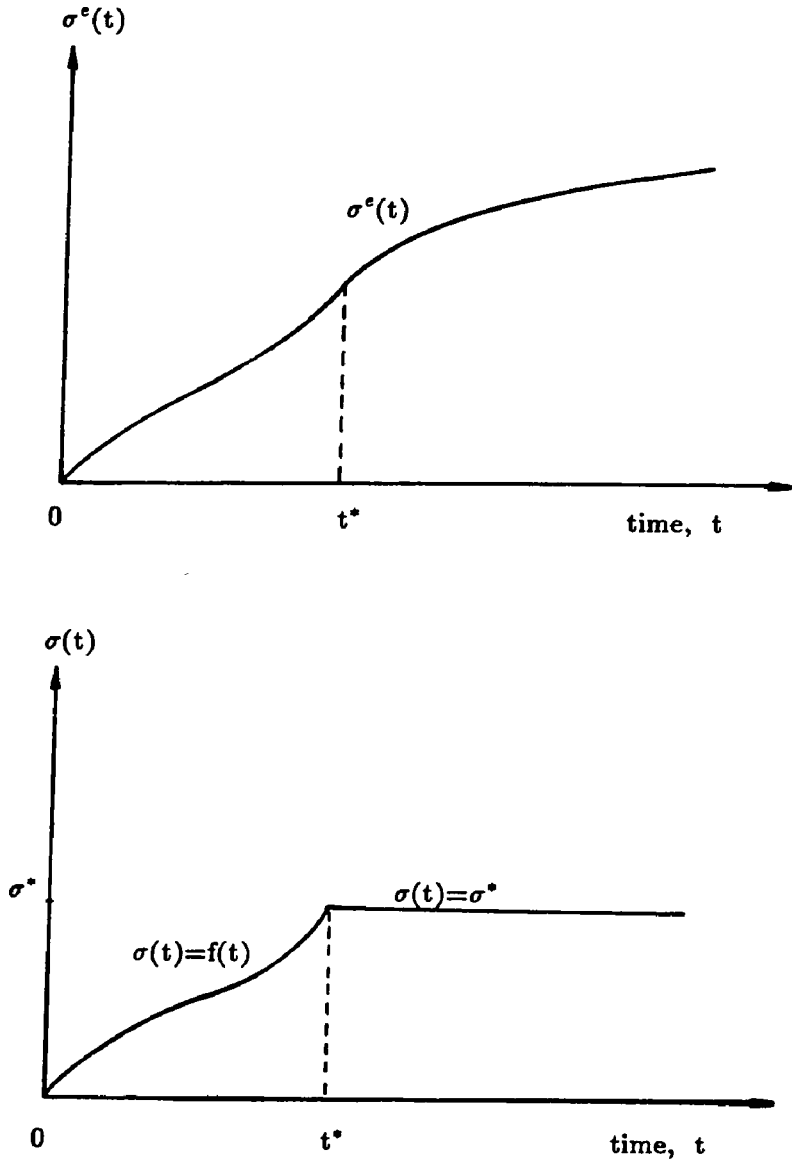

Fig.7.4 Creep behavior of a ligament due to applied stress history

[$\sigma^e(t)$ is the theoretically determined elastic stress response corresponds to the creep strain $\epsilon(t)$]

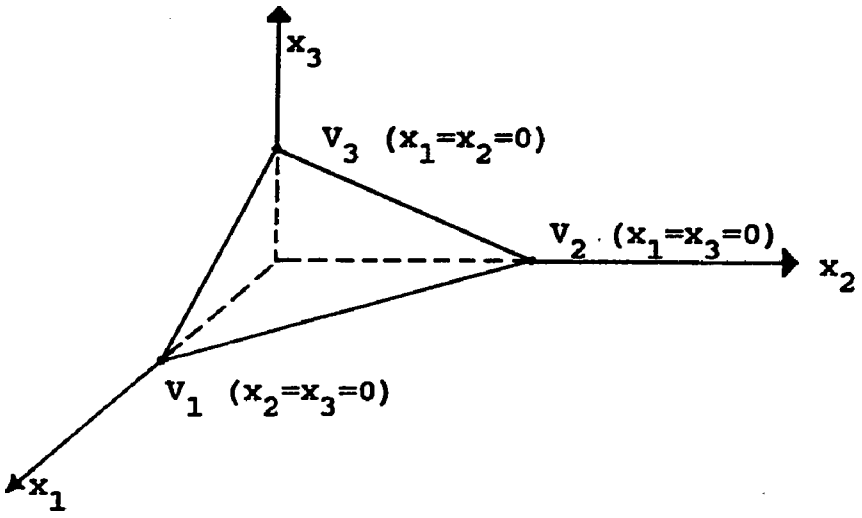

Fig.(1A). Solution boundary of case 1 (1 eqn.)

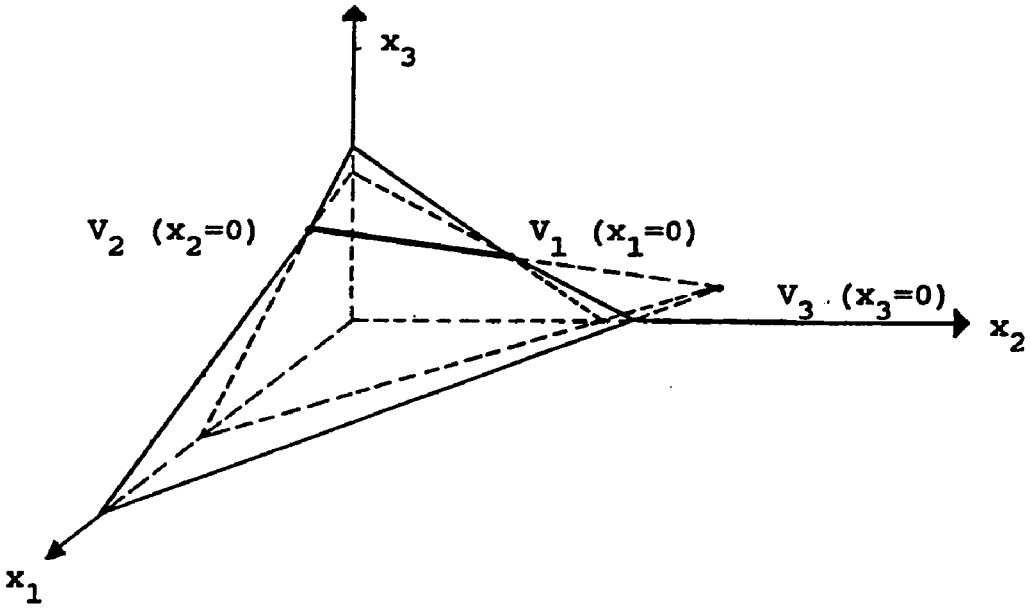

Fig.(2A). Solution boundary of case 2 (2 eqn's.)

REFERENCES

1. Johnston, T. B. et. al., ed., "Gray's Anatomy, 32-nd ed.," Longmans, Green and Co., N. Y., 1958.

2. Hellsing, G., Holmlund, A., Nordenram, A. and Wredmark, T., "Arthroscopy of the Temporomandibular Joint," Int. J. Oral Surg., Vol.13, pp.69-74, 1984.

3. Murakami, K. I., Matsuki, M., Iizuka, T. and Ono, T., "Diagnostic Arthroscopy of the TMJ: Differential Diagnoses in Patients with Limited Jaw Opening," J. Craniomandibular Practice, Vol.4, No.2, pp.117-126, 1986.

4. Anderson, J. E., ed., "Grant's Atlas of Anatomy, 7-th ed.," Williams and Wilkins, Baltimore, 1978.

5. Waters, R. L. and Morris, J. M., "An in Vitro Study of Normal and Scoliotic Interspinous Ligaments," J. Biomech., Vol.6, pp.343-348, 1973.

6. Woo, S. L-Y. , Gomez, M. A. and Akeson, W. H., "The Time and History -Dependent Viscoelastic Properties of the Canine Medial Collateral Ligament," J. Biomechanical Engr., Trans. ASME, Vol.103, pp.293-298, 1981.

7. Butler, D. L., Kay, M. D. and Stouffer, D. C., "Comparison of Material Properties in Facicle-Bone Units from Human Patellar Tendon and Knee Ligaments," J. Biomech., Vol.17, pp.425-432, 1986.

8. Pruim, G. J., de Jongh, H. J. and ten Bosch, J. J., "Forces Acting on the Mandible During Bilateral Static Bite at Different Bite Force Levels," J. Biomech., Vol.13, pp.755-763, 1980.

9. Vitti, M. and Basmajian, J. V., "Integrated Action of Masticatory Muscles; Simultaneous EMG from Eight Intramuscular Electrodes," Anatomical Record, Vol.187, pp.173-189, 1977.

10. Barbenel, J. C., "The Biomechanics of the Temporomandibular Joint: A Theoretical Study," J. Biomech., Vol.5, pp.251-256, 1972.

11. Grant, P. G., "Biomechanical Significance of the Instantaneous Center of Rotation: The Human Temporomandibular Joint," J. Biomech., Vol.6, pp.109-113, 1973.

12. Wheeler, R. C., "A Textbook of Dental Anatomy and Physiology," W.B.Saunders Co., Philadelphia, 1965.

13. Nachemson, A. L., and Evans, J.H., "Some Mechanical Properties of the Third Human Lumbar Interlaminar Ligament (Ligament Flavum)," J. Biomech., Vol.1, pp.211-220, 1968.

14. Viidik, A., "Functional Properties of Collagenous Tissues," Int. Review of Connective Tissue Research, Hall, D. A., ed., Vol.6, pp.127-215, 1973.

15. Dumas, G. A., Beaudoin, L. and Drouin, G., "In Situ Mechanical Behavior of Posterior Spinal Ligaments in the Lumbar Region. An in Vitro Study," J. Biomech., Vol.20, pp.301-310, 1985.

16. Fung, Y. C., "Stress-Strain-History Relation of Soft Tissues in Simple Elongation," Biomechanics: Its Foundations and Objectives, Fung et. al., eds., pp.293-298, 1972.

17. Butler, D. L., Grood, E. S., Noyes, F. R., Zernicke, R. F. and Brackett, K., "Effects of Structure and Strain Measurement Technique on the Material Properties of Young Human Tendons and Fascia," J. Biomech., Vol.17, No.8, pp.579-596, 1984.

18. Stromberg, D. D. and Wiederhielm, C. A., "Viscoelastic Description of a collagenous tissue in simple elongation," J.Applied Physiology, Vol.26, No.6, pp.857-862, 1969.

19. Haut, R. C. and Little, R. W., "A Constitutive Equation for Collagen Fibers," J. Biomech., Vol.5, pp.423-430, 1972.

20. Schmitz, J. V., "Testing of Polymers,", Vol.1 and 2, Interscience Publishers, 1965.

21. Aklonis, J. J., and McKnight, W. J., "Introduction to Polymer Viscoelasticity," John Wiley and Sons, 1983.

22. Fung, Y. C., "Biomechanics, Mechanical Properties of Living Tissues," Springer-Verlag N.Y. Inc., 1981.

23. Abramowitz, M. and Stegun, I. A., "Handbook of Mathematical Functions," Dover Publications, Inc., N.Y., 1970.

24. Pedersen, D. R., Brand, R. A., Cheng, C. and Arora, J. S., "Direct Comparison of Muscle Force Predictions Using Linear and Nonlinear Programming," J. Biomechanical Engr., Trans. ASME, Vol.109, pp.192-199, 1987.

25. Pruim, G. J., ten Bosch, J. J., and de Jongh, H. J., "Jaw Muscle EMG-Activity and Static Loading of the Mandible ," J. Biomech., Vol.11, pp.389-395, 1978.

26. An, K. N., Kwak, B. M., Chao, E. Y. and Morrey, B. F., "Determination of Muscle and Joint Forces: A New Technique to solve the Indeterminate Problem," J. Biomechanical Engr., Trans. ASME, Vol.106, pp.364-367, 1984.

27. Pierre, D. A., "Optimization Theory with Applications," John Wiley and Sons, Inc., N.Y., 1969.

28. Throckmorton, G. S. and Throckmorton, L. S., "Quantitative calculations of Temporomandibular Joint Reaction Forces - I. The Importance of the Magnitude of the Jaw Muscle Forces," J. Biomech., Vol.18, No.6, pp.445-452, 1985.

29. Throckmorton, G. S., "Quantitative calculations of Temporomandibular Joint Reaction Forces - II. The Importance of the Direction of the Jaw Muscle Forces," J. Biomech., Vol.18, No.6, pp.453-461, 1985.

30. Dortmans, L.J.M.G., Sauren, A.A.H.J. and Rousseau, E.P.M., "Parameter Estimation Using the Quasi-Linear Viscoelastic Model Proposed by Fung," J.Biomechanical Engr., Trans. ASME, Vol.106, pp.198-203, 1984.

31. Rousseau, E. P. M., Sauren, A. A. H. J., van Hout, M. C. and van Steenhoven, A. A., "Elastic and Viscoelastic Material Behaviour of Fresh and Glutaraldehyde-treated Porcine Aortic Valve Tissue," J. Biomech., Vol.16, pp.339-348, 1983.

32. Loeb, G. E. and Gans, C., "Electromyography for Experimentalists," University of Chicago Press, 1986.

APPENDIX (a). Relation between G(t) and J(t)

From eq.3.7, including all the past history of applied stress,

$$\sigma(t) = \int_{-\infty}^{t} G(t - \tau) \frac{d\sigma^e}{d\tau} d\tau. \qquad (a.1)$$

Integrating by parts,

$$\sigma(t) = [\ G(t-\tau)\, \sigma^e(\tau)\ ]_{-\infty}^{t} - \int_{-\infty}^{t} \sigma^e(\tau) \frac{dG(t-\tau)}{d\tau} d\tau. \qquad (a.2)$$

Assuming $\sigma(-\infty) = 0$ and let $t - \tau = u$,

$$\sigma(t) = G(0)\, \sigma^e(t) + \int_0^{\infty} \sigma^e(t - u) \frac{dG(u)}{du} du\ . \qquad (a.3)$$

Taking Laplace Transform of eq.(a.3),

$$\mathcal{L}\{\sigma(t)\} = G(0)\ \mathcal{L}\{\sigma^e(t)\} + \int_0^{\infty} e^{-st} \int_0^{\infty} \sigma^e(t-u) \frac{dG(u)}{du} du\, dt$$

$$= G(0)\ \mathcal{L}\{\sigma^e(t)\} + \int_0^{\infty} \frac{dG(u)}{du} \int_0^{\infty} e^{-st}\, \sigma^e(t-u)\, dt\, du$$

$$= G(0)\ \mathcal{L}\{\sigma^e(t)\} + \int_0^{\infty} \frac{dG(u)}{du}\ \mathcal{L}\{\sigma^e(t-u)\}\ du$$

$$= G(0)\ \mathcal{L}\{\sigma^e(t)\} + \int_0^{\infty} \frac{dG(u)}{du}\ e^{-us}\, \mathcal{L}\{\sigma^e(t)\}\ du$$

$$= G(0)\ \mathcal{L}\{\sigma^e(t)\} + \mathcal{L}\left\{\frac{dG(u)}{du}\right\}\ \mathcal{L}\{\sigma^e(t)\}$$

$$= G(0)\ \mathcal{L}\{\sigma^e(t)\} + [-G(0) + s\ \mathcal{L}\{G(t)\}]\ \mathcal{L}\{\sigma^e(t)\}$$

$$= s\ \mathcal{L}\{\sigma^e(t)\}\ \mathcal{L}\{G(t)\}\ . \qquad \text{(a.4)}$$

In the similar way, from eq.3.22,

$$\mathcal{L}\{\sigma^e(t)\} = s\ \mathcal{L}\{\sigma(t)\}\ \mathcal{L}\{J(t)\}\ . \qquad \text{(a.5)}$$

From eqs. (a.4) and (a.5),

$$\frac{1}{s^2} = \mathcal{L}\{G(t)\}\ \mathcal{L}\{J(t)\}\ . \qquad \text{(a.6)}$$

The inverse transform gives us,

$$t = G(t) * J(t)$$

$$= \int_0^t G(\tau)\ J(t-\tau)\ d\tau\ , \qquad \text{(a.7)}$$

where $*$ denotes the convolution integral .

APPENDIX (b). Computational Basis of the Simplex Method

Suppose we are to minimize or maximize a linear function $P(x_1,x_2,x_3)$, which is generally called the performance measure, in the solution set of equations for three unknowns x_1, x_2 and x_3, where the number of equations is less than that of the unknowns;

e.g.,

$$P(x_1, x_2, x_3) = c_1 x_1 + c_2 x_2 + c_3 x_3 , \tag{b.1}$$

the extreme value of which is to be determined in the solution set of the equation

$$a_{1j} x_1 + a_{2j} x_2 + a_{3j} x_3 = b_j , \tag{b.2}$$

where the number of equations j is less than 3 in this example.

The constraint for all x_i's is

$$x_i \geq 0 , \qquad i = 1, 2, 3 . \tag{b.3}$$

The solution set of eq.(b.2) can be geometrically represented in three dimensional space to the plane $V_1V_2V_3$ when $j = 1$, and the line V_1V_2 when $j = 1, 2$, as shown in Figs.(1A) and (2A) . In Fig.(2A), the line V_1V_3 which is the extension of the line V_1V_2 in the space $x_1 < 0$, should be discarded by the constraint given in eq.(b.3).

The performance measure $P(x_i)$ being represented by a set of parallel planes, it has the limit value on one of three points V_1, V_2 and V_3.

Expanding the problem to an n-dimensional one, the solution set of system of equations (b.2) will be a polyhedron in n-dimensional space. The number of vertices will be ${}_nC_m$, where m is the number of equations. By sweeping through all vertices,

we can get the values $P_1, P_2, P_3, \cdots\cdots, P_N$ for all the vertices, where N is the number of vertices. By considering the constraint, eq.(b.3), and comparing the values, we can get the optimum solution correspond to the limit value of P.

If the system contains inequality conditions such as,

$$a_{1k}\, x_1 + a_{2k}\, x_2 + \cdots\cdots + a_{nk}\, x_n \leq b_k , \qquad \text{(b.4)}$$

by introducing a slack variable x_s for each inequality, and converting the condition as;

$$a_{1k}\, x_1 + a_{2k}\, x_2 + \cdots\cdots + a_{nk}\, x_n + x_s = b_k , \quad \text{where} \quad x_s > 0 , \qquad \text{(b.5)}$$

we can have the same type of the system of equations. But in this case, the dimension of the system will be increased by each slack variable.

Now we return to the system of muscle force equations which has three equations for seven unknowns - five magnitudes of muscle forces, R_x and R_y. By converting R_x and R_y into $R\cos\phi$ and $R\sin\phi$, where R is the magnitude of the joint reaction force and ϕ is its direction, we can meet the constraint condition that all the variables should not be less than zero. With ϕ being dealt with as a parameter, the system is reduced to a six-dimensional problem with one parameter.

The solution set will be a polyhedron in six-dimensional space and the number of vertices of the polyhedron will be 20 $(= {}_6C_3)$. The performance measure $P(x_i)$ will have the limit value on one of these vertices. To find the optimum solution, we pick one vertex by taking three of unknown forces to be zero, and we solve the system of equations for the remaining three unknown forces, which now has a unique solution set and corresponding value of the performance measure $P(x_i)$. Similarly, taking another set of three variables zero, we can get another solution set and corresponding value of the performance measure for another vertex. After sweeping through all the vertices in the same way, comparing the performance measures, we can pick the limit value of the performance measure $P(x_i)$ and corresponding solution set of muscle forces.

Practically, the system was solved utilizing subroutine ZX3LP in IMSL5 subroutine packages, which is the most simplified easy-to use version. The parameter ϕ should be swept through from -180° to 180° with an appropriate interval and the detailed procedure is illustrated in the text.

VITA

The author was born on August 5, 1949 in Hahdong, Korea as the second son of Mr. and Mrs. Chul-Young Kang. In March 1967, he entered Seoul National University and graduated with a Bachelor of Science in Mechanical Engineering in February 1972. After finishing military service with Korean Army, he worked with Daejeon Machine Depot, Daejeon, Korea for six years as a research engineer. During his work with Daejeon Machine Depot, he was enrolled as an associate student in the graduate school of Aircraft Design Department, Cranfield Institute of Technology, England, United Kingdom from October 1979 to July 1980.

He came to the United States in August, 1982 for graduate study. He attended University of Maine, Orono, where he was awarded a Master of Science in Mechanical Engineering in August, 1984. His studies at Lehigh University began in August, 1984.

The author is married to Mee-Young, the eldest daughter of Mr. and Mrs. Chong-In Hahn and has two daughters, Min-Jung (Jessica) and Eui-Jung (Jamie).